AIAA Undergraduate Individual Aircraft Design Competition 2018 - 2019

The Pteslasaur

Author: Nathan Simon

AIAA # 952743

Nathan Simon

Advisor: Dr. R. Barrett-Gonzalez

AIAA # 022393

Ron Barrett

The University of Kansas
Aerospace Engineering Department

Abstract

The purpose of this report is to outline the design of the Pteslasaur in response to the American Institute of Aeronautics and Astronautics (AIAA) Request of Proposal. This aircraft will be able to exceed the payload requirements for the power line surveying within 6 hours, under the standard 8 hour work day. By surpassing the mission specifications, this aircraft should be able to dominate the emerging market of UAS civilian-use surveillance systems. STAMPED analysis will be used to project the size of the aircraft and design it to out perform any competitors. With the initial sizing of the aircraft complete, several configurations will be created and then selected based on the objective function. The design of this aircraft was selected to resemble a Pterosaur was to reduce the transportation storage volume by using the membrane wing structure as well as maximizing the objective to dominate the powerline surveying UAS industry.

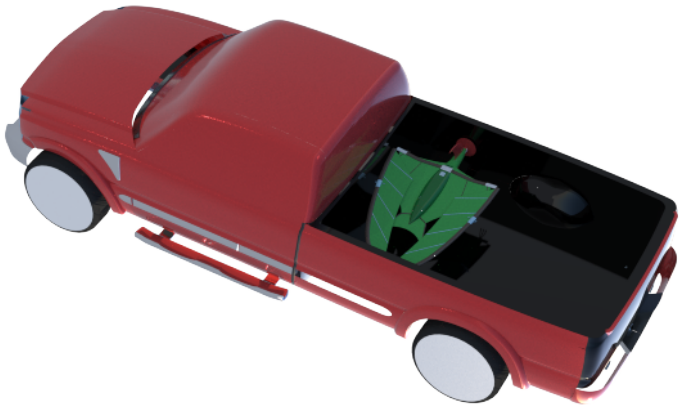

Acknowledgments

The author would like to thank his AE 721 teammates for working through these report sections to learn the process for each report block, making AE 521 reports much easier. The designer would also like to thank Dr. R. Barrett-Gonzalez and his tempting words of "do you know what would be cool" that inspired the design of the aircraft. Another person the author would like to thank is Dr. Alexander in the evolutionary biology department for taking the time to talk about pterosaurs and how an RC pterosaur could work.

Table of Contents

List of Figures

List of Tables

List of Symbols

Symbol	Description	Units
a	Regression Line Constant	~
A	Aspect Ratio	~
b	Span	ft
c	Chord Length	ft
C_D	Coefficient of Drag	~
C_{Do}	Zero-Lift Drag Coefficient	~
C_L	Aircraft Lift Coefficient	~
C_l	Airfoil Coefficient of Lift	~
D	Drag	lbf
E	Endurance	hrs
e	Oswald Efficiency Factor	~
L	Lift	lbf
M	Pitching Moment	ft*lbf
n	Load Factor	~
P	Power	W,ft*lbf
$\bar{q}$	Dynamic Pressure	psf
R	Range	mi
Re	Reynolds Number	~
S	Wing Area	ft^2
T	Thrust	lbf
T/W	Thrust-to-Weight Ratio	~
V	True Airspeed	ft/s
W	Weight	lbf
W/S	Wing Loading	psf
$\bar{X}$	Distance Normalized by MGC	

Greek Symbols

α	Angle of Attack	deg
β	Sideslip Angle	deg
ε	Wash	~
λ	Taper Ratio	~
μ	Dynamic Viscosity	slug/s*ft
Λ	Sweep Angle	deg
ρ	Air Density	$slugs/ft^3$

Symbol	Description
Subscripts	
AC	Aerodynamic Center
CG	Center of Gravity
D	Drag
e	Empty
f	Friction
f	Fuselage
F	Fuel
h	Horizontal Tail
l	Rolling Moment
l	Airfoil Lift
L	Wing Lift
m	Pitching Moment
max	Maximum
n	Yawing Moment
PL	Payload
tent	Tentative
TO	Takeoff
v	Vertical Tail
wet	Wetted
w	Wing
Acronyms	
Advanced Aircraft Analysis	AAA
American Institute of Aeronautics and Astronautics	AIAA
Federal Aviation Administration	FAA
Federal Aviation Regulation	FAR
Finite Element Model	FEM
Low Observable	LO
Mean Geometric Chord	MGC
Request for Proposal	RFP
Statistical Time and Market Predictive Engineering Design	STAMPED
Short Take Off and Landing	STOL
Vertical Take Off and Landing	VTOL

1. INTRODUCTION, MISSION SPECIFICATION & PROFILE

This report follows the design of an aircraft that satisfies the Request for Proposal (RFP) issued by the American Institute of Aeronautics and Astronautics (AIAA).

With the advancements in small aircraft motors and power supplies, the use of Unmanned Aerial Systems (UAS) has expanded to several industries. The RFP requires a UAS that can monitor the condition and the surroundings of powerlines to direct maintenance crews to specific locations. The key design parameters for the UAS are being able to survey 100 miles in a single day where the launch site is located at the midpoint, the 50-mile mark. For the surveying, the UAS must carry a LiDAR system, a GPS based autopilot and an ADS-B transponder with broadcasting capabilities. Additional tradable capabilities can be found in the RFP.

1.1 MISSION SPECIFICATION

Table 1 outlines the mission specifications derived from the RFP issued by the AIAA for the 2017-2018 Design Competition.

Table 1.1: UAS Mission Specifications (Ref.1)

Flight Requirements	
Survey Distance	100 linear miles in 1 day
Take-Off/Landing Conditions	Dirt and grass roads or clearings
Take-Off/Landing Distance	500 ft runway with 50 ft trees at the end
Min/Max Flight Altitude	150/400 ft AGL
Meet FAA Part 107 Certification, Beyond Line of Sight (BVLOS) exception	
Payload Requirements	
RIEGL miniVUX-1UAV	Point Cloud Density of 25 points per sq. meter
GPS-based Autopilot for Autonomous Operations	
ADS-B Transponder with Broadcast Capability	
Design Objectives	
Minimize Production Cost Based on the Potential Market Size	
Launch Within 15 Minutes of Arriving at the Takeoff Site	
Replace Failed Parts Within 10 Minutes	
Entry into Service in 2020	
Operations are Based from a 2018 Ford F-150 SuperCrew Cab	

1.2 MISSION PROFILE, PERFORMANCE, PAYLOAD-RANGE REQUIREMENTS

The mission specifications require that the flight starts at the 50-mile mark which splits the survey distance into 50 miles of power lines in each direction. This sets a minimum flight range of 2 - 100 mile segments with a maximum 10-minute overhaul in between. The take-off and landing zone is a 500 ft grass or dirt clearing with grass and 50 ft trees on the sides. Figure 1.1 shows the overall mission objective and Figure 1.2 shows the mission profile.

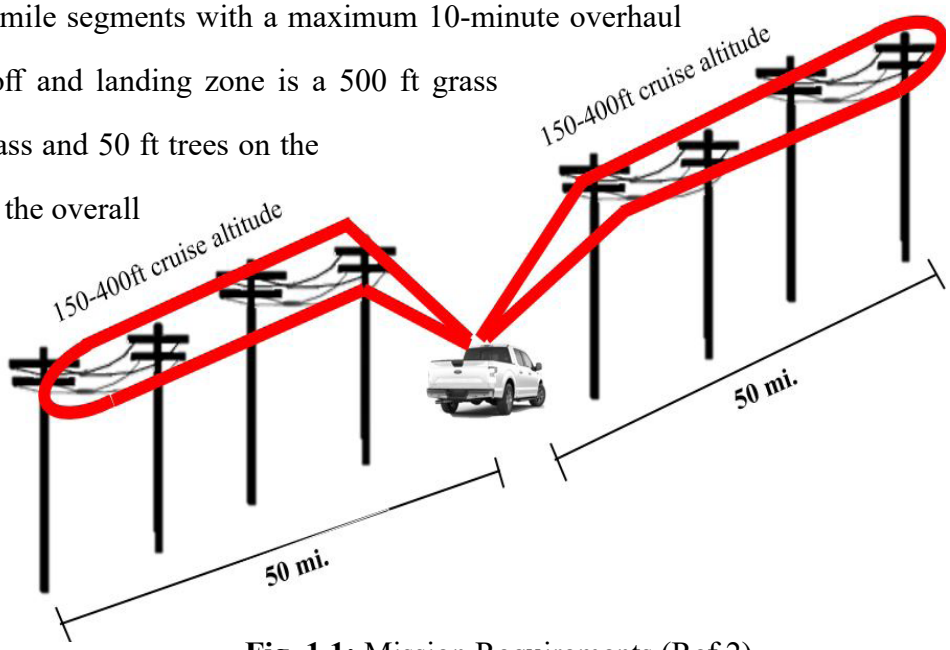

Fig. 1.1: Mission Requirements (Ref 2)

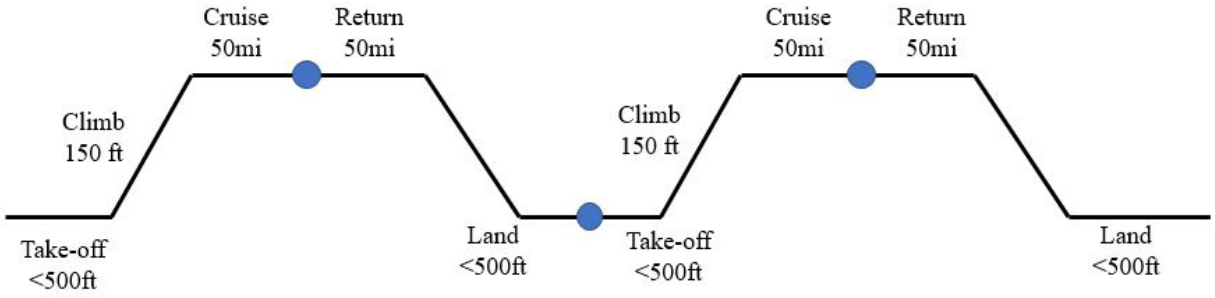

Fig. 1.2: Mission Flight Profile

1.3 OVERALL DESIGN METHODS AND PROCESS

Steps for the design process are based off Dr. Jan Roskam's Aircraft Design Series (References 3-10). Calculations for the design process were done in Microsoft Excel and hand calculations will be attached in the report where they are used. Click on the hand calculation image to enlarge the photo, and click a second time to return the image to the smaller size. The generalized steps for the aircraft design process are described below.

1. Analyze the RFP to determine the aircraft requirements and the mission profile;
2. Use Statistical Time and Market Predictive Engineering Design (STAMPED) Analysis for general aircraft sizing parameters to analyze what design characteristics have been successful for similar types of missions;
3. Using the STAMPED data, determine the initial sizing parameters based on the flight conditions. Through the Class I Design, the sizing parameters will be used to develop several potential configurations. These configurations will be analyzed to select a final design for Class II Design analysis;
4. The Class II Design analysis and calculations are performed on the final Class I design to verify that the aircraft meets the RFP design requirements.

1.4 INTRODUCTION TO THE SELECTED DESIGN

For this mission, the selected design takes resemblance to the Pterosaur with the primary interest of utilizing the membrane wing. The ability to use the membrane on the wing for flight has been biologically proven millions of years ago. There is also current research looking into using the membrane for the wing structure, so this concept can be used in place of the traditional airfoil wing structure used in most aircraft. Transportation of the aircraft and mission supplies will be using the Ford F-150, so the purpose of the membrane wing is to reduce the packing volume of the aircraft. The membrane wing will be at most an eighth of an inch thick, and it will be able to be folded onto itself during storage. The required wing area will be selected in Chapter 6, and then Chapter 10 will further discuss the advantages of the membrane structure over a rigid wing.

2. HISTORICAL REVIEW & COMPETITION IN THE MARKET

The purpose of this section is to analyze previous aircraft that have mission profiles similar to the RFP, and what characteristics made them successful.

The Penguin C (Figure 2.1) is a 50 lb_f maximum take-off weight, internal combustion UAV that is suitable for reconnaissance and surveillance (Ref. 11). This platform would allow for photo mapping and environmental monitoring which are two mission requirements for this RFP using the LiDAR. The equipment only has a maximum range of 60 miles. But with the communications set up along the power lines the range should be extended to its 12-hour endurance at 49mph cruise velocity, giving it almost a 600-mile range. So, this aircraft would complete the mission, but it is far heavier than what is needed.

Fig. 2.1: UAV Factory Penguin C (Ref 12)

The Silent Falcon (Figure 2.2) is an electric powered aircraft that has a max take-off weight of 25 lb_f (Ref. 11). This aircraft has its base options of having IR cameras which would allow the platform to do the tradable requirement of taking thermal imaging scans of the powerlines. This aircraft has a range of 60 to 240 miles depending on the wing configuration which also far exceeds the flight requirements. But the cruise velocity is 20mph which would require 10 hours to complete the 200-mile flight, exceeding the standard 8-hour work day.

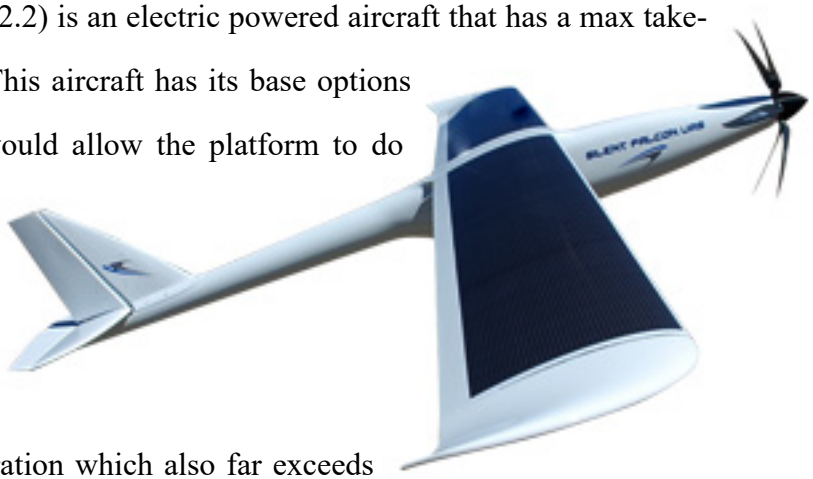

Fig. 2.2: Silent Falcon (Ref 13)

Applied Aeronautics has a UAS named the Albatross, which has a maximum take-off weight of 22 lb_f with uses including (but not limited to) surveillance and precision agriculture (Ref 14,15). This would likely include high resolution cameras as well as infrared camera packages satisfying both of the tradeable payload options in the RFP. Their system also has GPS navigation and 10 pounds of payload space which can hold the LiDAR along with other equipment as well. With multiple battery options, the range can reach 240 miles which also exceeds the requirements laid out by the RFP. This aircraft being light weight will allow for easier transportation as well.

Fig. 2.3: Applied Aeronautics Albatross (Ref 14)

Table 2.1 shows historical data for more of the UAS platforms that will be used for the STAMPED analysis in Chapter 4.

Table 2.1: Characteristics of Historical Aircraft (Ref 11-18)

Aircraft	Empty-to-takeoff Weight Ratio W_e/W_{to} (lbf/lbf)	Maximum Lift to Drag Ratio $(L/D)_{max}$	Wing Loading W/S (psf)
ScanEagle	0.64	20.5	5.9
Penguin C	0.44	19.4	5.3
Penguin B	0.47	19.4	5.0
CSV-20	0.50	20	6.2
Puma	0.86	32.5	1.7
Penguin BE Electric	0.83	19.3	3.1
Sensintel Coyote	0.93	19.2	7.8
Silent Falcon	0.75	-	1.3
AR4 Evolution	0.80	8.3	2.7
TAM-5	0.43	10.6	0.7
Albatross UAV	0.56	28	2.9

3. DESIGN VECTOR & WEIGHTS ESTABLISHMENT

The Pteslasaur was designs to maximize the objective function that the designer created based on input from companies that work on UAS surveying and the RFP (Ref. 1). Each variable in the objective function was given a weighting based on the perceived importance from the operators. Using the weighting, the designs can be compared directly to decide which configuration will have the highest performance.

3.1. OBJECTIVE FUNCTION

Based on the RFP and customer input, the following objective function will be used for the design:

OF=Range(=2 if over 200 miles, =1 if over 100 miles, 0 otherwise)

+(1 if it meets the 500ft clearing, 0 otherwise)

+(1 if Meets Payload Requirements, 0 otherwise)

+(8 hours/actual flight time, 0 if over 10 hours)^2

+($25K/(Fly Away Cost))

+(Visually Appealing/Public Acceptance)

+(Safe for Operators=1 yes, or 0)

+(Interference resistance, 1=yes, 0 otherwise)

+([1 for each: Thermal imaging, HD optical, Vegetation Health]/3)

3.2. CUSTOMERS AND OPERATORS FOR WEIGHTS DETERMINATION

Several employees at White River Valley Electric Cooperative were consulted about the type of work that they do with their UAS and what they would want to have in new technology. The takeaways from this consultation were (Ref. 19):

- Infrared imaging isn't important, they can find shorts in lines quickly;
- IR camera would only be used in the mornings;
- Maximum cost of $100K if the UAS can measure the right of way, tree species identification, brush density and dead tree identification.

For further input the designer was able to contact Tim Handley, the president of FlyGuys; a company that does UAV surveying for a wide variety of industries including transmission lines. Based on his input, it costs 100$ per hour or 1000$ per mile of transmission line for a pilot. For large repeated projects he gave an approximate value of $20K to purchase the UAV. The payload requirement would have to include both thermal and HD optical imaging. A major factor is that the UAV must be able resist interference from the magnetic fields of the powerlines. An added bonus, in his words was “if someone can make a good fixed wing VTOL, that would be bitchen” (Ref. 20).

3.3. WEIGHTING SURVEY AND RESULTS

The following weighting scale prioritized the ability to complete the mission objective of flying 100 miles with the payload such that the job is completed. Small scale UAVs aren’t too dangerous as long as the operators are paying attention when it takes off and returns for landing so the safety was more of a secondary requirement. After completing the mission, the next design objective would be to reduce the operating cost through the production value and the operating costs.

Table 3.1: Weights for Design Vector Variables from Survey of Customers & Operators

	VARIABLE TYPE	OPTIMIZATION DIRECTION	WEIGHTED PERCENTAGE
Range	Binary	Must Meet	15%
Takeoff and Landing Zone	Binary	Must Meet	15%
Required Payload	Binary	Must Meet	20%
Flight Time	Gradient	Minimize	10%
Cost	Gradient	Minimize	10%
Appealing and Public Acceptance	Binary	Meet	5%
Safe for Operators	Binary	Meet	5%
Interference Resistance	Binary	Must meet	15%
Additional Payload	Gradient	Maximize	5%
		Total:	100%

4. Statistical Time and Market Predictive Engineering Design (STAMPED) Analysis Techniques

The STAMPED Analysis Technique is a method that allows designers to track key sizing variables of historic aircraft and project them into the future to create a competitive design for the entry into service (EIS) date. In years leading up to the current date, the design parameter is plotted against its market share. The mean and standard deviation will be found to decide on an aggressive or conservative design and can be plotted similar to Figure 4.1. Then setting the market share distributions between each year along a 3rd axis, the trend of the market share can be tracked from the past to the current date. This will then be projected to the EIS date similar to Figure 4.2. Using the market distribution versus the entry into service plot, the aircraft characteristics can be sized to be aggressive to dominate the market but risk market acceptance, or to be sized conservatively with the market and stay competitive in the market.

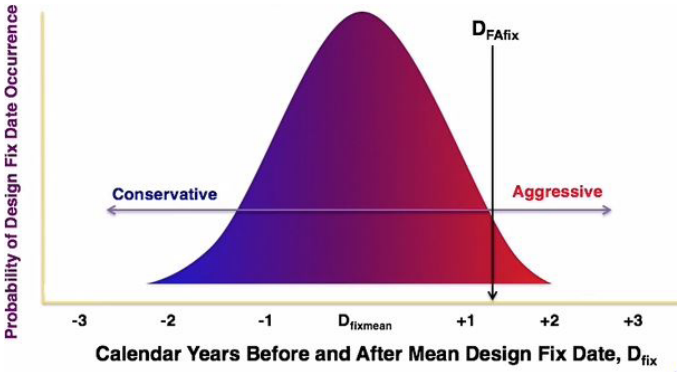

Fig. 4.1: Aggressive and Conservative Design Meaning (Ref. 21)

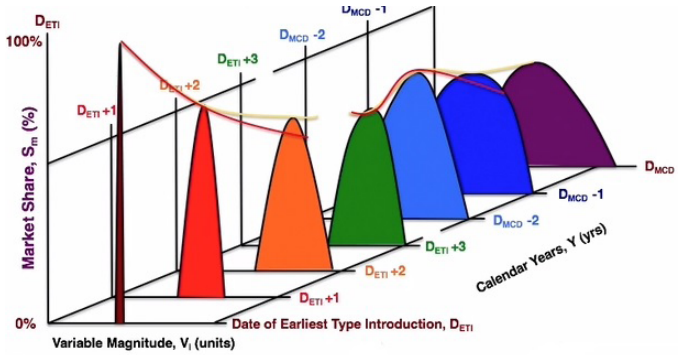

Fig. 4.2: Design Tracking and Projection (Ref 21)

Since the UAS market is relatively new and has many competitors, there isn't too much information that has been shared with a wide variety in aircraft. For this reason, the standard STAMPED method will not be as effective for determining market competition. Instead of using the market distribution in each year, the analysis will be done simply plotting the sizing characteristic against the production year to determine where the market appears to be going. This process will then use the standard deviation of all data to develop the standard deviation range to decide on an aggressive or conservative design approach.

5. WEIGHT SIZING

Using the STAMPED Data for the aircraft, the UAS weight was sized to lead the market in empty to take-off weight ratio with a low weight for ease of use.

5.1. EMPTY-TO-TAKEOFF WEIGHT RATIO

Figure 5.1 shows the STAMPED Analysis for the empty to takeoff weight ratios for some of the UAS platforms that are under the FAA Part 107 - 55 lb_f limit. To try and dominate the market, the UAS will be sized with an empty to takeoff weight ratio of 0.55. This value is below the -1 standard deviation line so it will outperform more than 85% of the market, thus being highly competitive for its payload options. This design point will still be reasonable since the Penguin UAS gas systems still have a lower empty to takeoff weight ratio.

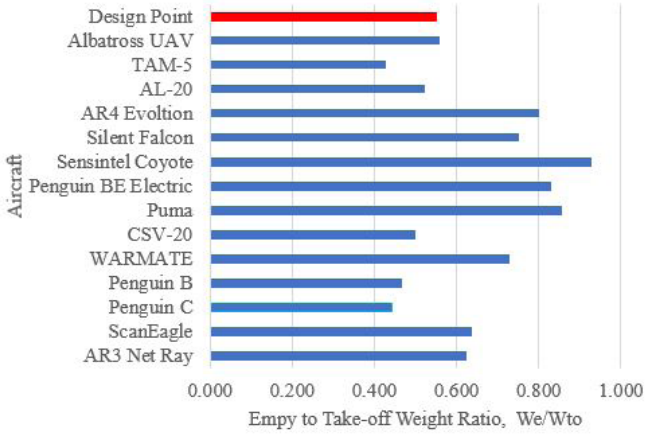

Fig. 5.1: Empty-to-Takeoff for UAS Systems

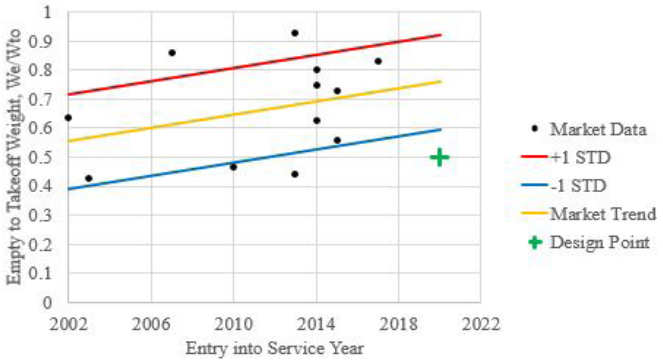

Fig. 5.2: Empty-to-Takeoff Projection for UAS Systems

5.2. DETERMINATION OF PRE-LIMINARY DESIGN AND BATTERY WEIGHTS

The current UAVs that comply with FAA Part 107 requirements have a large range of weights from less than 10 pounds to the maximum 55 pounds. For ease of use and transportation, the lighter aircraft will likely dominate the market but the battery and payload sizing will ultimately determine the aircraft weight.

The payload required for the mission are shown in Table 5.1 including both tradable payload. This will include the weights and total power required for the flight that will factor into the sizing of the aircraft.

Table 5.1: Payload Requirements (Ref 22-28)

Payload	Required or Tradable	Weight (lbf)	Power (W)
miniVUX-1UAV LiDAR	R	3.4	16
ADS-b transponder	R	0.044	20
Pixhawk 4.1	R	0.035	5
Sequoia Multi-band sensor	T	0.24	8
Thermal Camera	T	0.25	0.5
Thermal Camera Control	T	0.35	0.5
UBlox GPS x2	T	0.002	0.17
Total	**-**	**4.33**	**48.67**

The process for determining the battery sizing follows an iterative sizing process that is outlined by Dr. Barrett in Reference 29. Aircraft and battery sizing will affect each other since having a lower empty weight will lower the battery weight, which then changes the aircraft weight. The sizing of the wing will also have an affect on the battery sizing, so iteration will take place between Chapters 5 and 6 as well. To balance this relationship, the process is outlined below and hand calculations are shown in Figure 5.3. The battery size will be determined off of the Energy Density from Figure 5.4.

1. Determine the Payload Weight, $W_{paylaod}$, see Table 5.1 above;
2. Guess a Value for Takeoff Weight, $W_{to,guess}$;
3. Determine the Weight of the Battery, W_f;
4. Calculate $W_{o,estimate}=W_{to,guess}-W_{payload}$;
5. Calculate $W_{e,estimate}=W_{o,estimate}-W_f$;
6. Calculate $W_e=W_{to,guess}*(W_e/W_{to})$;
7. Compare W_e and $W_{e,estimate}$;
8. Modify the Aircraft wing or estimated Aircraft weight until W_e is within 0.5% of $W_{e,estimate}$.

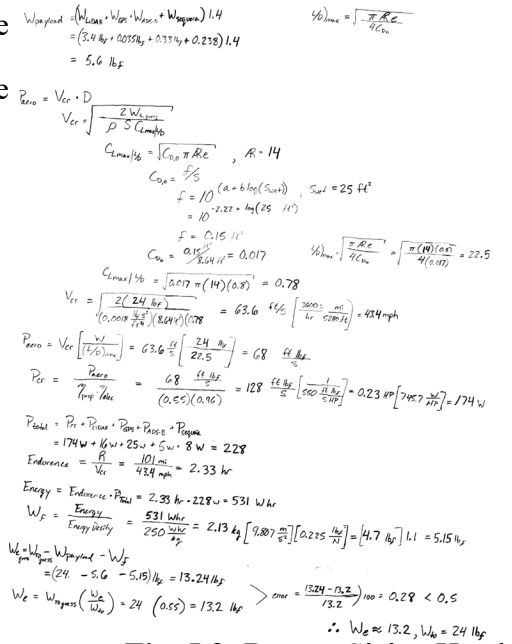

Fig. 5.3: Battery Sizing Hand Calculations

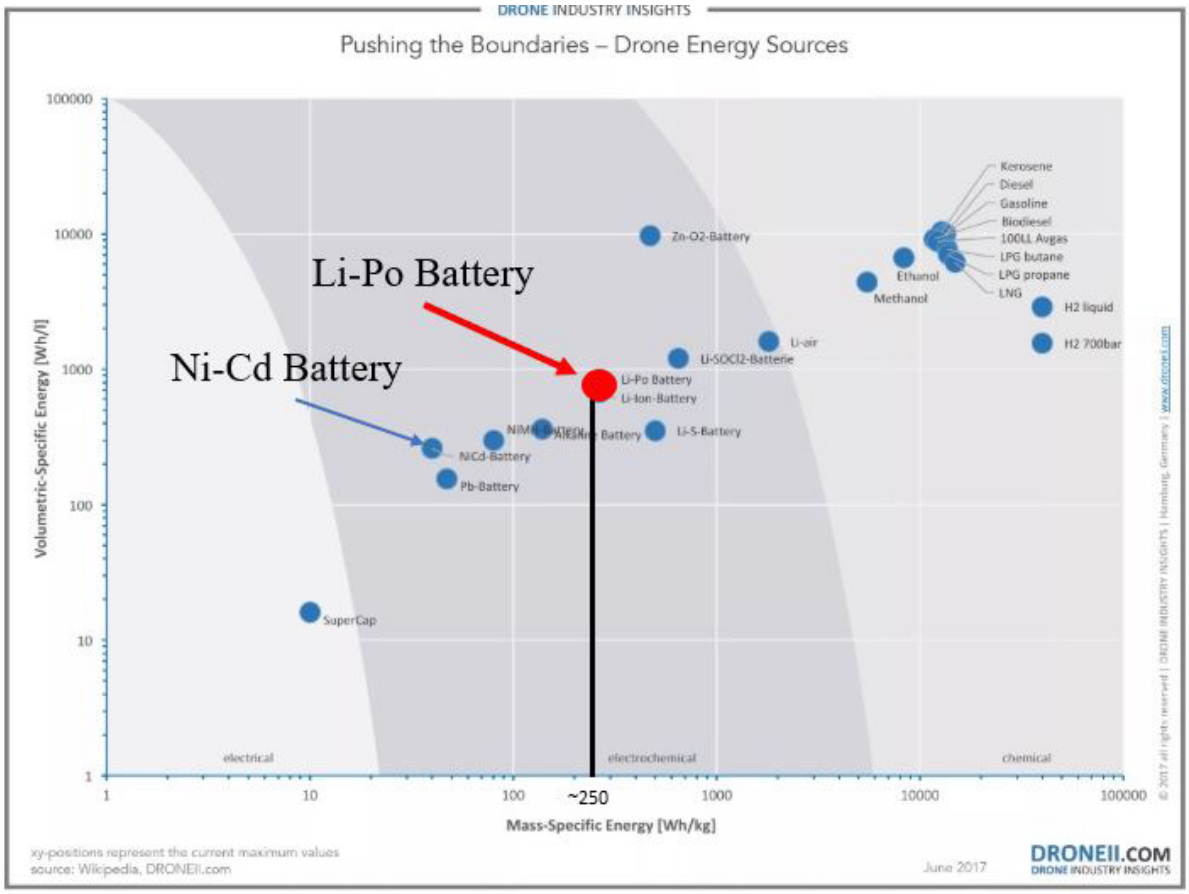

Fig. 5.4: Battery Energy Density (Ref 30)

To add a safety factor and future adjustments in the design, the battery weight was increased by 30% as well as being designed for a 101-mile range to ensure the aircraft has power for successful retrieval. In the interest of the customer, the payload capability was increased by 60% from the value listed in Table 5.1 for any additional add-on sensing the customer may want. The final weights for the preliminary design of the aircraft are:

Take Off Weight: 24 lb_f

Battery Weight: 6.1 lb_f

Payload Weight: 5.9 lb_f

Empty Weight: 12 lb_f

6. WING AND POWERPLANT SIZING

The purpose of this chapter is to size the wings and the thrust requirements. The intended takeoff system will either include a catapult launch system or a high launch system to lift the aircraft to 50ft, removing the need for take-off sizing requirements. Part 107 doesn't have any set climb requirements or stall requirements. The sizing requirements will be maneuver conditions, maneuver stall and the FAR Part 107 maximum speed stall sizing. For landing, the aircraft will be captured in a net, so landing sizing won't be needed. The sizing will be based off thrust to weight, similar to jet sizing, to provide a requirement for the motor and propeller sizing in a following chapter.

Another consideration for the UAS design with be its operation altitude and how that affects the air density. With the design interest of dominating the market, the UAV will be sized such that it can fly all the way at 10000 feet elevation which provides service to 99% of all power lines in the continental United States (data from Ref 31). A full distribution of the powerlines with respect to the altitude is shown in Figure 6.1.

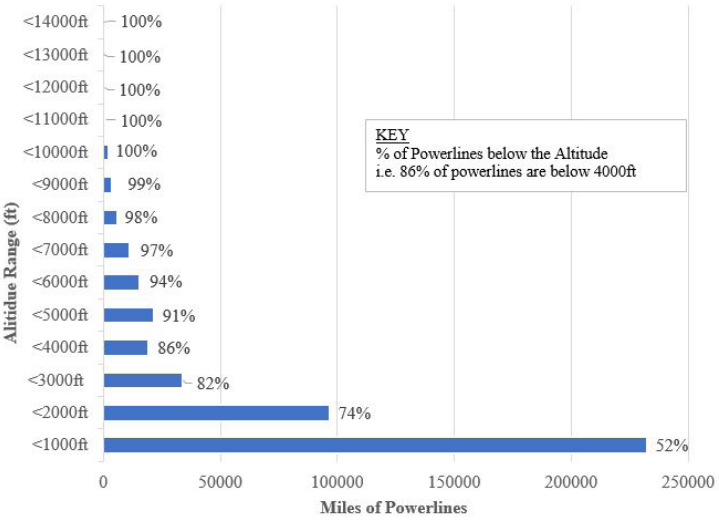

Fig. 6.1: Powerline Location by Altitude (Ref. 31)

6.1. PRELIMINARY DRAG POLAR

In order to be conservative in the design, a coefficient of drag of 0.006 was used along with a 0.8 oswald efficiency to under estimate the quality of design. The parasite area of the aircraft was determined based on the STAMPED data for the wetted area being 0.4 standard

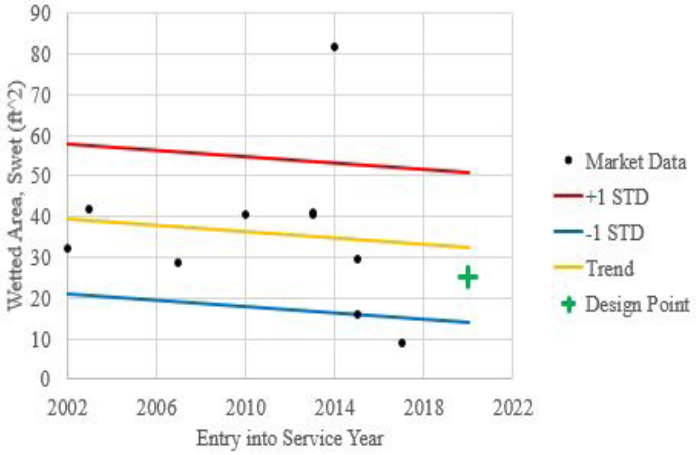

Fig. 6.2: STAMPED Swet Design Point

deviations lower than the 2020 trend as shown in Figure 6.2. The aspect ratio of the aircraft will be 14, based on the STAMPED data trend line in Figure 6.3. Using these values, the zero lift coefficient of drag is 0.017 and the resulting drag polar is shown in Figure 6.4.

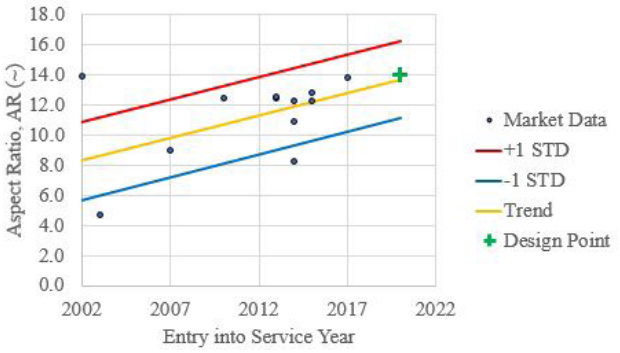

Fig. 6.3: STAMPED Aspect Ratio

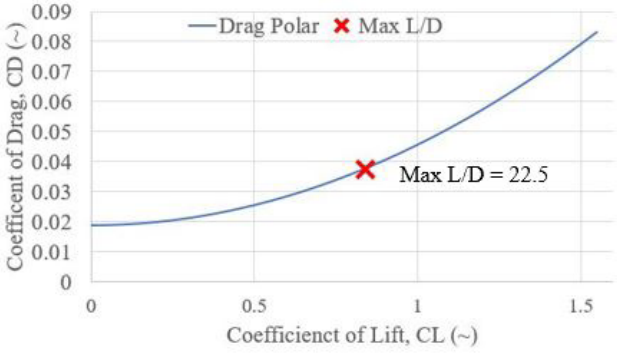

Fig. 6.4: Drag Polar

6.2. AIRCRAFT SIZING CHART ANALYSIS

From the sizing requirements, Figure 6.5 shows the design area in which this UAS can complete the flight requirements. As a check, the aircraft size was put into AAA to verify the maneuver sizing which is overlaid onto the calculated size in Figure 6.5. The FAR 107 requirement sets a maximum wing loading of 20.8 psf which is far larger than the maneuver stall so it is not included in the figure. To add robustness in the design, the Thrust to Weight ratio will be 10% higher than the minimum for the designed wing loading condition.

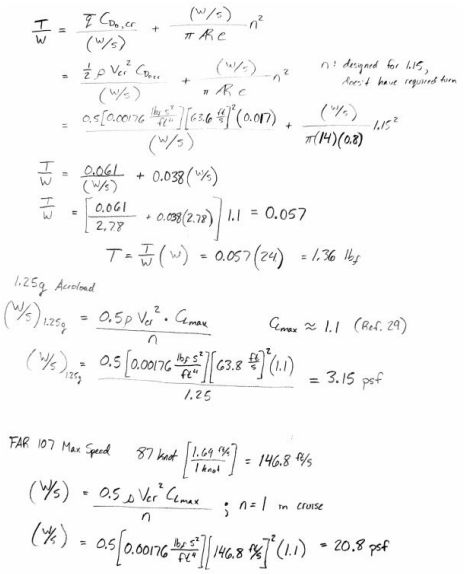

Fig. 6.5: Sizing Hand Calculations

The design point for the UAS will be as follows with the Sample Calculations shown in Figure 6.6:

Wing Loading: 2.8 psf

Thrust to Weight Ratio: 0.057

Wing Area, S: 8.6 ft^2

Aspect Ratio: 14

Thrust Required: 1.4 lbf

Fig. 6.6: Aircraft Sizing Area

6.3. LAUNCH SYSTEM REQUIREMENTS

To reduce the amount of battery needed on board the UAS, the launch system will be sized such that it can launch the vehicle over the 50ft trees at the ends of the clearing. Rolling take off requires a lot more ground time as well as battery which increases the weight. The target is to reach 55ft to clear the trees and being at the cruise velocity at that point. One method of doing this uses a pneumatic catapult launch system which is known for its reliability, but it is more costly than the bungee launch. For the initial design, the energy required at the launch is shown in the calculations in Figure 6.7 along with the launch energy acquired from the UAV Factory 6kJ pneumatic catapult shown in Figure 6.8 (Ref 32) which would be modified to have a slightly longer track to reduce the launching load on the UAS. The required launch velocity is 87.3ft/s so the catapult will also have an added pulley system to increase the launch velocity.

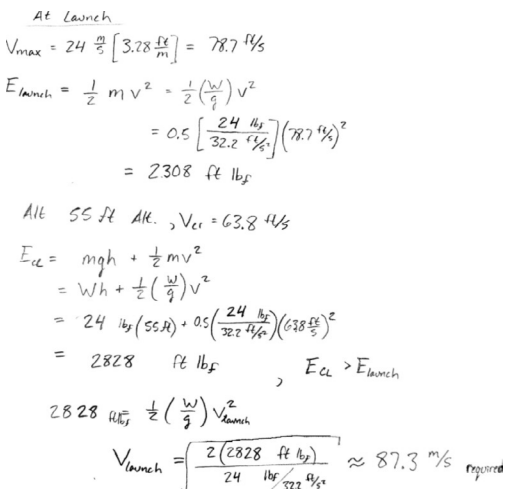

Fig. 6.7: Catapult Hand Calculations

Fig. 6.8: UAV Factory Catapult (Ref 31)

7. CLASS I CONFIGURATION MATRIX AND DOWN SELECTION

The purpose of this chapter is to create a sweep of possible aircraft configurations, and select the design that fits the mission profile.

7.1. MAJOR IMPACTS ON THE DESIGN

The configuration was based off the preliminary sizing from Chapter 6. More importantly, the aircraft was designed to meet the major impact items determined from the RFP by the designer. The design drivers for the UAS were:

- Must take off and land within 500 ft with 50ft trees;
- Landing zone is unprepared, grass and possible rocks;
- Must have 100 or 200 mile range;
- Minimize packing volume for easy transportation in a Ford F-150;
- Part 107 regulations, 55lbf, maximum 400ft above ground;
- Carry the required payload items.

7.2. COMPARATIVE STUDY OF SIMILAR AIRCRAFT

From the aircraft in Chapter 2, the Silent Falcon and the Albatross each have a mission package that can be used for the RFP. The Silent Falcon has the thermal imaging capability. The Albatross can be equipped for agriculture scanning, which can be translated to the vegetation scanning around the power lines. Both aircraft have the range capability, but the designer is concerned about the 10-hour flight time that would be required. The other concern is the Albatross can only carry 4.4 pounds of payload for maximum range flight, which doesn't allow the consumer to add too much beyond what is listed in Section 5.2.

7.3. CONFIGURATION SWEEP AND SELECTION

7.3.1. CONCEPT OF OPERATIONS

The aircraft is designed to inspect power lines for their health and for the vegetation clearance. For this type of mission, it will require steady flight for long ranges to get clear imaging of the power lines. Operated by inspection crews, it will use an autopilot with an FAA certified pilot available. To transmit data, it has a transceiver with communications along the power lines. A

catapult launch and net capture will be used to create a short take-off and landing (STOL) vehicle, reducing the power requirement compared to vertical and ground run take off. For takeoff and landing, the motor will be turned off with the motor folded in to help protect the operators. For transportation, the wings spar will be designed similar to a camping tent pole so there will be a folding joint between the 2nd and 3rd rib. This will allow the PTeslasaur to be stored in small 36" by 60" by 16" storage case with foam padding protecting the aircraft during transportation.

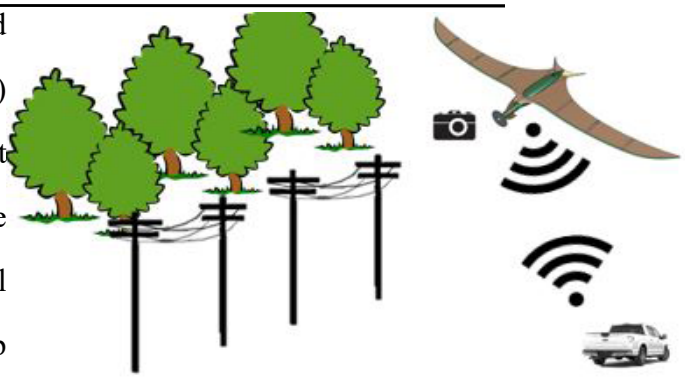

Fig. 7.1: Concept of Operations

7.3.2. SELECTION OF THE OVERALL CONFIGURATION

7.3.2.1. AIRCRAFT CATEGORY

The required aircraft for this mission will fall under the home built UAS category. This can stretch from faster, more acrobatic planes to sailplanes, so there are several configuration types available.

7.3.2.2. CONFIGURATION SWEEP

Possible design configurations made using MATLAB Aircraft Intuitive Design are shown below in Figure 7.2.

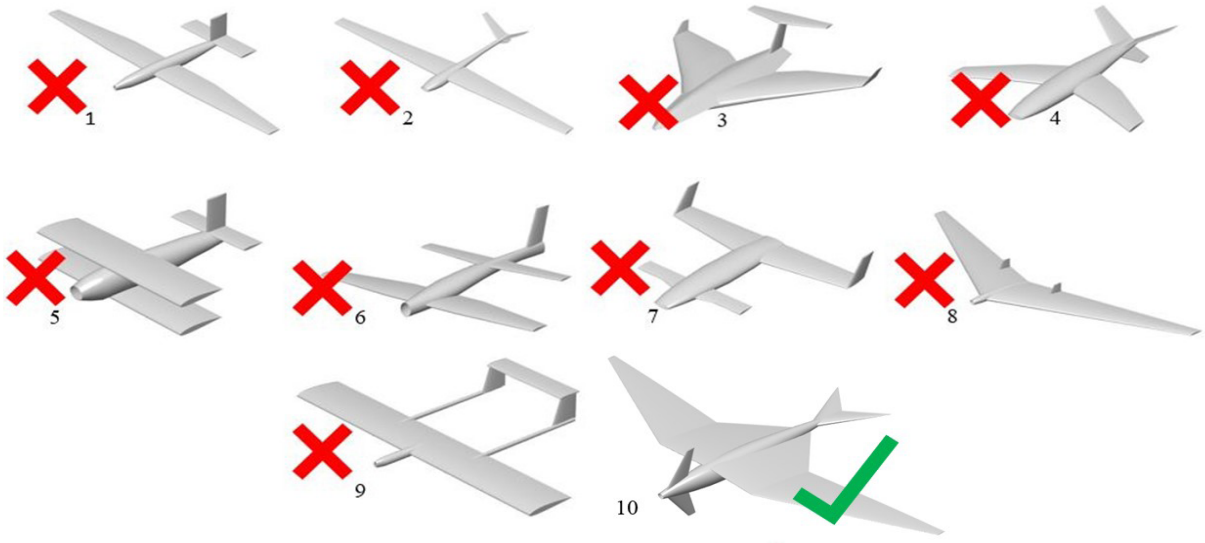

Fig. 7.1: Preliminary Designs (Not to Scale)

7.3.2.3. Configuration Down Selection Reasoning

With a restricted amount of time, there will only be one design that gets carried into Class I Sizing. Table 7.1 shows the reasons that the designer rejected the configurations. For power line surveying, the designer chose the glider design allow for a lower cruise velocity to improve image quality of the cameras.

Table 7.1: Preliminary Design Down Selection

Aircraft	Reason for Selection
1	Large amounts of empty fuselage space
2	Stick and Wing design does not allow for large payload
3	Large wetted area
4	Unconventional, may lose public acceptance
5	Bi-Wing production costs are higher
6	Unconventional, may lose public acceptance
7	Unconventional, may lose public acceptance
8	Added complexity with wing storage for replaceable payload
9	Tail damage can break wings through the tail booms
10	Glider type, Bird-like shape for public acceptance

7.4. Summary and Recommendations

Summary of Configuration Selection

Based on Chapter 7, the following configuration variables were chosen:

- High AR bird-like design for low power flight;
- Payload and battery storage in fuselage;
- Final Class I design shown in Figure 7.3.

Recommendations for Configuration Selection

The author recommends that:

- Take multiple designs through Class 1 design to compare their performance;
- Do a full analysis of the OF to determine the best aircraft for the RFP.

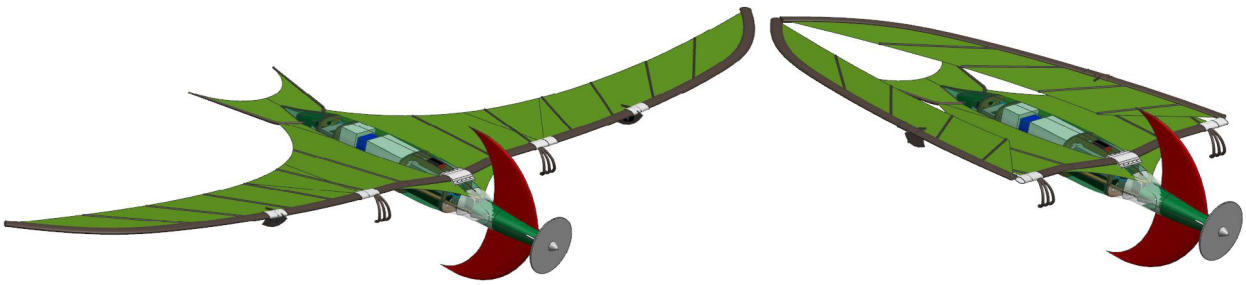

Fig. 7.2: Final Class 1 Design Configuration

8. LAYOUT OF THE COCKPIT AND THE FUSELAGE

The purpose of this section is to outline the design of the fuselage. There are two imaging devices that will require a clear cover to protect the lenses without affecting the image quality. The other consideration will be the camera viewing angle which needs to be maintained for unobstructed imaging. The fuselage design procedure is from Airplane Design Part II (Ref. 4).

8.1. LAYOUT DESIGN OF THE FUSELAGE

The shape of the body was determined from the payload requirements. First the batteries, motor and payload were centered along a common axis. Then the skins were shaped to fully enclose the payload without leaving empty space in the fuselage. The first consideration was the field of view for the multispectral and the thermal camera, neither of which had a published viewing angle. To ensure unobstructed imagining, the body and propeller were placed to give a wide field of view as shown in Figure 8.1. To protect the camera lenses, the cameras were placed inside the fuselage using a clear cover on the fuselage so the camera isn't covered. The motor and head fins are placed on an articulating section about the Z-axis that will be used for yaw control. The final layout of the fuselage is shown in Figure 8.2, outlining the location of the LiDAR and batteries.

8.2. COCKPIT AND FUSELAGE SUMMARY AND RECOMMENDATIONS

Summary of the Fuselage Design

The major findings for the fuselage were:

- Total length: 42 inches;
- Space around the batteries are for wing spars;
- Fineness Ratio of 6.8;
- Camera have wide field of view;
- Fully Exposed Motor for cooling.

Recommendations

The author recommends that

- A motor cowling for water protection should be added during weather;
- Modify the front articulating section to match the curvature of the main body to improve aerodynamics.

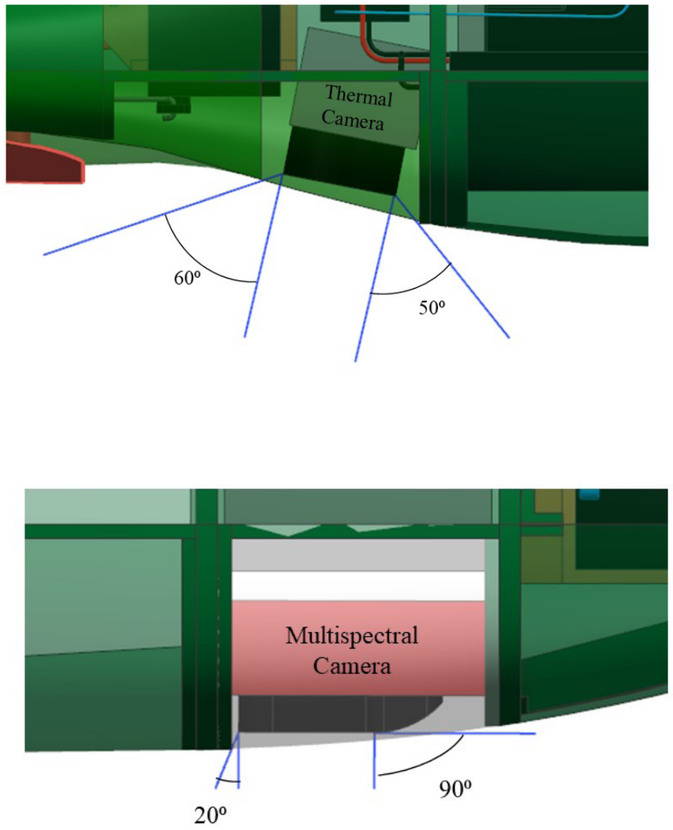

Fig. 8.1: Imaging Field of View, All Dimensions in Inches (Scale 1:5)

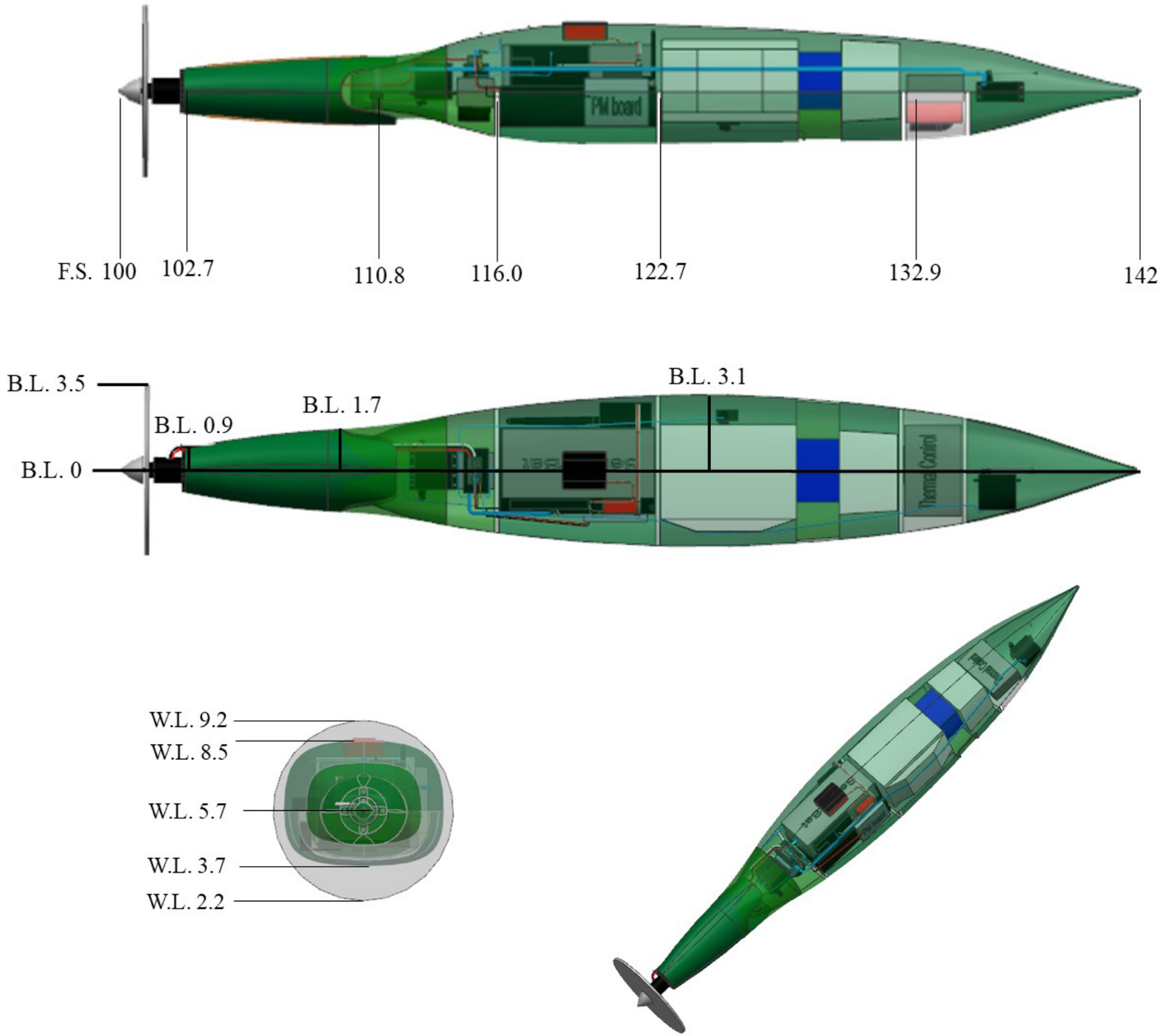

Fig. 8.2: Fuselage Sizing and Location, All Dimensions in Inches (Scale 1:5)

9. LAYOUT DESIGN OF THE PROPULSION INSTALLATION

The purpose of this section is to outline the requirements and the selection process of the propulsion system. This will include the electric motor, matching the propeller and sizing the battery. The design procedure comes from Aircraft Design Part 2 (Ref. 4).

9.1. MOTOR SIZING AND PROPELLOR MATCHING

The requirement of the motor and propeller is to be able to produce enough thrust to maintain the cruise velocity. Based on the Chapter 6 maneuver sizing, the required thrust to weight ratio is 0.054 which includes an added 10% safety factor. For the 24-pound aircraft, the propulsion system will require 1.3 pounds of thrust and a pitch speed greater than the flight speed of 44mph. To reduce the battery sizing, the other factor in motor selection will reducing the amount of power that is required to operate. To prevent overloading the motor, it is important to match the motor to a propellor. The final selection was a Cobra 2213/26 motor with a APC 7×6×2-E propeller. This combination provided the required thrust and pitch speed, and was selected because there is published data to show this combination is safe to run for extended periods of time. The performance characteristics are shown in Table 9.1 (Ref. 33) including the battery requirement for the 2.3-hour flight.

Fig. 9.1: Cobra 2213-26 Motor (Ref. 33)

Table 9.1: Motor and Propellor Performance Characteristics (Ref. 33)

Propeller	Input Voltage (V)	Input Current (A)	Thrust (lb_f)	Pitch Speed (mph)	Battery Capacity Required (mAh)
APC7×6×2-E	14.8	8.62	1.36	63	20070

9.2. BATTERY SELECTION

To provide power for both the propulsion and the flight payload, two separate batteries will be used. Using multiple batteries will allow for more control over the placement in the fuselage using smaller individual cross sections compared to having one giant battery. For the motor, the

battery will be sized for 22000mAh for standard battery sizes. The other consideration is for the motor requiring an input voltage of 14.8 V. The selected propulsion battery is a TATTU 22000mAh 14.8V LiPo (Ref. 34). Two GPS chips near the wing tips will also run off the propulsion battery which will be used to minimize the interference from the power lines magnetic field.

The remaining sensors and operating equipment will be powered of a second battery. The capacity requirement for each item is shown in Table 9.2. The operating current was determined from the power and voltage data for the payload item. The selected battery was the MaxAmps 12000XL 4S 14.8V battery pack (Ref. 35).

Table 9.2: Auxiliary Power Requirements (Ref. 22-27)

Payload	Power (W)	Input Voltage (V)	Input Current (A)	Battery Capacity Required (mAh)
LiDAR	16	11	1.45	3387
Pixhawk	5	5	1	2329
Sequoia Camera and Sensor	6	5	1.2	2795
Thermal Camera and Control	0.5	5	0.1	233
ADS-B	20	14.5	1.37	3212
Total Capacity (mAh)				**11955**

9.3. PROPULSION INSTALLATION SUMMARY AND RECOMMENDATIONS

Summary of Propulsion System Selection

The major findings for the propulsion system were:

- Motor: Cobra 2213/26
- Propeller: APC 7×6×2-E
- Propulsion Battery: TATTU 22000mAh 14.8V LiPo
- Auxiliary Battery: MaxAmps 12000XL 4S 14.8V

Recommendations

The author recommends to:

- Research Motors available by 2020
- Research Batteries available by 2020
- Investigate possible weight savings for internal combustion engines

10. CLASS I LAYOUT OF THE WING

The purpose of this section is to outline the selection of the wing design and its location. The design procedure is from Airplane Design Part III (Ref. 5). The initial process was analyzing characteristics created by mother nature, as evolution has shaped creatures to specialize in flight. For this reason, the wing design will go back to the Cretaceous Period; about 70 to 140 million years ago. Using traits found on the Pterosaur, the wing will feature a membrane airfoil which is believed to be similar to modern day bats.

10.1. WING DESIGN LAYOUT

Following the initial sizing from Chapter 6, a wing span of 11 feet and an aspect ratio of 14 will be used for the wing design. For a short body design, it will be important to keep the aerodynamic center close to the aircraft center of gravity to improve controllability.

Fig. 10.1: Bat Wing (Ref. 36)

An important consideration in the shape of membrane surfaces is being able to keep the membrane in tension. To do this, each wing section must keep a concave curvature on the trailing edge; a wing characteristic that can be seen in Figure 10.1 for bats. This was brought to the designers attention in a technical discussion with Dr. Barrett (Ref. 37). To prevent the flutter, rigid ribs will be placed along the span since a full span section will has been shown to experience flutter for low angles of attack (Ref. 38). The single rib design in Figure 10.2 had the flutter issue, so multiple ribs were used in the design.

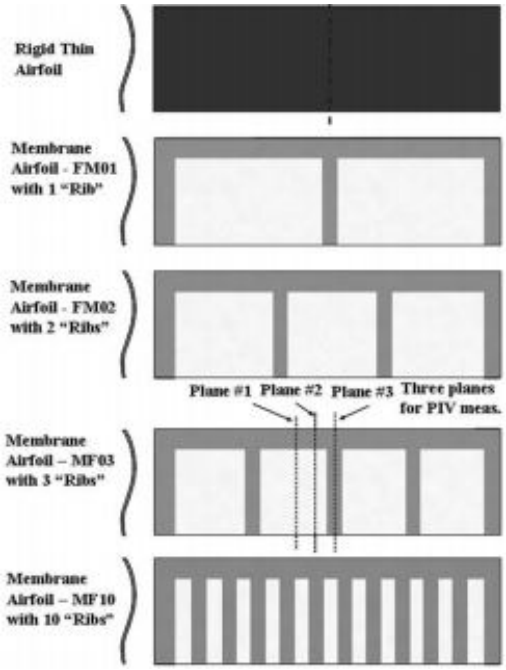

Fig. 10.2: Membrane Rib Placements (Ref. 38)

Compared to rigid thin airfoils, the membranes were found to have better lift coefficients especially at higher angles of attack delaying stall. Another advantage is the reduction in the drag coefficient since the membrane conforms to the airflow (Ref. 38). Figure 10.3 shows the comparison between the lift and drag coefficient between rigid airfoils (solid circles) and the ribbed design that is being used for the aircraft (squares). Figure 10.4

and Figure 10.5 show the flow separation over the rigid plate compared to the continuous flow over the membrane airfoil.

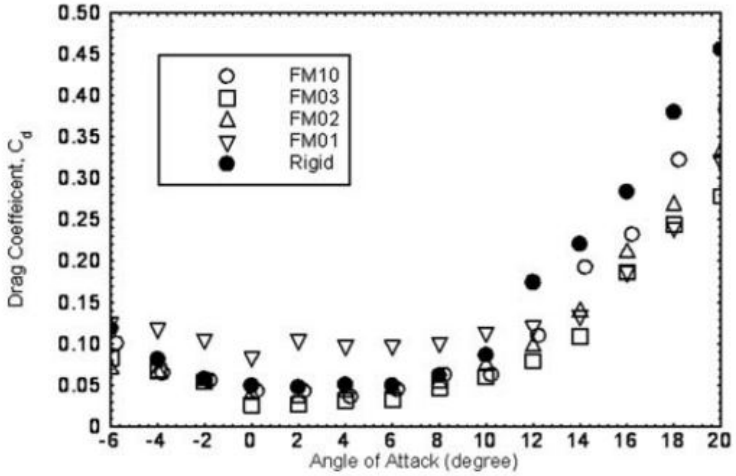

Fig. 10.3: Coefficient of Drag for Membrane Airfoils (Ref. 38)

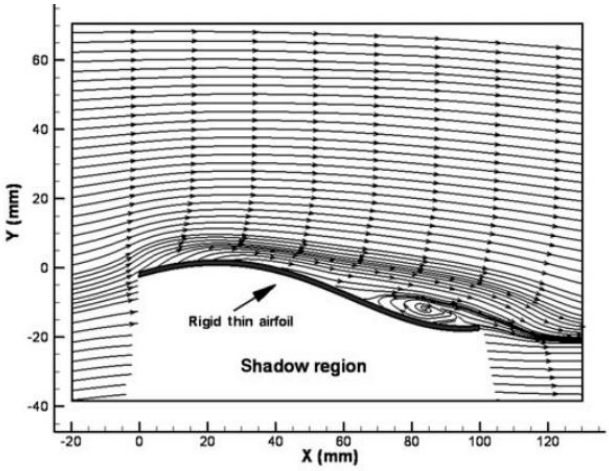

Fig. 10.4: Streamlines for Rigid Airfoil (Ref. 38)

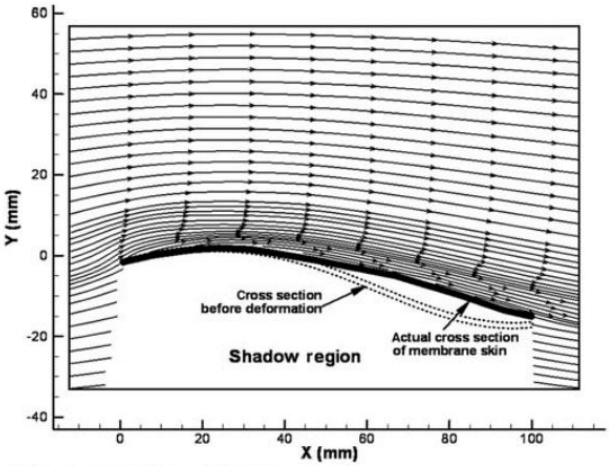

Fig. 10.5: Streamlines for Membrane Skin (Ref. 38)

Figure 10.6 shows the effect that the angle of attack has on the membrane shape in flight (Ref. 39). Figure 10.7 shows how the pitching moment changes with respect to the angle of attack (Ref. 39).

With a wing type that can fly at high angles of attack, the aircraft will be able to do a perching maneuver into a net landing. Without stalling at high angles of attack, the aircraft will be able to maintain controlled

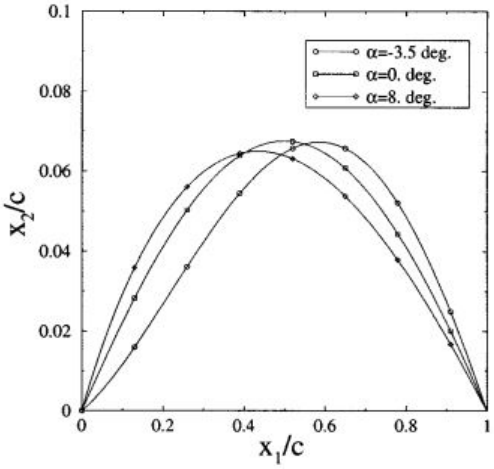

Fig. 10.6: Effect of Angle of Attack on Membrane Shape (Ref. 39)

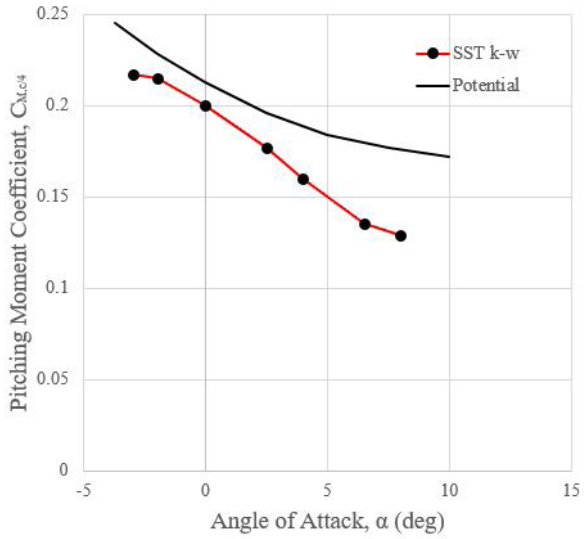

Fig. 10.7: Membrane Pitching Moment vs Alpha (Ref. 39)

flight on the descent which improves the safety of the aircraft. But more importantly it will improve the safety of the operators to avoid high speed collisions upon landing.

The other ability that the membrane airfoil presents is the resistance to wind. Since the wing will morph with the airflow, the effect of perturbations in angle of attack on the coefficient of lift should be reduced compared to rigid airfoils. This will provide the membrane wing with advantages under high wind conditions or around mountains where the wind drafts can be unpredictable.

Fig. 10.8: Pterosaur With Wings Folded (Ref. 40)

With an 11-foot wingspan, storage and transportation would become difficult for a solid wing. The inspiration from the Pterosaur membrane wing comes from the interest of a thinner, folding wing. Figure 10.8 shows how the Pterosaur wings, in white, could fold down tightly around the bone of arm/wing. For comparison, a rectangle wing of the same span and area would have a 9.5 inch chord. Using a 15% thickness to chord ratio airfoil, the wing would be almost 1.5 inches thick. Splitting the wing into 2 part to fit in an F-150, that requires a storage space of 11”x68”x12” (with 2 inches of padding for protection); or 9000 in^3 in storage volume. The membrane wing in this design can easily fold into a 11”x68”x3” space, or 2200 in^3 in storage volume. This is a 75% reduction in storage volume by switching from the traditional structure to a membrane wing. This space savings will mean the bed of the F-150 will be less cramped as shown in Figure 10.9, thus decreasing the likelihood of damaging the aircraft during transportation. The extra space can also allow the crew to bring more equipment for surveillance or repairs of the

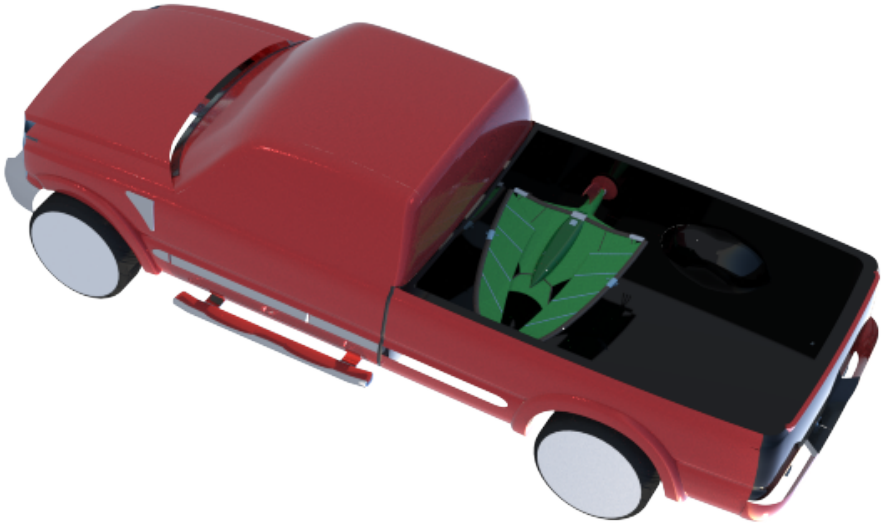

Fig. 10.9: Pteslasaur in Transportation Configuration

power lines.

For interference protection in the navigation system while around the powerlines, two additional GPS receivers were placed at the wing tips. The increased number of GPS receivers will provide more accurate position following. Then having two of them spread out will also provide a way to measure the amount of feedback noise in the system.

10.2. WING DESIGN SUMMARY AND RECOMMENDATIONS

Summary of Class 1 Wing Design

The major findings from this section are:

- The wing will use a membrane airfoil with ribs spaced along the span;
- Folding wings for storage and transportation;
- High lift and stall angle of attack allows for a controlled perch landing;
- Wing Span of 11ft, Aspect Ratio of 14
- Root Chord: 23 in., Taper Ratio: 0
- Dihedral Angle: 3° Sweep Angle (c/4): 6°
- Class 1 Wing Design shown in Figure 10.9;

Recommendations

The author recommends:

- Conduct testing on rib locations for flutter and aerodynamic performance;
- Analyze the scale increase from the experiments to the 11ft wing span aircraft,

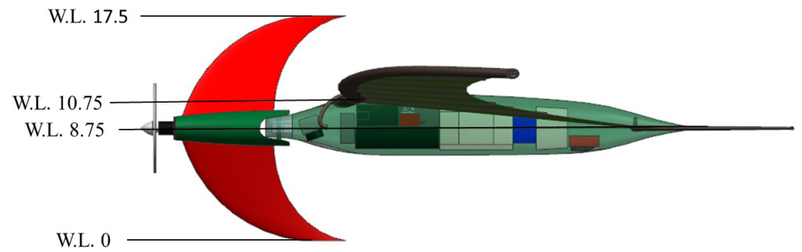

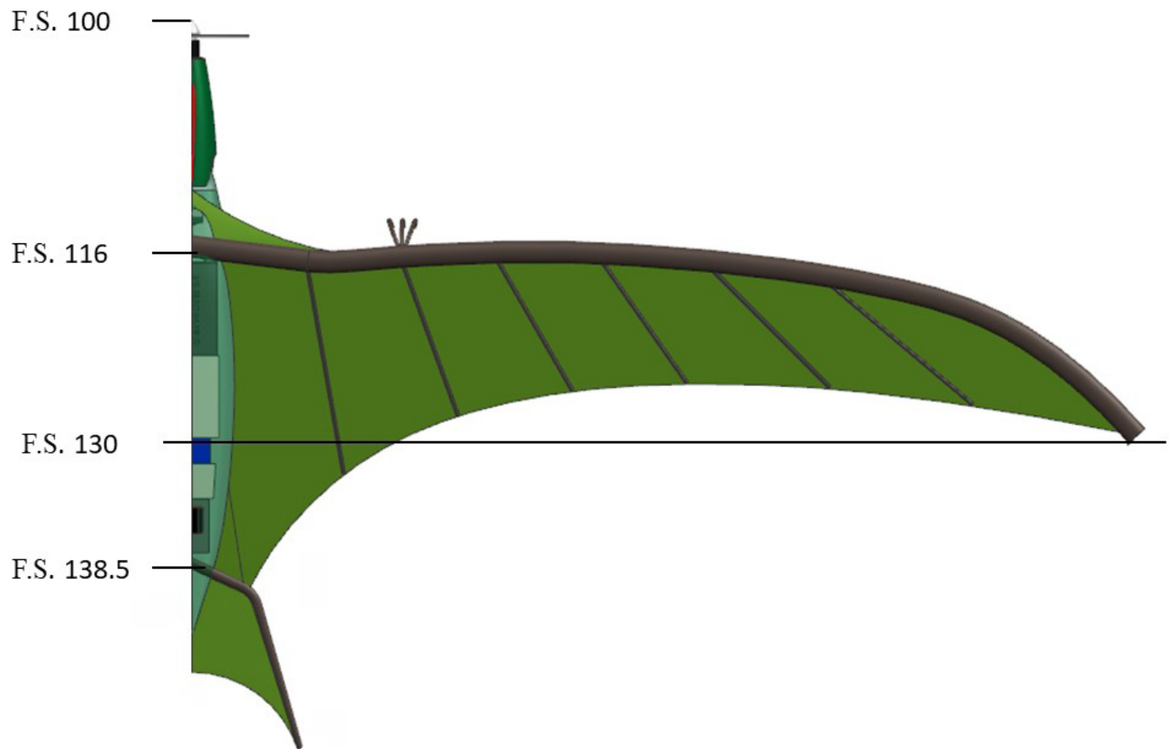

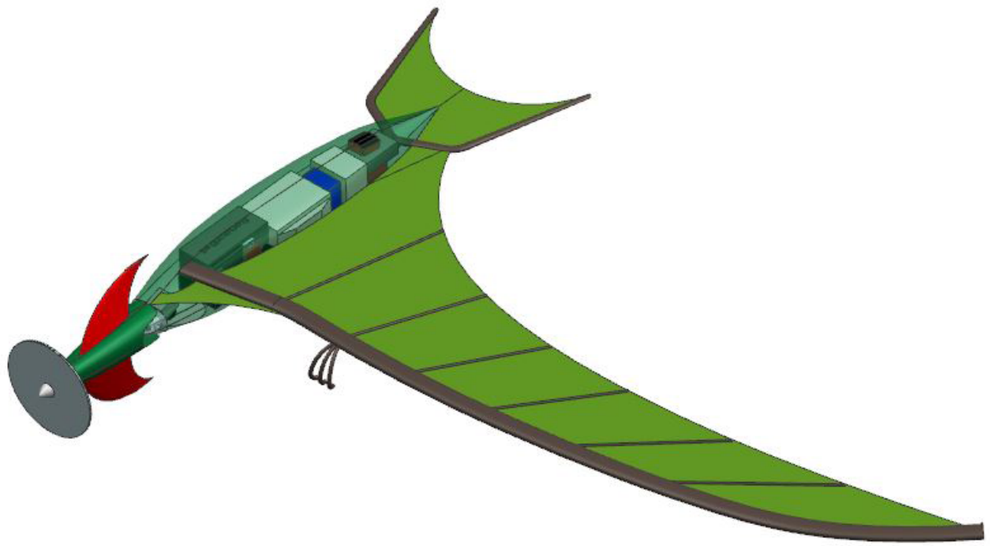

Fig. 10.9: Fuselage Sizing and Location, All Dimensions in Inches (Scale 1:10)

11. CLASS I DESIGN OF THE HIGH LIFT DEVICES

Due to the membrane structure, the aircraft will not be able to accommodate any high lift devices. So the purpose of this section is to show that a high lift device is not needed for this design. To determine the coefficient of lift, the Pteslasaur wing will be compared to another membrane wing that was created for a dissertation at the Technical University of Munich (Ref. 40). In the dissertation, the Reynolds numbers were based off of the mean geometric chord. Then the coefficient of lift plots of the wing are compared using the MGC Reynolds number. For this reason, the wing coefficient of lift will be predicted from comparing the MGC Reynolds number to the plots from the dissertation. To estimate the aircraft $C_{L,aircraft}$, the wing $C_{L,wing}$ is divided by 1.1 since it is a short coupled design. Figure 11.1 shows the coefficient of lift plots from Reference 40, where K_m is the pre-stress state or the tension of the membrane without airflow. Figure 11.2 shows the hand calculations for the high lift requirement.

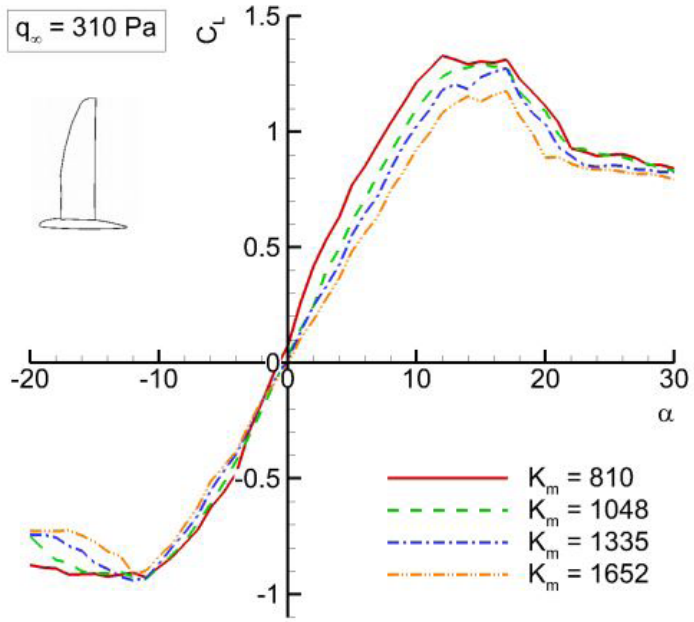

Fig. 11.1: Wing Lift Coefficient (Ref. 40)

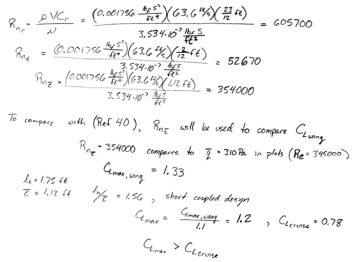

Fig. 11.2: High Lift Hand Calculations

11.1. HIGH LIFT SUMMARY AND RECOMMENDATIONS

High Lift Devices Summary

The major findings from this chapter are:

- High lift devices are not required;
- $C_{L,max}$=1.2.

Recommendations

The author recommends:

- Build a wing structure to test $C_{L,max}$ and verify that no high lift devices are required.

12. CLASS I LAYOUT OF THE EMPENNAGE

The purpose of this section is to go over the design of the empennage. The procedure for the design is from Airplane Design Part II (Ref. 4). The empennage will be used to provide both pitch and yaw control.

12.1. EMPENNAGE DESIGN PROCEDURE

The design of the empennage is a modified X tail configuration. The horizontal tail follows conventional design with the location on the midplane of the fuselage. The vertical tail is designed similar to the crest of a Pterosaur. Since the "head" of the Pteslasaur will be articulating for yaw control, the crest will be split between the top and bottom of the fuselage to balance the weight across the x-y body coordinate plane. This will also reduce the effect that sideslip has on the rolling moment, so the crest will only control the aircraft yaw. The challenge with a forward placed vertical tail is the instability in $C_{n,\beta}$ but using an autopilot, a controller can be designed to maintain stability during flight. The horizontal tail will be sized based on the volume coefficients of several avian species since there are no preserved fossils of pterosaur tail membranes. The crest sizing will be based off palaeontological recreations of the crest whether they were more bone like structures, or a membrane. The volume coefficients of the selected avian species tails and pterosaurs are shown in Table 12.1. Figure 12.1 shows the design and locations of key components on the empennage.

Table 12.1: Volume Coefficients Used for Configuration Design

AVIAN SPECIES	V_h	**Pterosaur Species**	V_v
BALD EAGLE	0.13	TUPANDACTYLUS IMPERATOR	0.023
WANDERING ALBATROSS	0.05	DSUNGARIPTERUS	0.003
PACIFIC GULL	0.09	PTERANODON LONGIPES	0.001
ARTIC TERN	0.10	THALASSODROMEUS SETHI	0.013
TURKEY VULTURE	0.08	TUPUXUARA LEONARDII	0.014
BLACK VULTURE	0.07		
GREAT WHITE PELICAN	0.01		
COMMON LOON	0.04		
TRUMPETER SWAN	0.14		
HARPY EAGLE	0.16		
DESIGN POINT	**0.074**	**DESIGN POINT**	**0.08**

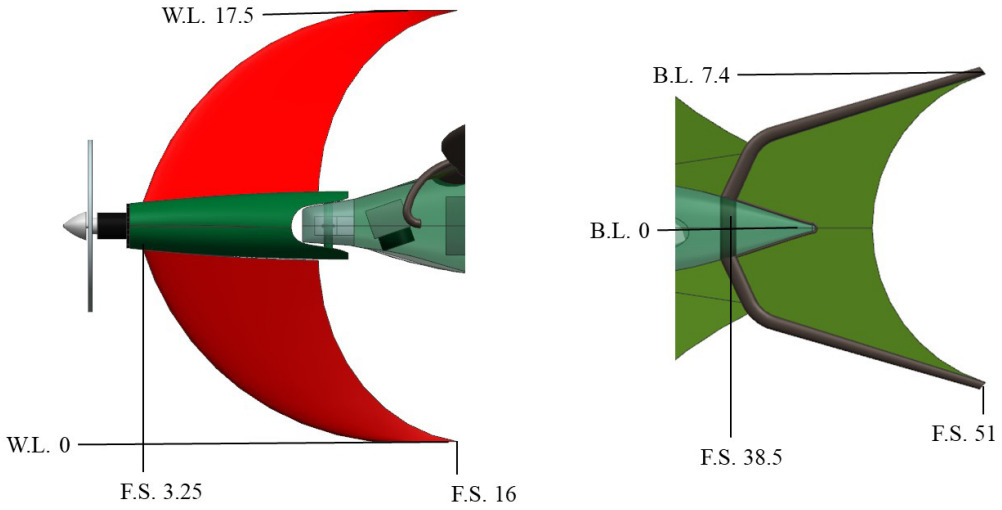

Fig. 12.1: Empennage Planform, All Dimensions in Inches (Scale 1:8)

12.2. DESIGN OF HORIZONTAL TAIL

The structural design of the horizontal tail will be similar to that of the wing, using a leading edge spar and then a membrane structure for the lifting surface. The purpose of the bird's tail is actually a topic that encompasses several different theories. The first theory proposes that the tails act as a spilt flap that modifies the flow over the wing which increases the maximum lift coefficient of the wing (Ref. 41). The second theory suggests that the tail acts as a stabilizer similar to an aircraft horizontal tail to balance the pitching moments in slow flight (Ref. 41). For this design, the horizontal tail will be analyzed as a stabilator, using the entire horizontal tail for pitch control. Table 12.2 shows the key parameters of the horizontal tail design.

Table 12.2: Horizontal Tail Characteristics

Characteristic	Design Value
Horizontal Tail Area, S_h (ft^2)	0.45
Aspect Ratio, AR_h	3.3
Sweep Angle, $\Lambda_{c/4}$	30°
Taper Ratio, λ_h	0

12.3. DESIGN OF VERTICAL CREST

The real explanation for why pterosaurs evolved to have such large crests on their head is

still unknown, since there is no way to study their behaviour. There are arguments that the crest was element of display for mating, similar to the feathers on birds of paradise. The other theory is that the crest did evolve for yaw control. In either case, such a large structure must have provided an element of flight control so the pterosaur crest size is useful for sizing the UAV vertical crest. To balance the weight and protect the propeller from ground strikes in an emergency landing, the crest will be split to be on top and bottom of the head. Table 12.3 shows the key parameters of the vertical crest.

Table 12.3: Vertical Crest Characteristics

Characteristic	Design Value
Vertical Tail Area, S_v (ft^2)	0.6
Aspect Ratio, AR_v	3.55
Sweep Angle, $\Lambda_{c/4}$	47°
Taper Ratio, λ_v	0.5

12.4. EMPENNAGE DESIGN SUMMARY AND RECOMMENDATIONS

Summary

The major findings in this chapter are:

- The horizontal tail aspect ratio, AR_h=3.3;
- The vertical crest aspect ratio, AR_v=3.55;
- The horizontal tail has the membrane structure like the wing;
- The vertical crest airfoil is a NACA 0012;
- The horizontal tail is a stabilator.
- Hand Calculations are shown in Figure 12.2

Recommendations

This author recommends that:

- Have a variable area horizontal tail for cruise (lower S_h) and recovery (higher S_h), most evident on the Harpy Eagle;

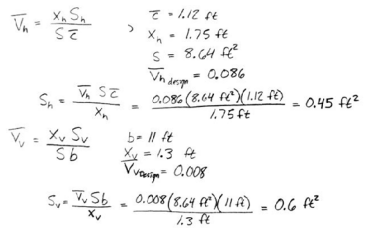

Fig. 12.2: Empennage Sizing Hand Calculations

13. Class I Design of the Launch and Recovery

Since the design will not be using a landing gear for takeoff or landing, this section will be used to discuss the design for the catapult and the net for recovery. The design process of the catapult will be based off achieving an adequate launch velocity to get above the 50ft tall trees. The other consideration is the length of the catapult which determines load factor on the aircraft to reach the launch velocity. The design of the net will be based on the stall speed of the aircraft since it will be using a perching maneuver to land in the net.

13.1. Catapult Design

The most important considerations for the catapult design are achieving the desired launch velocity and being able to be transported in the truck. To reduce the power requirement of the aircraft, the catapult will be designed to reach 55 ft in altitude at the cruise velocity. This sets a launch velocity of 88 ft/s. The other consideration is to consider the acceleration on the aircraft to reduce the load. But if the design load factor (discussed in Chapter 15) is above the launching load factor, then the acceleration won't be the driving factor of the catapult design. The carriage of the catapult must be design such that the aircraft won't hit the carriage during the release. The track will be built in two sections, one that is 6.5 feet long to fit inside the bed of the truck. The other section will be 13.5 feet long and will be fixed onto the truck. The total length will be 20 feet. Figure 13.1 shows the set-up of the catapult on the truck. Figure 13.2 shows the aircraft on the carriage. Figure 13.3 shows the hand calculations to solve for the launch velocity requirement and the load factor due to the acceleration of the carriage.

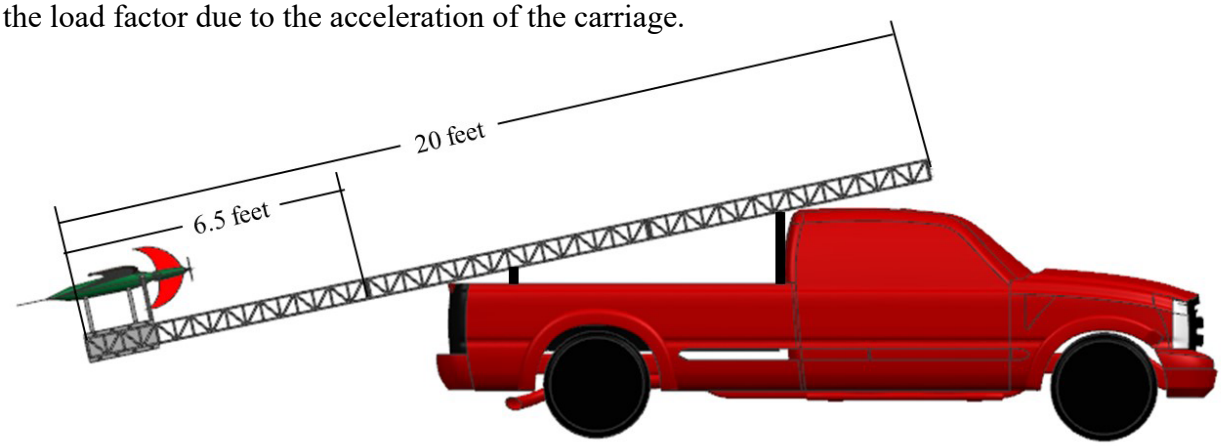

Fig. 13.1: Catapult Design (Ref. 43)

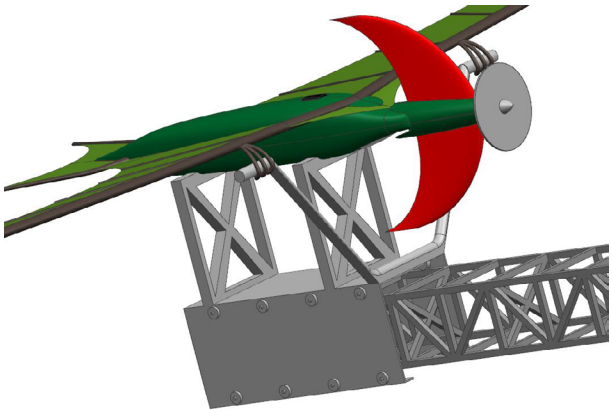

Fig. 13.2: Carriage Design

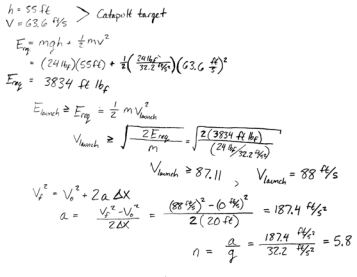

Fig. 13.3: Catapult Calculation

13.2. NET DESIGN

With an 11-foot wingspan, the width of the net will be 20 feet to allow for plenty of room for error without hitting the net posts. The height of the net will be 15 feet to give room for error during the perching maneuver. The net will be held under low tension to reduce the impact loading as the aircraft lands. In the interest of protecting the aircraft, the claws will be used to catch the net and prevent the aircraft from falling. But the net will be J-shape so if the claws don't catch on the net, the aircraft will just fall into the bottom of the net. The net posts will be designed to collapse into 5 foot sections, and the net will be folded for transportation.

13.3. LANDING GEAR DESIGN SUMMARY AND RECOMMENDATIONS

Summary

The major findings in this chapter are:

- With only one section of the track to put together, crews should easily complete the 15 minute launch time;
- Launch Velocity= 88 ft/s;
- Launch Load Factor= 5.9;
- The net can be put together during flight;
- Net Size: 20ft by 15 ft.

Recommendations

The author recommends that:

- Use a reflective net material around the outside of the net for easy visual identification;
- Make sure to turn the propeller off before going into the net.

14. CLASS I WEIGHT AND BALANCE ANALYSIS

The purpose of this section is to complete a weight and CG analysis under the different operating payload combinations that can be done using a modular design. The payload and powerplant component weights are published data. The structure sizing will be based on approximations of material and adjusted to withstand large load factors involved with flight and transportation. The procedures for the weight and balance come from Airplane Design Part V (Ref. 7).

14.1. CLASS I WEIGHTS BREAKDOWN

Figure 14.1 shows the preliminary 3-view from the Class 1 design. The first step is to find the total weight of the known payload items shown in Table 5.1.

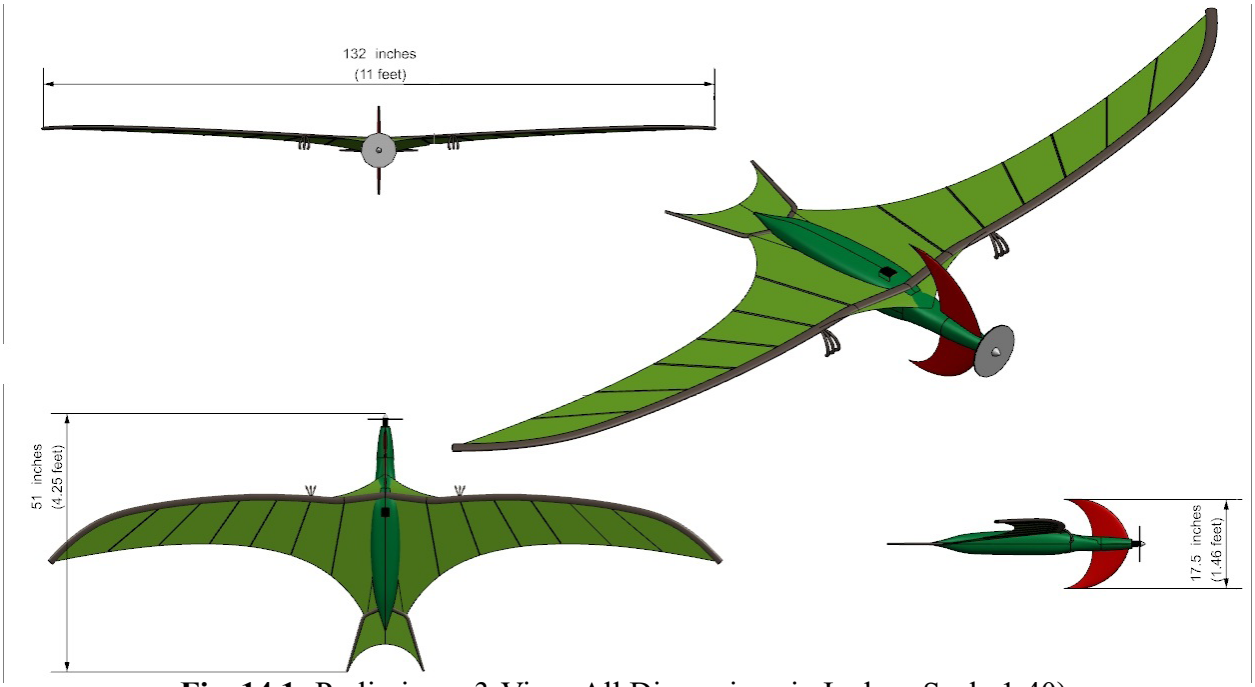

Fig. 14.1: Preliminary 3-View, All Dimensions in Inches. Scale 1:40)

Table 14.1: Weight Fractions

Component	Weight Fraction	Component Weight (lbf)
Payload	0.18	4.32
Powerplant	0.27	6.5
Wing	0.155	3.7
Tail	0.029	0.7
Crest	0.04	1
Fuselage	0.323	7.75

The powerplant, defined as the motor battery, payload battery, motor, propeller and ESC, was determined from the production information. The weight of the wires was approximated to be 1/8th pound. To approximate the weight of the wing and horizontal tail membranes, Dacron Sailcloth was used. A little extra weight was added since the membrane will have some elastic properties, and elastic material would generally weigh more than a stiff material like Dacron. The spars were approximated using weights for carbon fiber tubes, and the ribs were approximated with fiberglass rods. Table 14.1 shows the weight fractions for the major sections of the aircraft.

The fuselage weight, making up the remaining weight, appears to be high for only being 40 inches long, but this was done for added strength and durability. With membrane wings, there is a chance to tear the wing material increasing the life cycle cost. The fuselage will then be made for high load factors giving it durability during transportation which is higher than the flight loads (discussed more in Chapter 15). This reduces the life cycle cost since it will not need to be replaced.

14.2. CLASS I WEIGHT AND BALANCE CALCULATION

To calculate the aircraft center of gravity, the approximate center of gravity and weight for each component will be used. Since the aircraft is symmetric about the x-z body coordinate plane, the lateral center of gravity will be centered on the aircraft. For this reason, only the longitudinal and horizontal centers of gravity will need to be calculated. Table 14.2 has the weight and location of the approximate center of gravity of each component. Figure 14.2 shows the component location in the fuselage. The GPS chips are actually located on the tips of the wings, not in the fuselage.

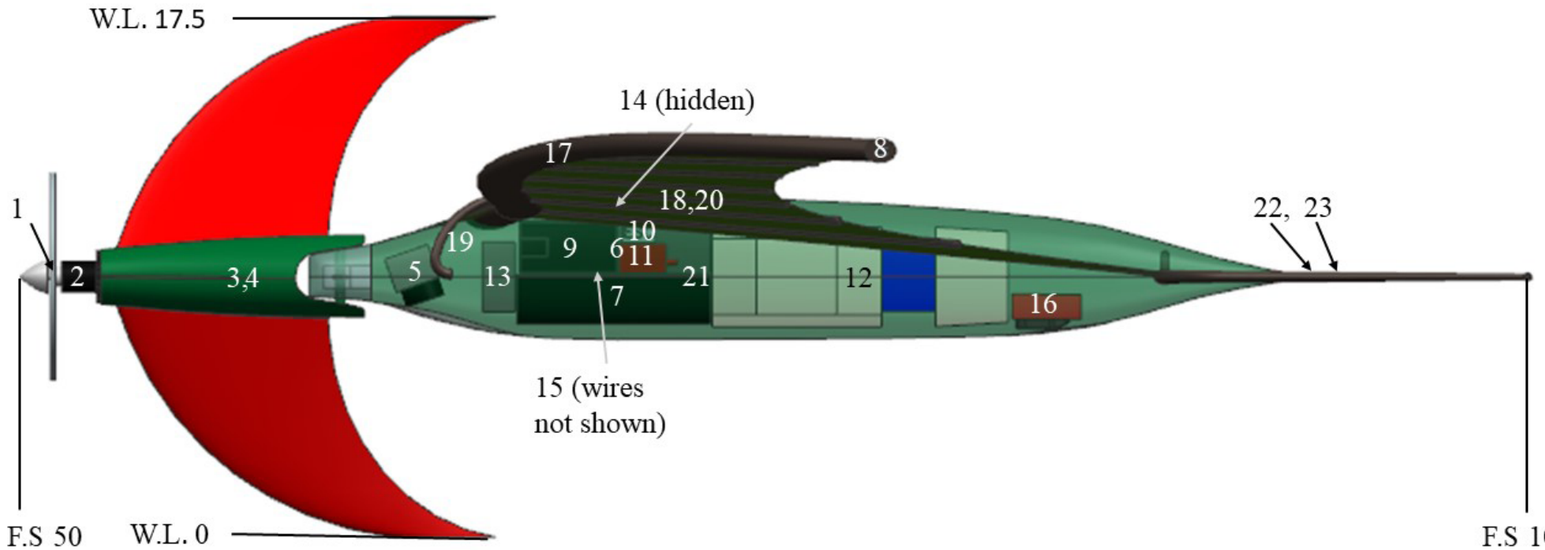

Fig. 14.2: CG Location of Major Aircraft Components, All dimensions in inches (scale 1:5)

Table 14.2: Component CG Locations

Item Number	Item	Weight (lbf)	F.S. (in)	WL (in)
1	Propeller	0.02	51.0	8.75
2	Engine	0.13	52.0	8.75
3	Head	2.00	57.2	8.75
4	Crest	1.00	58.1	8.75
5	Thermal Cam	0.25	63.0	8.79
6	Sensor Battery	2.45	70.0	9.74
7	Motor Battery	3.75	70.8	7.99
8	GPS (x2)	0.00	80.0	12.99
9	Pixhawk	0.04	78.5	9.74
10	ESC	0.02	70.8	10.29
11	ADS-B	0.04	71.0	9.34
12	LiDAR	3.40	77.5	8.75
13	Thermal Control	0.36	56.2	8.75
14	Sun Sensor	0.08	69.6	11.19
15	Wires	0.13	70.3	8.75
16	Multi-Spec Camera	0.16	84.6	7.75
17	Wing Spar	2.22	68.7	12.14
18	Wing Membrane	1.30	73.7	11.49
19	Wing Claw	0.20	64.5	9.69
20	Wing Rib	0.02	71.4	11.49
21	Fuselage	5.75	72.3	8.75
22	Htail Spar	0.44	92.0	8.75
23	Htail Membrane	0.25	93.0	8.75
		C.G	**70.6**	**9.2**

14.3. CG EXCURSION DIAGRAM

With several payload items designed for the UAV, the operator has the option of whether or not to have them onboard for each flight. The aircraft payload is loaded into the aircraft while laying on the ground or truck, so the CG excursion will not affect the stability while sitting on the ground. Once loaded with payload, the aircraft CG will not change during flight. For this reason, a point CG diagram is only required to show the flight stability for each loading condition. Figure 14.3 shows the CG excursion plot for each payload configuration of the modular design. Table 14.3 shows the payload options and the point number for the respective point on the plot.

Table 14.3: Payload Configurations

C.G. Excursion	Point Number	Weight	C.G. (FS)	%Cbar	C.G. (WL)
Empty Weight	0	19.761	69.648	0.185	9.307
Design Condition	1	24.004	70.59	0.255	9.210
No LiDAR	2	20.604	69.45	0.170	9.286
No Thermal Camera	3	23.397	70.89	0.278	9.222
No Multispectral Camera	4	23.768	70.13	0.221	9.167
No Cameras	5	23.161	70.42	0.243	9.178
No LiDAR, Added Motor Battery	6	24.354	70.690	0.263	9.203
(same CG placement)		**Maximum Shift**	**1.440**	**0.107**	**0.139**

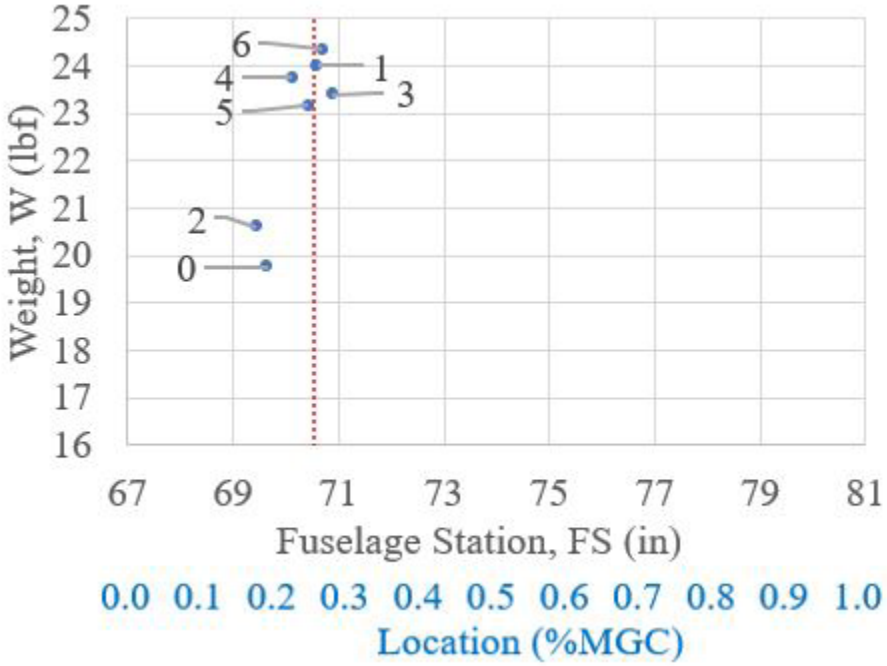

Fig. 14.3: CG Excursion Diagram

This plot shows the adjusted payload locations. The initial design had the thermal camera controller and the sun sensor placed in the tail near the multispectral camera. From this position, the center of gravity was behind the quarter chord of the wing for most of the payload conditions. In the interest of reducing the static margin change for each flight condition, the thermal controller and sun sensor were move forward. This adjustment placed the approximate average CG location between each payload option close to the aerodynamic center of the wing.

The CG shift in the longitudinal direction with respect to the chord was about the same for each iteration, so that didn't influence the 2nd iteration. The total CG shift between the furthest forward and aft CG location is 10.7% of the mean geometric chord (MGC), which is higher than what is ideal but should be manageable. If the user doesn't fly on empty weight or without replacing the LiDAR with another battery, the CG shift is only 5.7%. The C.G shift along the z-axis between each payload configuration is only an eighth of an inch, so vertical adjustments weren't required.

14.4. SUMMARY AND RECOMMENDATIONS

Summary

The major findings of this chapter are:

- Maximum CG shift between flight payloads was 10.7% of the MGC;
- CG locations are centered around the wing quarter chord;
- The in-flight CG will not change
- Hand Calculations shown in Figure 14.3

Recommendations

The author recommends that:

- A reduction in the CG shift would be ideal
- Moving the CG forward would increase the static margin

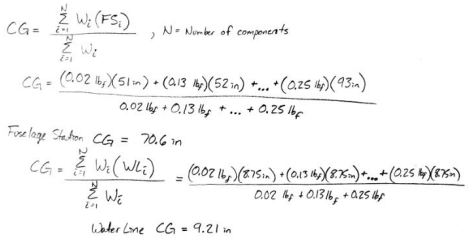

Fig. 14.4: CG Hand Calculations

15. V-N DIAGRAM

This chapter will show the steps for the creation of the V-N diagram for this design, and discuss the decisions for the load factor that the aircraft will be designed for.

15.1. PRESENTATION OF THE V-N DIAGRAM

The V-n diagram shows the relation that the flight velocity has on the allowable load factor. The blue line shows the designed maneuver load with the turn load factor of 1.15. The red lines show the design points from the catapult launch. The grey line is for wind gusts of up to 25 knots, and the yellow represents 35 knot gusts. The other loads to consider are for transportation which can reach load factors of 6 in trucks, and up to 30 on railcars (Ref. 44). With the use of a foam padded case, the maximum load factor will be 15 which would occur during transportation. Figure 15.1 shows each of the load conditions, but the design point will be for n=12 to sustain all gust loads and transportation. Having a large load factor will increase the up-front cost of the UAV. But this design point will reduce how often the aircraft should need to be repaired or replaced, decreasing the life cycle cost for the user. Hand calculations are shown in Figure 15.2.

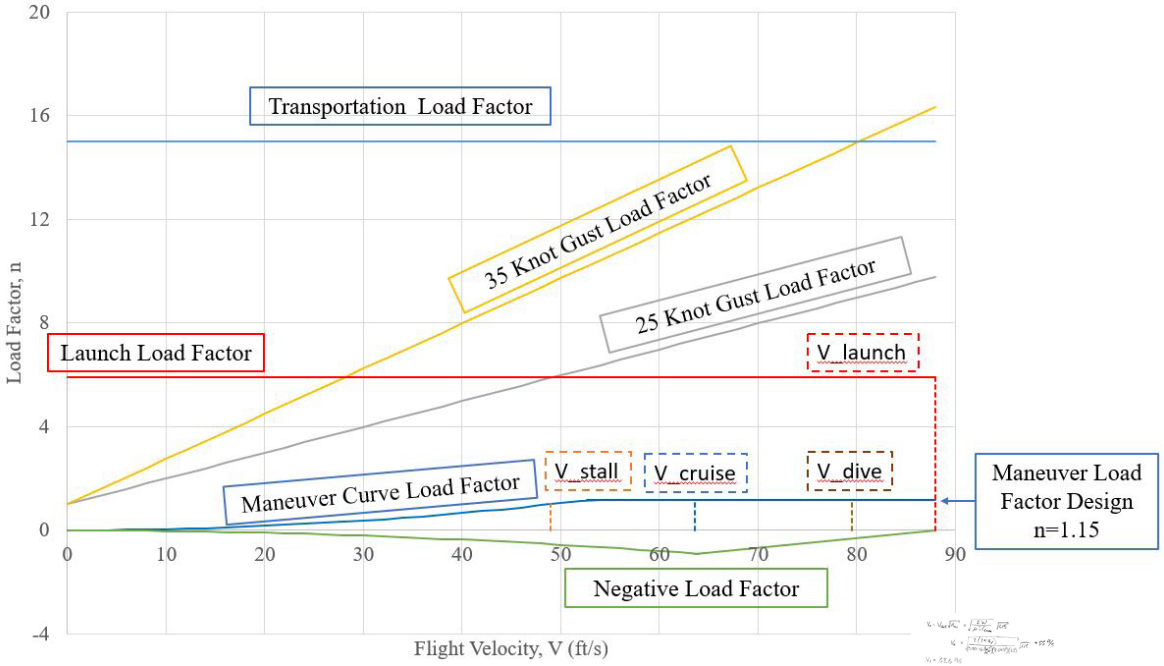

Fig. 15.1: V-n Diagram

Fig. 15.2: V-n Hand Calculations

16. Class I Stability and Control Analysis

This chapter discusses the analysis of the longitudinal and directional stability and control of the Pteslasaur. With an unstable design, the control feedback gain will be analyzed for the engine off conditions since that is where the most control authority will be required. The procedures for the analysis are based off Airplane Design Part II and Part VI (Ref. 4 and 8).

16.1. Longitudinal Stability Analysis

The requirement for longitudinal stability is to have a positive static margin. To reduce trim-drag the aircraft should be designed with a lower static margin, generally from -10% to 5% (Ref. 45). The aircraft will be designed with a static margin between 0% and 5% to be inherently stable since the powerline right of way is small while also having some maneuverability. However, pilots generally are unable to control an aircraft with static margins of under 6% and the recommended static margin is 10% for stability (Ref. 45). To achieve this, a feedback controller will be designed to create a static margin of 10%.

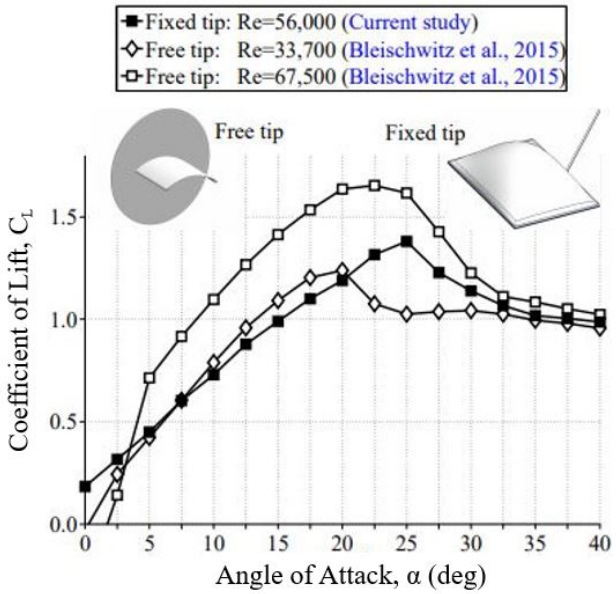

Fig. 16.1: Horizontal Tail Coefficient of Lift (Ref. 46).

The aerodynamic center is dependent on the aerodynamic center of the wing, horizontal tail and the fuselage. The lift curve slope of the wing was determined from the slope of the linear section of Figure 11.1. The horizontal tail has a membrane structure with 3 ends fixed on the spar, and one free end. This should behave similar to the fixed tip curve of Figure 16.1 (Ref. 46). The static margin is defined as the difference between the aerodynamic center of the aircraft and the center of gravity, normalized by the mean geometric chord. The center of gravity for each flight condition is shown in Table 14.3. Figure 16.2 shows the static margin for the most forward placed CG and the designed flight configuration CG.

Using the static margin, the feedback gain (K_α) was determined for each operating condition.

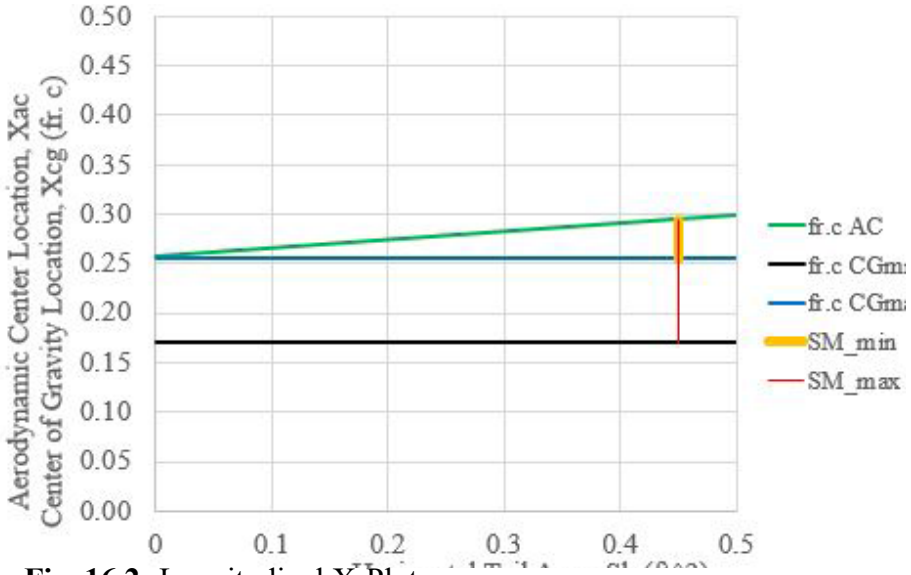

Fig. 16.2: Longitudinal X-Plot.

Fig. 16.3: Hand Calcs 1.

Fig. 16.4: Hand Calcs 2.

Fig. 16.5: Hand Calcs 3.

Table 16.1: Longitudinal Stability Analysis

Configuration	0	1	2	3	4	5	6
$C_{L\alpha,W}$ (per deg.)	0.101						
$\bar{X}_{AC,wf}$	5.26						
$C_{L\alpha,h}$ (per deg.)	0.051						
$\bar{X}_{AC,h}$	6.75						
$C_{L\alpha,A}$ (per deg.)	0.104						
$\bar{X}_{AC,A}$	5.29						
$C_{M,ih}$ (per deg.)	-0.01						
SM (%)	11.0	3.9	12.4	1.7	7.4	5.2	3.2
K_{α} (deg/deg)	0.10	-0.62	0.25	-0.84	-0.27	-0.49	-0.69

Depending on the flight configuration chosen by the operator, the control gain can be adjusted to the feedback gain calculated so the de-facto static margin is always 10%. Table 16.1 shows the key aerodynamic and control characteristics. Figures 16.3, 16.4 and 16.5 show the hand calculations.

16.2. DIRECTIONAL STABILITY ANALYSIS

The directional stability of the aircraft is determined by the yawing moment due to sideslip, commonly known as weathercock stability. The recommended stability criteria is a $C_{n\beta}$ greater or equal to 0.001/deg. Due to the Pteslasaur crest acting as a forward placed vertical tail creating an inherently unstable aircraft, the stability criteria will have to be met using a feedback gain. Figure 16.6 shows the relation between the crest planform area has on the yawing coefficient due to side

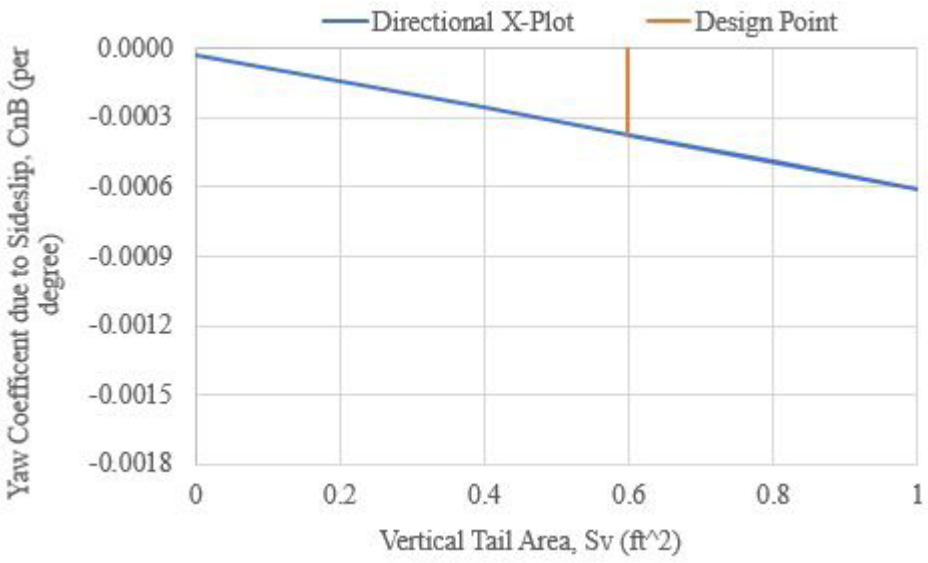

Fig. 16.6: Directional X-Plot

Fig. 16.7: Hand Calcs 1

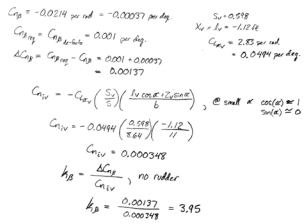

Fig. 16.8: Hand Calcs 2

slip. Table 16.2 shows the key aerodynamic and control characteristics for directional control. Figure 16.7 and 16.8 show the hand calculations. The One-Engine-Inoperative analysis does not have to be calculated since there is only one motor on the UAV.

Table 16.2: Directional Stability Analysis

X_V (distance from AC_h to CG) (ft)	-1.12
S_V (ft^2)	0.6
$C_{n\,\beta,f}$ (per deg.)	-0.00003
$C_{n\,\beta,design}$ (per deg.)	-0.00037
K_β (deg/deg)	3.95
$C_{n\,\beta,de\text{-}facto}$ (per deg.)	0.001

16.3. STABILITY AND CONTROLS SUMMARY AND RECOMMENDATIONS

Summary

The major findings in this chapter are:

- The design feedback gain, K_α is -0.62;
- The horizontal tail area is 0.45 ft^2;
- The design feedback gain K_β is 3.95;
- The vertical tail area is 0.6 $ft^{2.;}$
- The de-facto Static Margin is 10%;
- The de-facto $C_{n\,\beta}$ is 0.001 per degree.

Recommendations

The author recommends that:

- The crest servo will need high torque and operating frequency;
- Use two servos for redundancy since the yaw control is unstable.

17. CLASS I DRAG POLAR AND PERFORMANCE ANALYSIS

The final part of Class 1 design is to take the take the aircraft sizing from each of the previous chapters to analysis the lift to drag ratios. The lift to drag ratio of the designed aircraft should equal the initial estimates from Chapters 5 and 6. The procedure is from Airplane Design Part II (Ref. 4).

17.1. WETTED AREA BREAKDOWN

The wetted area of the UAV was determined from the CAD model making sure that surfaces were trimmed accurately, and are shown in Table 17.1. To verify the CAD model, hand calculations were done following estimates from Part II Airplane Design and are shown in Figure 17.1. The perimeter plot of the fuselage is shown in Figure 17.2.

Table 17.1: Wetted Area of Components

Component	Wetted Area
Wing	21 ft^2
Fuselage	3.7 ft^2
Horizontal Tail	1.2 ft^2
Vertical Tail	1.2 ft^2
Total	**27.1 ft^2**

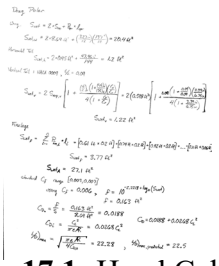

Fig. 17.1: Hand Calcs

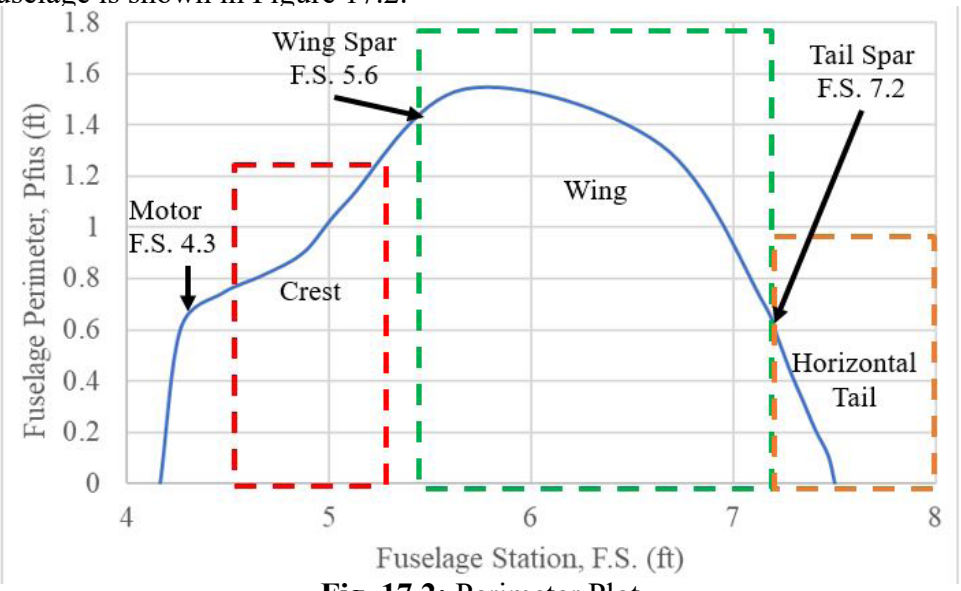

Fig. 17.2: Perimeter Plot

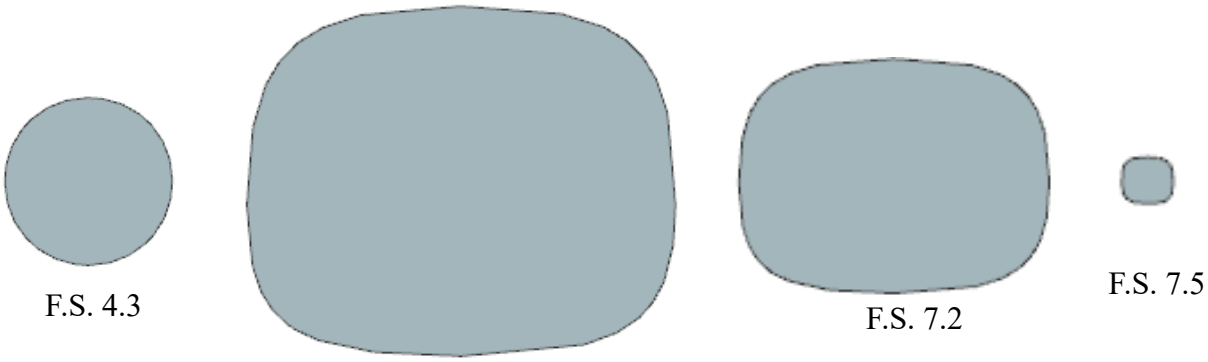

Fig. 17.3: Key Fuselage Cross Sections

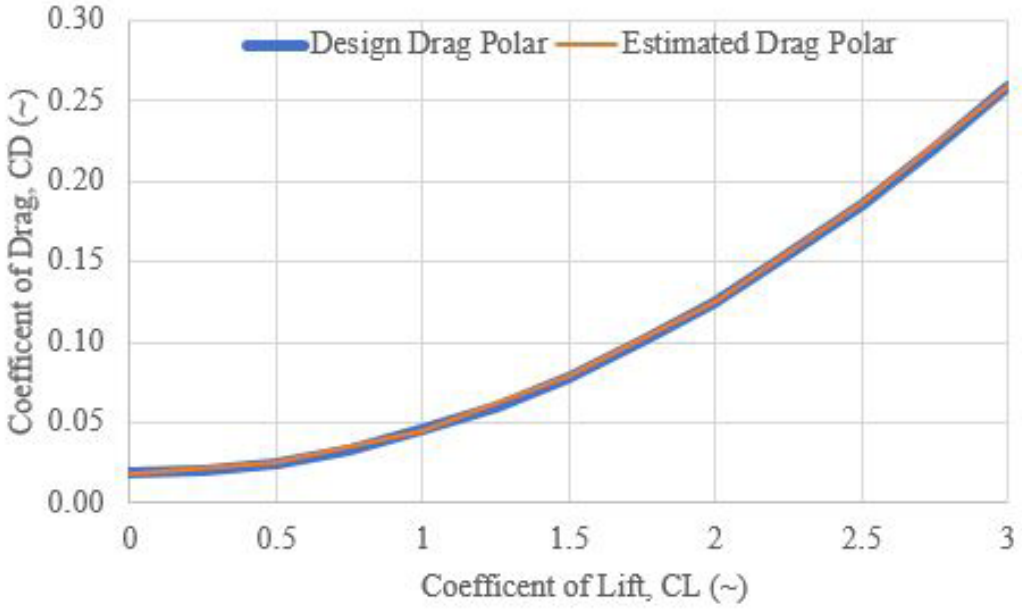

Fig. 17.4: Design Drag Polar

17.2. DESIGN DRAG POLAR

Using the wetted area from Section 17.1, a new aircraft skin coefficient was recalculated. The original design was set as a conservative value allowing for surface deformations. Using the design wetted area, the designed skin friction was changed from 0.006 down to 0.0058 to maintain the same performance. The new drag polar is shown in Figure 17.3.

17.3. DRAG POLAR AND PERFORMANCE SUMMARY AND RECOMMENDATIONS

Summary

The major findings in this chapter are:

- The designed wetted area is 27.1 ft^2;
- The skin coefficient, c_F, is 0.0058;
- The parasite drag coefficient, c_{D0} is 0.018.

Recommendations

The author recommends that:

- Reduce the volume of the aft section of the fuselage to reduce the wetted area, and increase the allowable skin friction coefficient.

18. ANALYSIS OF WEIGHT AND BALANCE, STABILITY AND CONTROL

This section will make conclusions about the Class 1 weight and balance, stability and control based off of the previous chapters. The design iterations that occurred will be discussed to summarize the decisions that lead to the final design. The procedure is from Airplane Design Part I (Ref. 3).

18.1. IMPACT OF WEIGHT AND BALANCE, STABILITY AND CONTROL

The stability and control analysis showed that the placement of the center of gravity and the design of the lifting surfaces acceptable. Using feedback gains, the horizontal and vertical tails will provide the control authority required for flight. The class 1 design of the catapult and retrieval net provide a safe launch and landing conditions for the aircraft and the surveying crew.

18.2. ANALYSIS OF CRITICAL L/D RESULTS

New lift to drag calculations were made for major flight conditions to validate the sizing of the design. During flight the weight will not change so the cruise condition is the same for flying out and the return flight, the difference is the operating altitude depending on the powerline locations. Table 18.1 shows the flight conditions and compares the initial design L/D to the real lift to drag ratio.

Table 18.1: Design Lift to Drag Ratios

	alt. (ft)	W (lbf)	V (ft/s)	C_L	C_D	$(L/D)_{Designed}$	L/D
Cruise, High Altitude	10,000	24	61.4	0.83	0.0373	22.3	22.5
Crusie, Low Altitude	0	24	63.6	0.687	0.0427	22.3	21

18.3. DESIGN ITERATIONS PERFORMED

To reach the final design of the aircraft, a couple iterations were required. During the weight and balance section, the first design had all the components spaced out along the length of the fuselage. The goal for the chapter was to place the CG close to the aerodynamic center of the wing, so that the aircraft would be stable due to the AC shift from the horizontal tail. To accomplish this, the first iteration was moving batteries and LiDAR forward by a half-inch. This decreased the static margin from 8.2% down to 5.7%. The second iteration was moving the Pixhawk, sun

sensor, and ADS-B forward to be placed next to the batteries which moved the center of gravity to fuselage station 70.6. Using this center of gravity location, a static margin of 3.9% was achieved which was within the -10% to 5% target range that reduces trim drag and can still be controlled with an feedback gain applied.

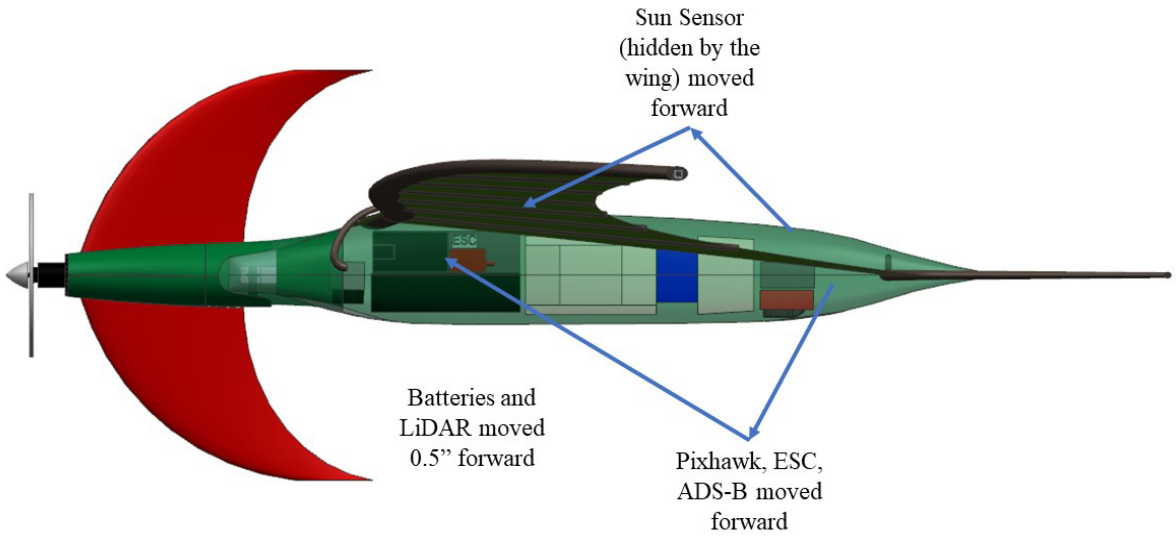

Fig. 18.1: Design Iterations (not to scale)

18.4. WEIGHT AND BALANCE SUMMARY AND RECOMMENDATIONS

Summary

The major findings in this chapter are:

- The aircraft does not need to be resized;
- A flexible cowling was added over the crest joint to reduce drag.
- Estimated L/D was 22.3
- Real L/D is 22.5 at 10,000ft ASL
- Real L/D is 21 at Sea Level

Recommendations

The author recommends that:

- Complete a sizing analysis for flight at low altitudes;
- Move onto the Class II design.

19. CLASS I AIRCRAFT CHARACTERISTICS

The purpose of this sections is to provide the major characteristics of the Class 1 aircraft design and outline the advantages that this design provides.

19.1. TABLE OF CLASS I AIRCRAFT CHARACTERISTICS

Table 19.1: Summary of Class I Design Characteristics

	Wing	Horizontal Tail	Vertical Tail
Area (ft^2)	8.64	0.45	0.6
Span (ft)	11	1.25	1.46
Aspect Ratio	14	3.4	3.5
MGC (ft)	1.12	0.55	0.4
MGC L.E. F.S.	65	89.4	57
Sweep Angle (c/4) (deg)	6	53	45
Taper Ratio	0	0	0.42
Airfoil/Stucture	L.E. Spar, Membrane skin	L.E. Spar, Membrane skin	NACA 0009
Dihedral Angle (deg)	3	0	0
Control Surface	N/A	Horizontal Stabilator	Vertical Stabilator

Fuselage Length (in)	40
Fuselage Maximum Height (in)	4.8
Fuselage Maximum Width (in)	6.25

19.2. CLASS I AIRCRAFT DESCRIPTION

The design is based off of a Pterosaur, which is a standard aircraft with a forward placed vertical tail. The total take-off weight of the aircraft is only 24 pounds making it easy to transport and set-up. The payload options for the aircraft include the LiDAR from the RFP, with an additional thermal camera to monitor the temperature of the powerlines and a multispectral camera that has an optical camera and can monitor the vegetation around the power lines. The aircraft has a maximum range of 106 miles which ensures that the aircraft will be able to travel the 100 miles in one direction (50 mile scan) with a simple battery change to fly the other direction to complete the 100 miles of powerlines. Using feedback gains, the aircraft will remain stable during the flight even with the inherently unstable crest placement. Through the use of membrane wings, the aircraft will be able to perform better during wind gusts since the wing will delay the stall until angles of attack of at least 20 degrees (from Ref. 40 and 45).

20. DESCRIPTION OF MAJOR SYSTEMS

This section will cover the outline of major systems on the UAV. The procedure for the systems will be based off common systems that are currently used in UAVs. An important topic in system design that will be addressed is the conflict of redundancy versus simplicity which will later affect the cost of the aircraft. The procedure for this section is from Aircraft Design Part II (Ref. 4).

20.1. LIST OF MAJOR SYSTEMS

The systems involved with the design are the flight control system, the sensor system and the electrical system. The flight control system consists of the flight motor and the servo motors for control surfaces. The sensor system consists of the flight payload and the protective cover for the LiDAR. The electrical system consists of the required wiring and flight instruments. The key components of each are shown in Figure 20.1 with the flight controls labeled in black, and the electrical and sensor system is labeled in blue.

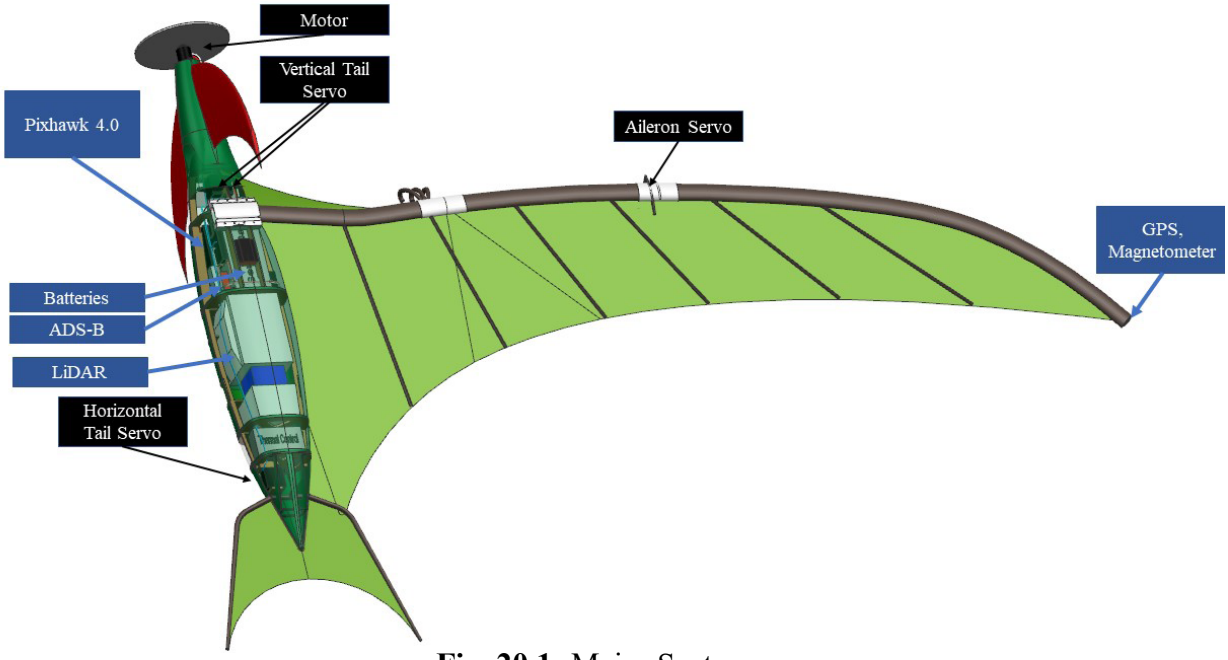

Fig. 20.1: Major Systems

20.2. DESCRIPTION OF THE FLIGHT CONTROL SYSTEM

The flight control system will resemble the same systems for flight control as most UAVs, using servo motors and plastic control arms for actuation. For servo motor selection, the force on the control surface was analyzed under the deep stall condition. With the selected control arm size,

the maximum torque of the servo was sized to be larger than the moment about the lifting surface hinges. Each control surface only has one servo to simplify the system which makes maintenance easier and won't require extra crew training since the layout is the same as most UAVs. The motor being used for the UAV is a Cobra 2213 motor with an APC 7*6-E propeller connected to a Talon 15 Amp electronic speed controller. Figure 20.2 shows the hand calculation for servo sizing and selection. Table 20.1 shows the servo selection and actuation requirements. Figure 20.3 shows the flight control systems labeled on the aircraft. The servos used for this aircraft will be the stock servo shown in table 20.1, using the gear ratios supplied by the manufacturer.

Table 20.1: Control Surface Servo Selection

	Servo Selection	Servo Torque Rating (oz-in)	Maximum Force on Control Surface (lbf)	Maximum Servo Torque Requirement (oz-in)	Actuation Deflection (Deg)
Aileron	HiTec D950-TW	292	4.4	282	+/- 30°
Vetical Stabilator	HiTec HSB-9465SH	112	1.7	98	+/- 20°
Horizontal Stabilator	HiTec HSB-9465SH	112	1.3	87	+/- 45°

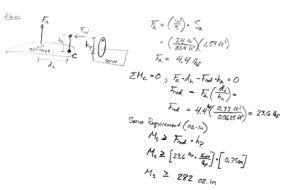

Fig. 20.2: Hand Calcs

Fig. 20.3: Flight Control System (not to scale)

20.3. DESCRIPTION OF THE SENSOR SYSTEM

The sensor equipment on board the UAV is based off the RFP and recommendations from industry. The largest payload requirement from the RFP for both weight and power is the RIEGL miniVUX-1UAV LiDAR. Since the LiDAR uses laser imaging, it is important to protect the glass screen. To do this, a retractable window will be place to expose the camera portion of the LiDAR during flight and cover it during launch, landing and transportation. Additional sensors include an infrared camera that will allow the UAV to monitor the temperature of the powerlines. Another problem that was mentioned was how the surrounding vegetation can damage the powerlines during a storm. For this reason, a multi-spectral camera that is commonly used in agriculture will be used to provide a High-Definition camera as well as other sensors to monitor the vegetation conditions around the powerlines. Figure 20.4 shows the placement of the payload items in the aircraft.

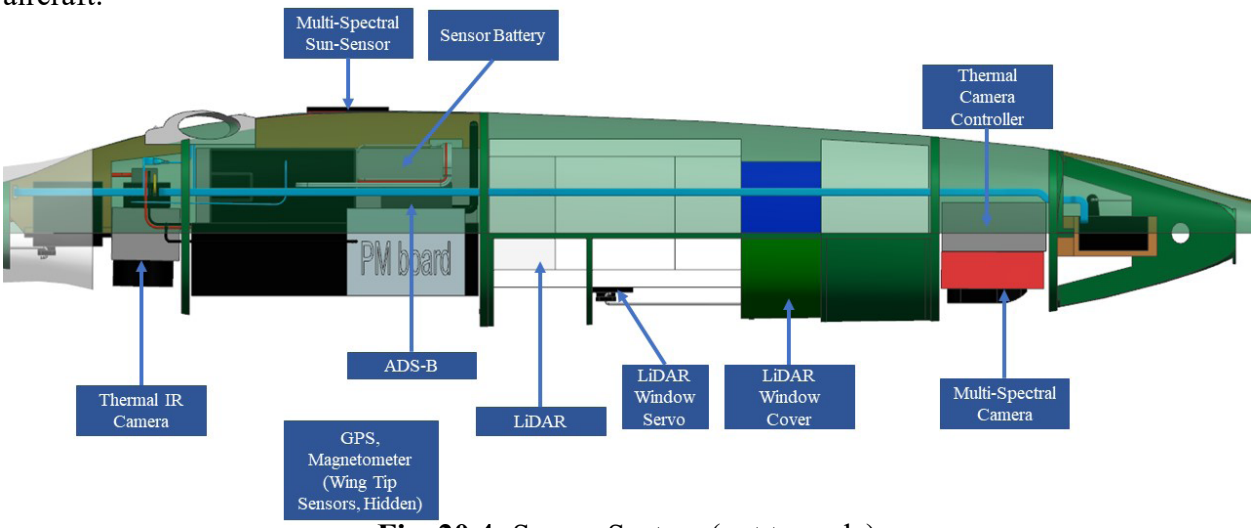

Fig. 20.4: Sensor System (not to scale)

20.4. DESCRIPTION OF THE ELECTRICAL SYSTEM

The electrical system includes any other equipment on board as well as the wiring to distribute power and control signals. The Flight control system and sensor system will be powered off of independent batteries so the sensor and communications will not receive any power signals from the motors. This will help prevent any of the collected data to be corrupted and reduce the amount of noise in the measurement. Since the UAV will be operating around high voltage powerlines, there will be an additional GPS chip and magnetometer on each wing tip. This will provide a method

to provide more accurate direction and location information for the auto-pilot. For FAR Part 107 requirements, an ADS-B trans-receiver will be used to communicate GPS location information between other aircraft. An additional telemetry radio will be used to transmit location data to and from the ground-station. All the sensors will use internal memory to store the data collection which can then be analyzed after the flight. Figure 20.5 shows the wiring diagram for all electrical components (click image to enlarge). Figure 20.6 shows the electrical system in the UAV.

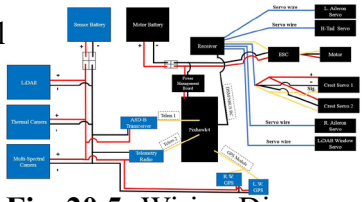

Fig. 20.5: Wiring Diagram

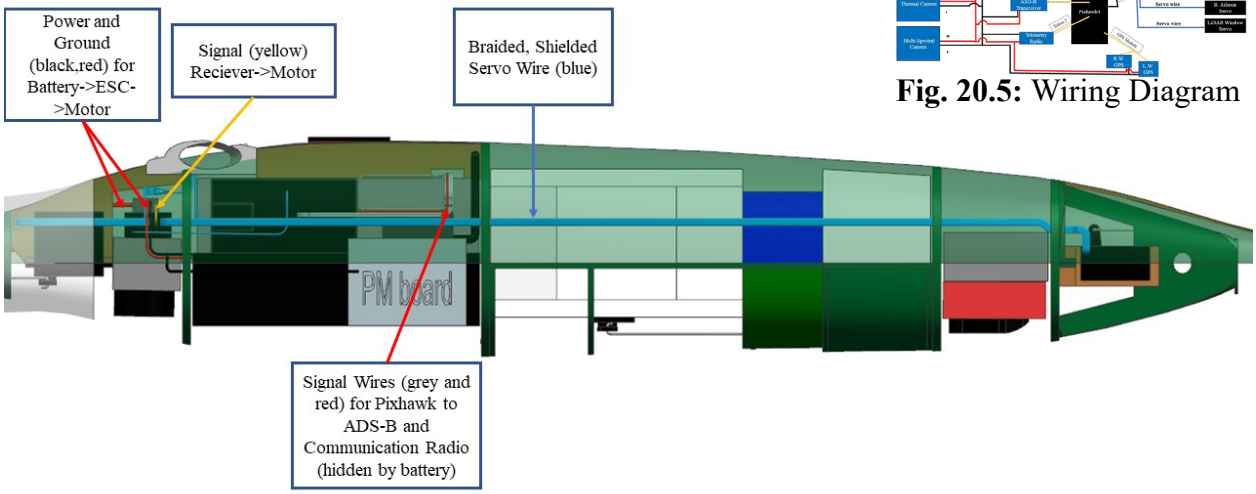

Fig. 20.6: Electrical System

To ensure the selected batteries have sufficient power, the energy required for each component is shown in Table 20.2. Figure 20.7 shows the power usage during each stage of flight. For the flight, the catapult and aircraft set-up will occur during the first 10 minutes of pre-flight. At the 10-minute mark, the propulsion motor and servo motors will be tested at full power. At the 14-minute mark, the sensors will be turned on. Then the catapult will launch at the 15-minute mark, meeting the set-up time requirement by the RFP. Since the catapult is sized to send the aircraft to a cruise velocity above the trees, the remaining time will be cruise. During cruise it will be assumed the servos are running at their stall currents in order to be conservative, which will ensure the battery has sufficient power for the full flight. 2 minutes before recovery, the motor is turned off to slow the aircraft down and prevent the propeller from getting tangled in the net. After capture, all systems will be turned off.

Table 20.2: Battery Power Loading

Motor Battery Item	Power Rating (W)	Sensor Battery Item	Power Rating (W)
Aileron Servo (2)	59.5	LiDAR	16
H-Tail Servo	31.2	ADS-B	20
V-Crest Servo (2)	62.4	Thermal Camera	0.5
Window Servo	5.8	Multi-Spectral Camera	6
Motor	128	GPS (2)	0.004
Total (W)	286	Magnetometer (2)	0.07
Battery Rating (W)	2035	Pixhawk	5
		Telemetry Ratio	0.6
		Total (W)	48.2
		Battery Rating (W)	1110

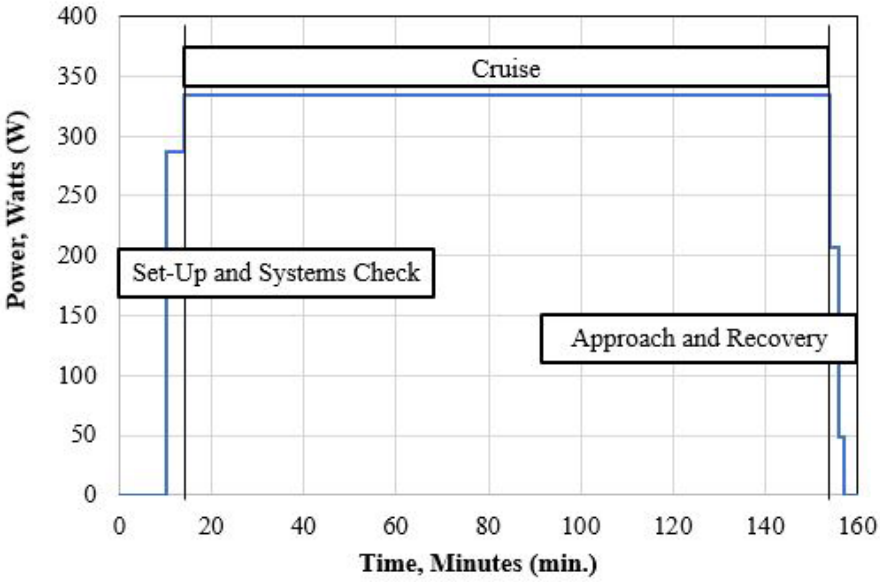

Fig. 20.7: Load Profile

To prevent loss of control during flight, it is important to protect the electrical system. To prevent the wires from moving freely and risk rubbing against structure which could cause the wire to fail, all wires will be secured to the structure. To protect the wires against interference from the magnetic fields around the powerlines and the on-board systems, all wires will be braided and shielded to prevent signal interference.

20.5. CONFLICT ANALYSIS

Around the batteries and the receiver, there are a lot of wires which will be packed tightly. Before flight, the operators should be sure to check to see that each wire is fully connected into the correct location so no wires come lose during flight. When checking the wires, the operator should be care to make sure not to pull out a wire and to make sure that no wires have a sharp bend which would decrease the life-span of the wire.

20.6. DESCRIPTION OF MAJOR SYSTEMS SUMMARY AND RECOMMENDATIONS

Summary

The major findings in this chapter are:

- Flight controls use single servos for ease of repair for surveying crews;
- Sensors meet the required LiDAR and GPS autopilot;
- Additional sensors include a HD camera, multispectral camera for vegetation surveying, and an IR camera for powerline temperature;
- Communications will used an ADS-B for aircraft to aircraft, and another radio for aircraft to ground station communication;
- For control, the UAV will have a Pixhawk 4.1 which provides GPS waypoint following or a method for pilot-controlled flight if desired.

Recommendations

The author recommends that:

- Use an antenna for data transfer that is capable of a 50 mile range in-case the communications along the powerlines fail;
- Use the optical and IR camera onto the UAV to provide a live-feed view of the powerlines so the post-processing of the data isn't required to find problems on the powerline.

21. Class II Sizing of the Take-off and Landing Systems

Since the take-off and landing uses a catapult and net, traditional landing gear sizing producers can't be used. Knowing the flight conditions that the catapult needs to achieve, the sizing for launch will be done using a kinematic analysis. The net will be sized based off nets that have been used for other UAVs.

21.1. Catapult Launch Sizing

From Chapter 13, the required energy to achieve cruise velocity at a height of 50 feet above ground level is 3.5 kJ and the length of the track is 20 feet. From the energy and length, the required spring constant is 12.7 lbf/ft. This requires 258 lbf to draw back for launch. For this reason, there will be a crank and gear assembly which will allow the operators to use it safely. Table 21.1 shows the characteristics of the catapult. Figure 21.1 shows the Class II catapult launch system with the crank in red.

Table 21.1: Launch System Characteristics

Track Length (ft)	20
Launch Energy (ft*lb_f)	2546
Spring Constant, k (lb_f/ft)	12.7
Force (x=0) (lb_f)	258
Acceleration (ft/s^2)	10.7
Force (x=0) (lb_f)	6.4
Acceleration (ft/s^2)	0.3
Maximum Load Factor	8

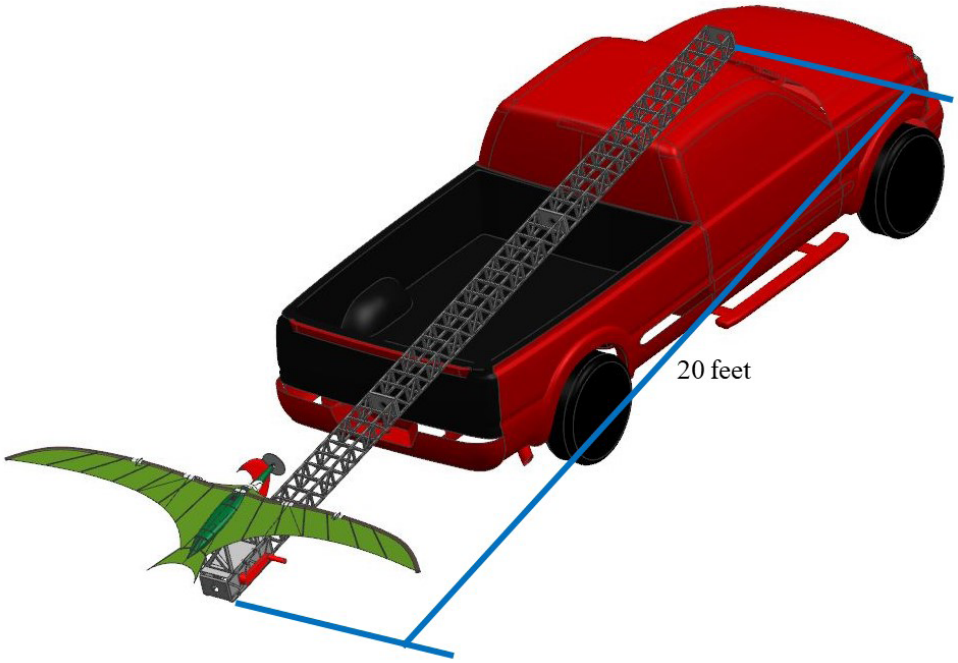

Fig. 21.1: Class II Catapult

21.2. Net Sizing

The net that will be used is the same net as the Textron Systems Aerosonde Mark-47. The Mark-47 has a weight of approximately 80 pounds with a cruise velocity of around 93 ft/s [Ref. 47]. The Mark-47 will have a higher capture approach energy than the 24 pound and 63 ft/s cruise velocity Pteslasaur. This system will allow the UAV to safely be captured without damage to the net. The Mark-47 has comes to stop after roughly 15 feet of net extension. For the assumption of a constant acceleration, the load factor from landing is 1.27 g's which is below the design point. This will allow the UAV to be recovered without damage. Figure 21.2 shows the net that will be used.

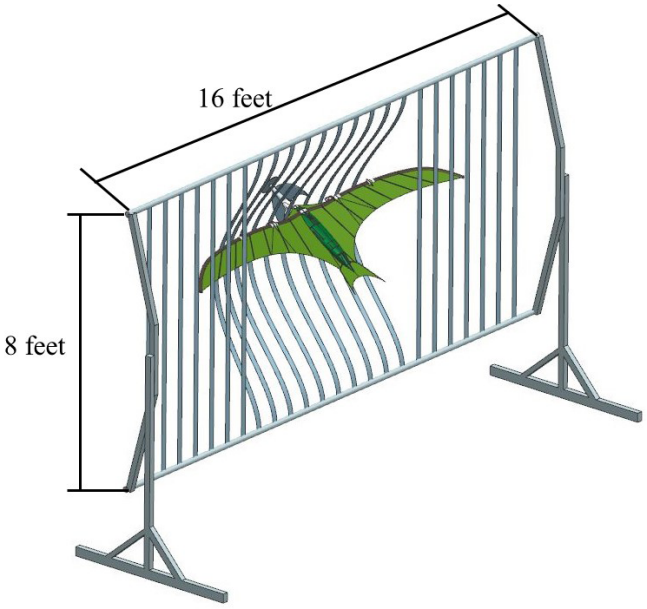

Fig. 21.2: Class II Net

21.3. Landing Gear Design Summary and Recommendations

Summary

The major findings in this chapter are:

- The catapult will require a spring with a 14.1 lbf/ft spring constant;
- The launch load factor of 8 is below the designed maximum load factor;
- The net will be the same net that the Aerosonde Mark-47 uses.

Recommendations

The author recommends that:

- Investigate the cost and size comparison between a spring launch and pneumatic launch system;
- Design a brand-new net specifically for this aircraft size to potentially reduce the transportation weight since the Aerosonde Net is oversized for this application

22. INITIAL STRUCTURAL ARRANGEMENT

The purpose of this section is to outline the location of structural elements to accommodate the payload. From the initial arrangement, the design can be given to the structural team to complete a full analysis. The structural arrangement process is based off of looking at the structure of RC aircraft of similar sizes.

22.1. LAYOUT OF FUSELAGE STRUCTURE

The primary structure of the fuselage will be a full carbon fiber skin which will provide most of the load bearing capability required for the design. Bulkheads will be made from a basswood sheet and will provide a way to support the payload during flight. The aircraft will be made with a modular design which will allow the operators to adjust what payload will be used for each flight. To do this, the bottom skin is split into sections between the bulkhead. To secure them during flight, springs loaded peg on the other to allow each section to be removed easily while also keeping them locked into position during flight. Figure 22.1 shows the full fuselage structure, and Figure 22.2 shows the lock and pin connections for the removable sections.

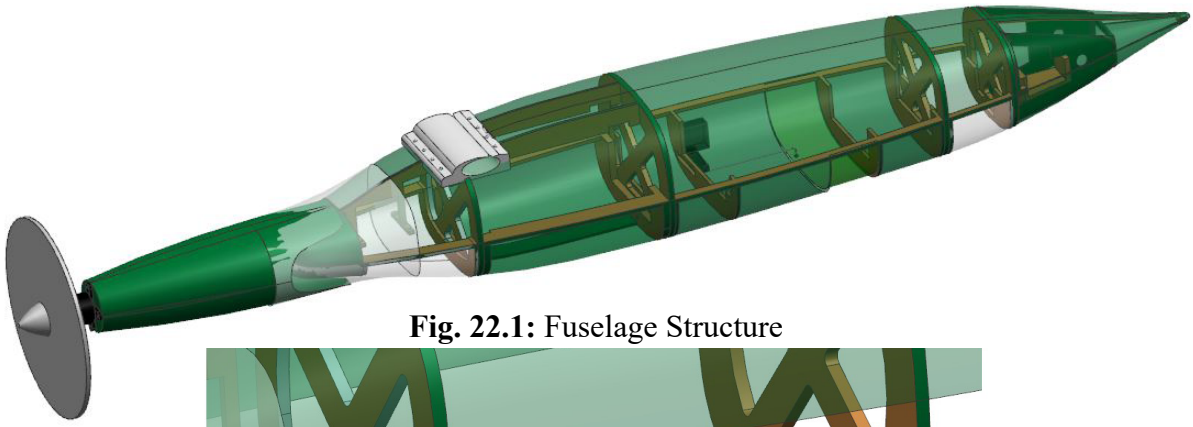

Fig. 22.1: Fuselage Structure

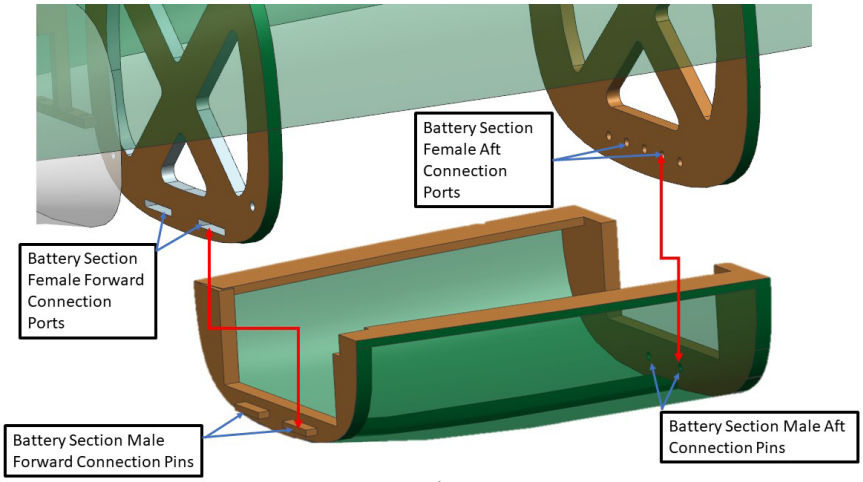

Fig. 22.2: Fuselage Structure

22.2. LAYOUT OF LIFTING SURFACE STRUCTURE

The lifting surfaces will be made using a carbon fiber spar with a membrane skin. Ribs made from fiberglass will be used to create stiffness along the trailing edge to prevent flutter, but thin enough to allow the fiberglass to still flex with the membrane. The properties of the ribs could be comparable to that of the tips of a fishing pole, strong enough to provide support while being flexible.

The membrane itself will be made from materials such as latex, silicon sheets, or Kevlar. The specific material would require testing for both strength and flexibility to maximize the aerodynamic performance. With a single membrane sheet, the visibility of the aircraft can be selected per customer request for a low observable aircraft with a zero-energy requirement. This will be discussed further in a coming chapter for aircraft variants.

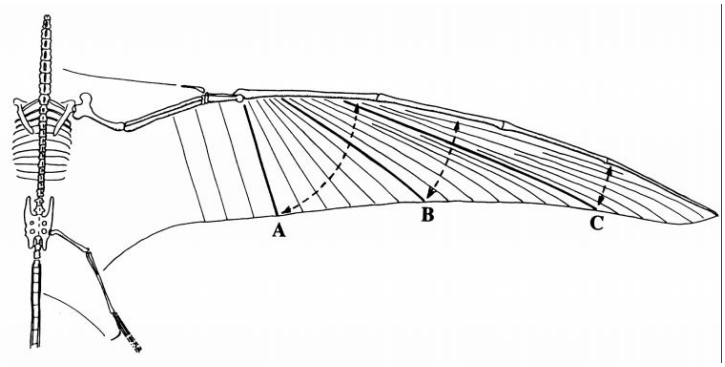

Fig. 22.3: Pterosaur Un-Folded Wing (Ref. 48).

Compared to a traditional wing design, the membrane structure inspired by the Pterosaurs will provide a unique advantage when it comes to storage. Since the wingspans of many competing aircraft from Chapter 2 are also around 10 feet, a solid wing becomes hard to transport in an F-150 and nearly impossible if the fuselage is attached. This would require the surveying teams take time to assemble and disassemble the aircraft, which only increases the chance of damage due to negligence. The membrane structure however, would allow the wing to be folded up in a fashion similar to the Pterosaur wings. While Pterosaur membranes are hard to

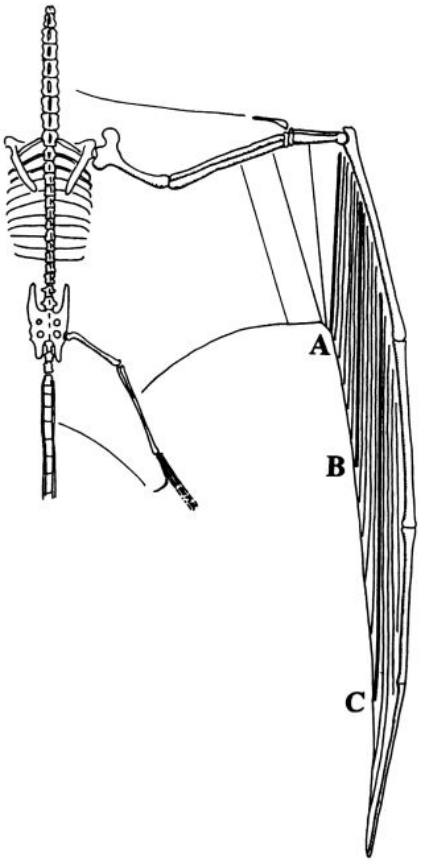

Fig. 22.4: Pterosaur Folded Wing (Ref. 49).

study since they are rarely preserved in fossils, it is believed that the wing structure has radial oriented fibers as shown in Figure 22.3 (Ref. 49). The actinofibrils of the Pterosaur would have provided the same function as the proposed fiberglass ribs. The radial pattern of the actinofibrils allow the wing membrane to have enough stiffness for flight while being able to fold as shown in Figure 22.4 (Ref. 49). To imitate this characteristic, the spar will have a male-female connection similar to camping tent poles. This fitting provides strength to the spar while being able to pull the spar apart to fold the membrane. Through the inside of the spar, an elastic band will provide a compressive force in the spar joint to prevent the outboard section from becoming disconnected during flight. This tent-pole design would significantly reduce the amount of time required to prepare the aircraft for flight. Instead of putting together the wing, and attaching the wing to the fuselage in 2 joints and 4-8 screws/bolts; the assembly is simplified to just putting the outboard spar back into the connection. Figure 22.5 shows one wing in the flight configuration, and the other wing in the folded configuration for transportation.

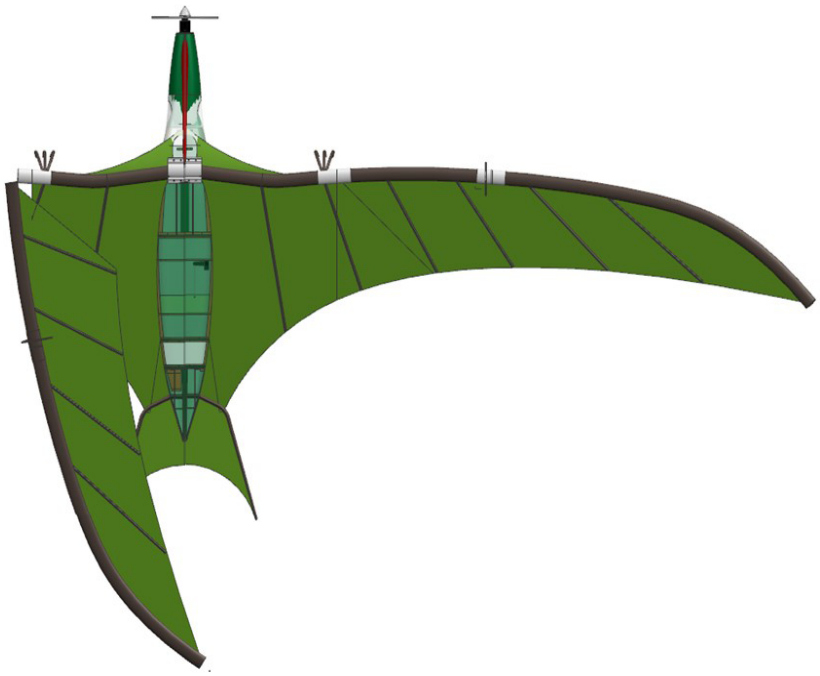

Fig. 22.5: Aircraft Wing Folding

The overall structure of the Pteslasaur wing closely resembles the wing structure that palaeontologists believed the Pterosaur had. Very few wing membranes were preserved when the creatures died off millions of years ago which has made the research on them difficult. Figure 22.6 shows the comparison between the UAV membrane wing (top 2 pictures) and the Pterosaur membrane structure (bottom picture).

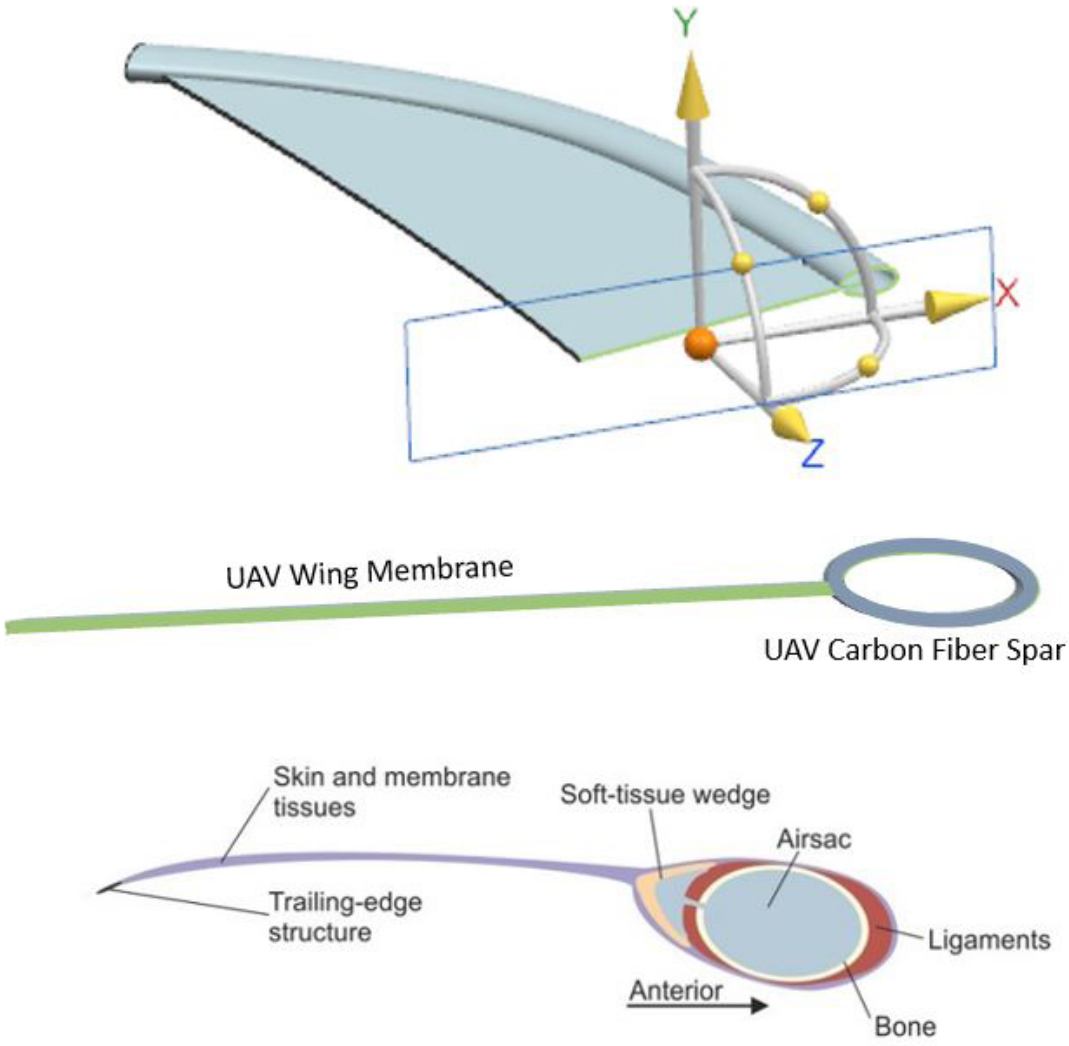

Fig. 22.6: Membrane Structure Comparison

A center support structure is placed to hold the wing to the aircraft, with a removable cover which allows for at-home wing replacement. Since wing damage would require a full replacement, the life-cycle cost will increase. To help reduce the cost, the wings can be purchased and then replaced at-home so customers will not be required to also pay for labor costs for wing replacements. For day-to-day usage, the wings will not have to be disconnected unless the wing becomes damaged.

22.3. CAD RENDERING OF THE STRUCTURAL LAYOUT

The full aircraft structure is shown in Figure 22.7, including the transportation configuration.

22.4. STRUCTURAL ARRANGEMENT SUMMARY AND RECOMMENDATIONS

Summary

The major findings in this chapter are:

- The fuselage structure is a fully monocoque composite skin with basswood inside structure for payload support;
- The wing structure is a fold-able carbon fiber spar with fiberglass ribs, and a membrane surface.

Recommendations

The author recommends that:

- Conduct a FEM analysis to ensure the composite skin can support flight loads;
- Do a cost-weight analysis of other materials like injection nylon, aluminum skins to select the best material for structural use and customer cost.

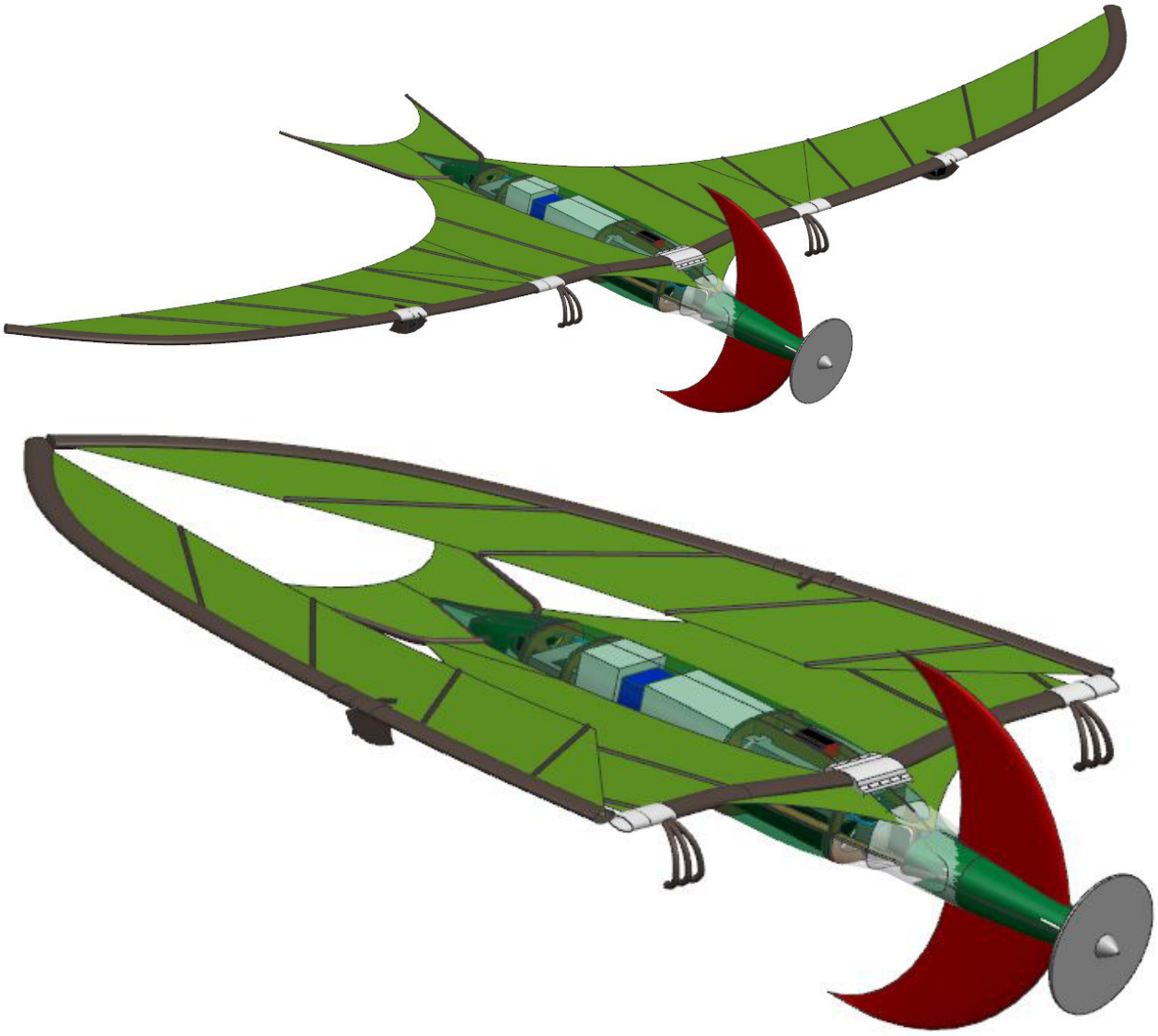

Fig. 22.7: Complete Initial Structure

23. Class III Weight and Balance

The class III weight and balance was conducted by using the center of gravity locations and component volumes from a CAD model, and density or weight information found online. Since all components are manufactured from materials shown in Chapter 28 or from currently sold equipment, this method will provide an exact CG location. Then a CG diagram will be made to show the operating flight conditions for the aircraft.

23.1. Class III Weight and Balance Calculations

Using the CAD model and material or equipment data, the center of gravity of the aircraft can be calculated. The fuselage structure is an IM7/C977-3 carbon fiber-epoxy composite with 17 plies on the top skin, and 10 plies on the bottom removeable pods. While this is thick for a 24 pound aircraft, there is a LiDAR worth over $50k so protecting that item became a priority. The wing and horizontal tail skins are made from a rubber-like material so the density of the material was based off of natural rubber latex and nitrile rubber. The spars were assumed to have the same density as the carbon fiber fuselage. Then the electronic and payload items weights were found on manufacturer's published data. Breaking the items into different categories, Table 23.1 shows the weight and CG locations of the major aircraft systems. A full list of component weights are found on the bill of materials in Chapter 28.

Table 23.1: Component Weight and CG Locations

System Number	System Name	Weight (lbf)	C.G. Location (FS, inches)
1	Fuselage	6.92	117.8
2	Crest	0.03	107.8
3	Wing	5.40	120.7
4	Tail	0.28	142.2
5	Propulsion and Controls	0.77	115.8
6	Sensors and Electronics	10.61	122.4
	Class III Weight and Balance	**24.01**	**120.7**
	Class I Weight and Balance	24.0	120.6

23.2. CLASS III CG POSITIONS ON THE AIRFRAME AND CG EXCURSION

Figure 23.1 shows the CG locations on a top view of the aircraft for each of the major systems. The system numbers from Chapter 23.1 correspond to the labels on the figure. The process to determine the center of gravity for each payload configuring is the same as what is shown in the hand calculations from Chapter 14. Figure 23.2 shows the CG location diagram for each payload condition. This diagram only uses the points opposed to the excursion diagram since the aircraft is loaded while the top of the fuselage is on the truck bed so there is no tip-over concern. During the flight the CG will not shift, so the operators only care about the CG of their loaded payload condition to adjust the feedback gain required for pitch control.

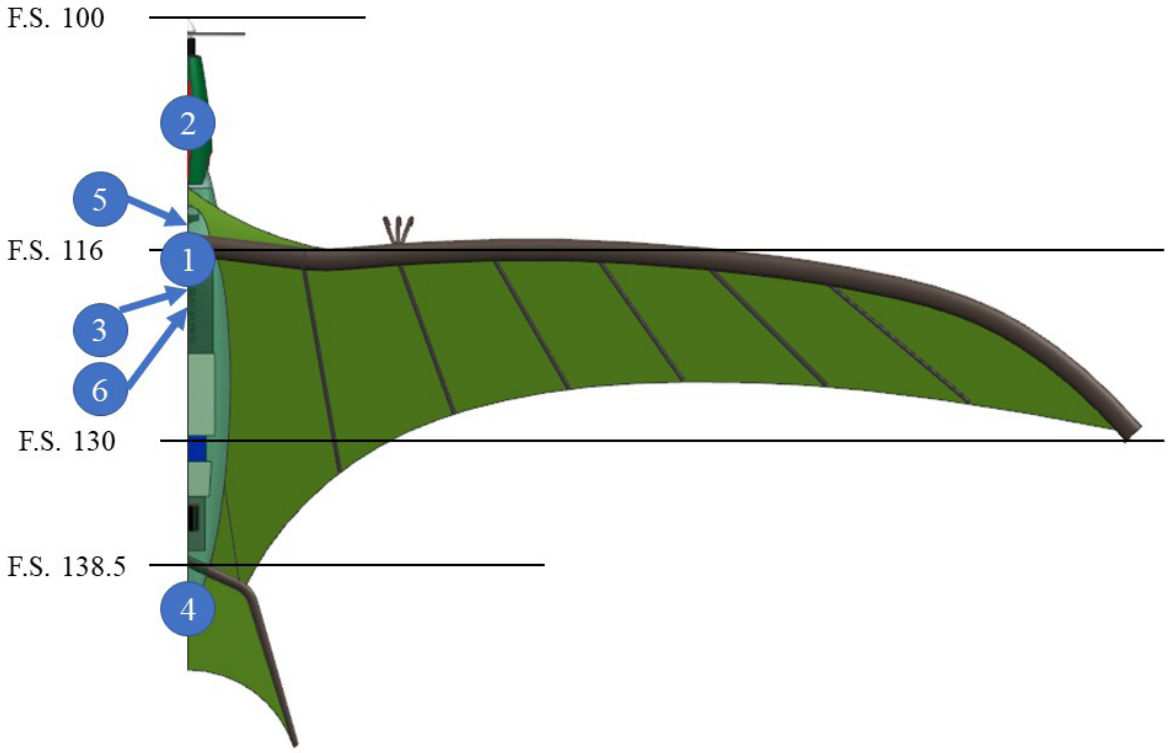

Fig. 23.1: Aircraft Component CG Locations

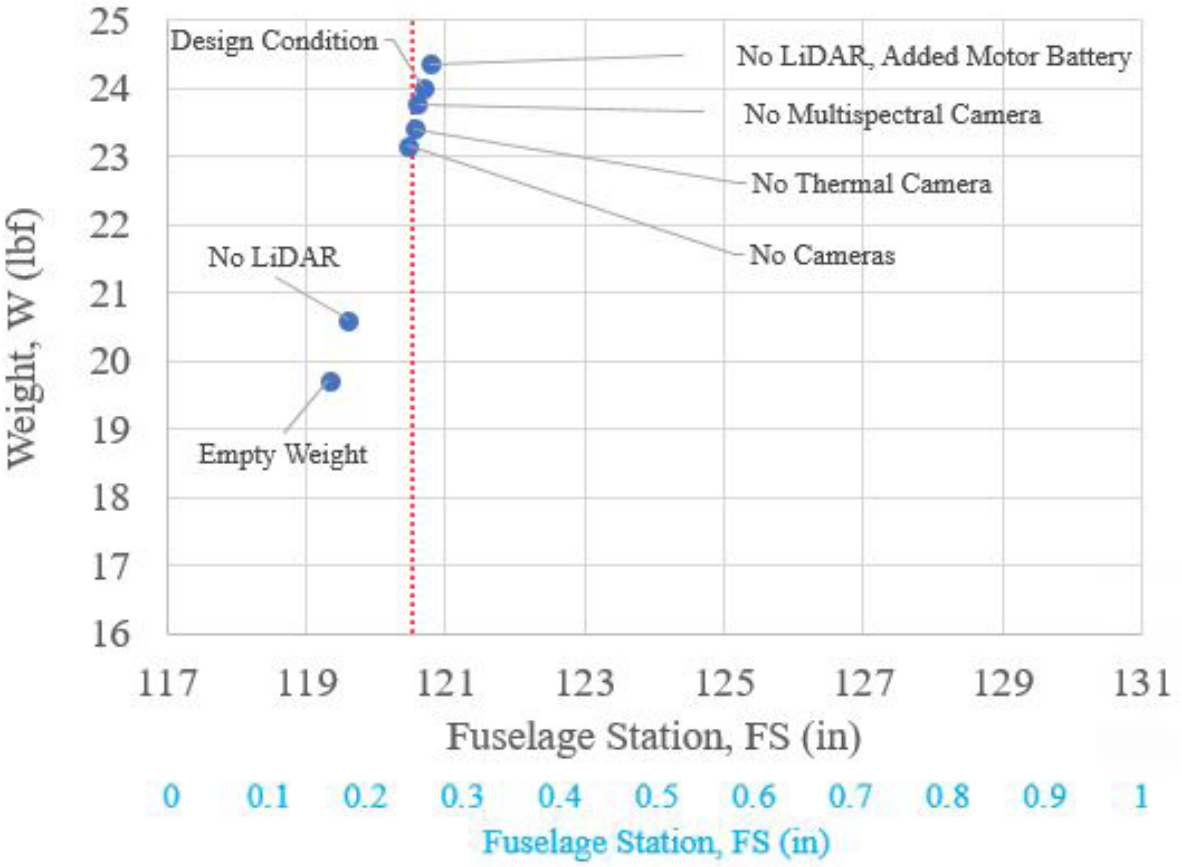

Fig. 23.2: CG Point Diagram for Each Payload Condition

23.3. CLASS III WEIGHT AND BALANCE SUMMARY AND RECOMMENDATIONS

Summary

The major findings of this section are:

- The standard payload configuration CG is at F.S. 121;
- The Weight is within 0.5% of the Class 1 Design;
- The maximum CG shift between configurations is 10.8%.

Recommendations

The author recommends that:

- Reducing the CG shift would allow for a single control gain design, reducing operator set-up error.

24. Class III Weight and Balance Analysis

With the Class III weight and CG calculated, an updated balance analysis should be done to ensure operating stability. The aircraft weight and CG locations were both within 0.1% of the Class I design estimations. This means that the Class I Weight and Balance Analysis provides an accurate insight into the stability of the aircraft. Without a landing gear, the aircraft doesn't have a tip-over issue. The CG shift is high, but the aircraft will not be used under the empty weight condition. If the operators don't use a LiDAR, then it is recommended to include an extra battery and complete the entire power line surveillance in 1 flight instead of 2 flights.

Figure 24.1 shows the updated x-plot for the Class III design. The standard payload configuration has a static margin of 3.2%. Using the same stability analysis method as Chapter 16, a feedback gain of -0.68 will give the aircraft a de-facto static margin of 10% which is acceptable for UAV controls. This design will provide the operators an easy to control aircraft to decrease the risk of crashing and damaging the aircraft.

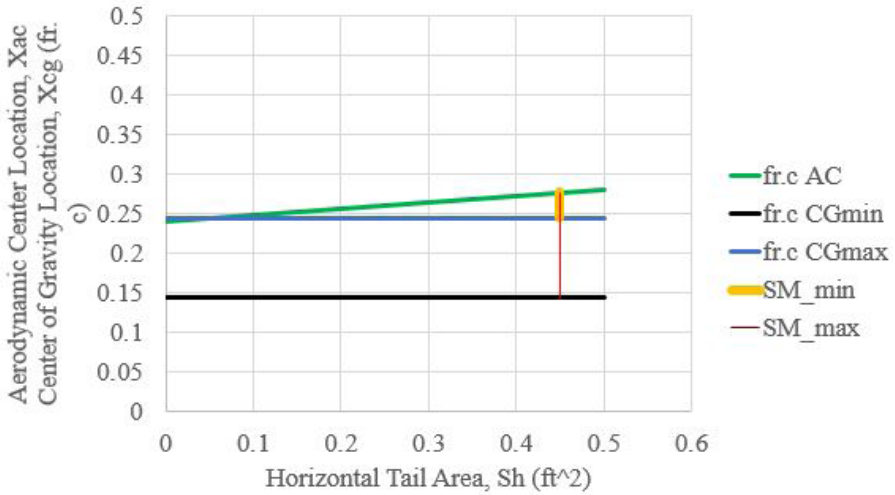

Fig. 24.1: Class III X-Plot

24.1. Class III Weight and Balance Analysis Summary and Recommendations

Summary

The major findings in this chapter are:

- The aircraft is stable with a 3.2% static margin;
- The feedback gain, K_a, of -0.68 provides a 10% de-facto static margin;

Recommendations

The author recommends considering

- Reducing the static margin to 0 reduces trim drag and a higher feedback can be used to maintain the 10% de-facto stability.

25. CLASS III STABILITY AND CONTROL ANALYSIS

The purpose of this chapter is to provide verification to the basic stability analysis steps laid out by Dr. Roskam in Chapter 16. This process will be done using AVL, a program designed for the analysis of the aerodynamics and flight-dynamics for fixed wing aircraft. The limitation of this program is that it does not accurately model the fuselage. But as shown in Chapter 16.2 this fuselage did not have a significant effect on the aircraft stability, so it was not modelled in AVL.

25.1. AVL MODEL AND RUN CASE

Each of the lifting surfaces were discretized into 6 sections to be used define the aircraft geometry. The software requires a data file containing the chordwise coordinates to define an airfoil. Which is something that can not be done since the Pteslasaur uses a membrane airfoil. To accommodate this, an airfoil was found to approximately match the lift-curve slope of the membrane wing from Chapter 11. The criteria were a Cl of approximately zero at zero angle of attack; and a maximum Cl of 1.3 at an angle of attack of 12 degrees. This airfoil would then have an equivalent Cl,α to the membrane wing. This would allow the airfoil to be used in place of the membrane if the wing is within an angle of attack range of zero to twelve degrees. Figure 25.1 shows the final AVL geometry model.

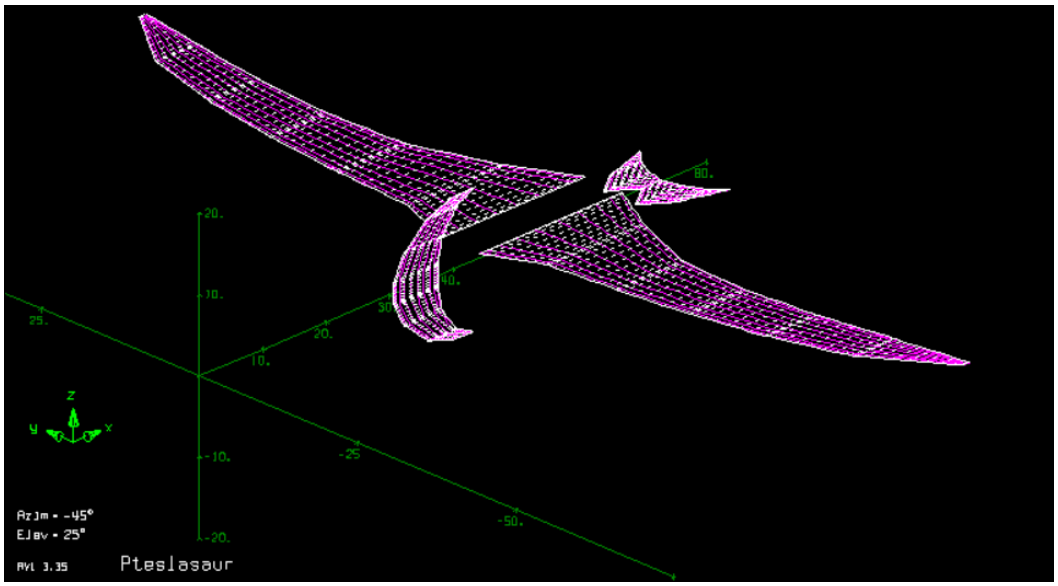

Fig. 25.1: AVL Geometry Plot

For the analysis of the stability, the following run case was used shown in Figure 25.2 For cruise condition, the coefficient of lift of 0.83 was set by the maximum L/D condition from Chapter 18. Then the elevator was used to trim the aircraft pitching moment to zero.

```
alpha        ->  CL          =   0.83000
beta         ->  beta        =   0.00000
pb/2V        ->  pb/2V       =   0.00000
qc/2V        ->  qc/2V       =   0.00000
rb/2V        ->  rb/2V       =   0.00000
flap         ->  flap        =   0.00000
aileron      ->  aileron     =   0.00000
elevator     ->  Cm pitchmom =   0.00000
rudder       ->  rudder      =   0.00000
```

Fig. 25.2: AVL Run Case

25.2. STABILITY AND CONTROL RESULTS AND ANALYSIS

After running AVL, the first check is to whether or not the airflow angles and the control surface deflection angles are reasonable. Table 25.1 shows the flight condition based on the AVL model and trim case. From Chapter 25.1, the requirement for the angle of attack to be within the zero to twelve degree range. The maximum incidence angle occurs at the wing root of 6.2 degrees, creates a total airflow angle (angle of attack + incidence angle) of 9.4 degree. This is within the acceptable range for the selected airfoil to represent the membrane structure. To trim the aircraft to zero pitching moment, an elevator deflection of 5 degrees was required. This allows the pilot to trim the aircraft, and still have a range of motion in the elevator to control the aircraft through perturbations from steady-state flight.

Table 25.1: Steady State, Level Wing Trim Condition	
Angle of Attack, α (deg)	3.19
Elevator Deflection, δe (deg)	5.03
Static Margin, SM (%)	3.9

The second check is to analyze the stability conditions in the control derivatives. Table ##.2 shows the major control derivatives that are used to analyze the stability of the aircraft during flight. The flight requirements and the typical ranges of the control derivatives were found from Dr. Roskam's Airplane Flight Dynamics and Automatic Flight Controls book (Ref. 50). The only unstable coefficient is the Angle of Sideslip stability, as expected from the forward place vertical crest. The solution to this would be to develop a controller to compensate from the instability. The remaining control derivatives all satisfy the stability requirement and are within the typical ranges.

Table 25.2: Stability Criteria and Pteslasaur Design Results

Control Derivative	Description	Stability Criteria (Ref. 50)	Typical Range (Ref. 50) (rad^{-1})	Pteslasaur Design, using AVL (rad^{-1})
$C_{m,\alpha}$	Angle of Attack Stability	< 0	[-4, 1]	-0.1618
$C_{y,\beta}$	Side Speed Stability	< 0	[-2, -0.1]	-0.2683
$C_{n,\beta}$	Angle of Sideslip Stability	> 0	[0, 0.4]	-0.0287
$C_{l,p}$	Roll Rate Stability	< 0	[-0.8, -0.1]	-0.5008
$C_{m,q}$	Pitch Rate Stability	< 0	[-90, 0]	-1.2685
$C_{n,r}$	Yaw Rate Stability	< 0	[-1, 0]	-0.0104

Figures 25.3 and 25.4 show the full AVL output for the forces and coefficients.

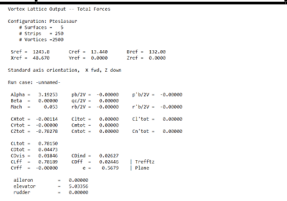

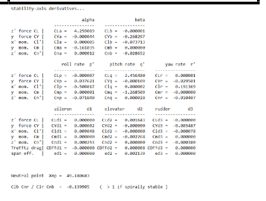

25.3. CLASS III STABILITY AN CONTROL ANALYSIS SUMMARY AND RECOMMENDATIONS

Summary

The major findings in this chapter are:

- The trim condition maintains reasonable angle of attack and elevator deflection;
- The only unstable control derivative is the Angle of Sideslip, as expected from the vertical crest.

Recommendations

The author recommends:

- Developing a controller that will compensate for the instability in the angle of sideslip.

26. Updated 3-View and Notable Variations

The design was not changed between Class I and Class III designs, so the official 3-view is shown in Chapter 19. The purpose of this section is to discuss the different variants that this aircraft can have based off the base design that has been described so far. These variants will offer designs that would better fit available markets, and focus on public acceptance. The base design is strictly focused on being able to complete the mission. This provides 100 linear miles of flight using a LiDAR as the primary data collection system as requested in the RFP.

One of the operating concerns is that during flight around populated areas, civilians might not want to see a Pterosaur flying overhead. While most kids would love to see the flying dinosaur, an angry adult poses a threat to the safety of the aircraft. For this reason, the wing membrane material can remain rubber-like but be upgraded to a transparent color. Doing this will create the Low-Observable variant called the PtesLOsaur. Compared to adjustable LED lights for a low observable design which has a very high-power requirement, the transparent material would provide for a cheap and easy solution to the possible public disturbance. Along with the membrane, the fiberglass ribs could be replaced with a clear polycarbonate rib making the wings nearly invisible. Figure 25.1 shows the model of the PtesLOsaur and Figure 25.2 shows how the transparent wings will change the visual cross section of the aircraft.

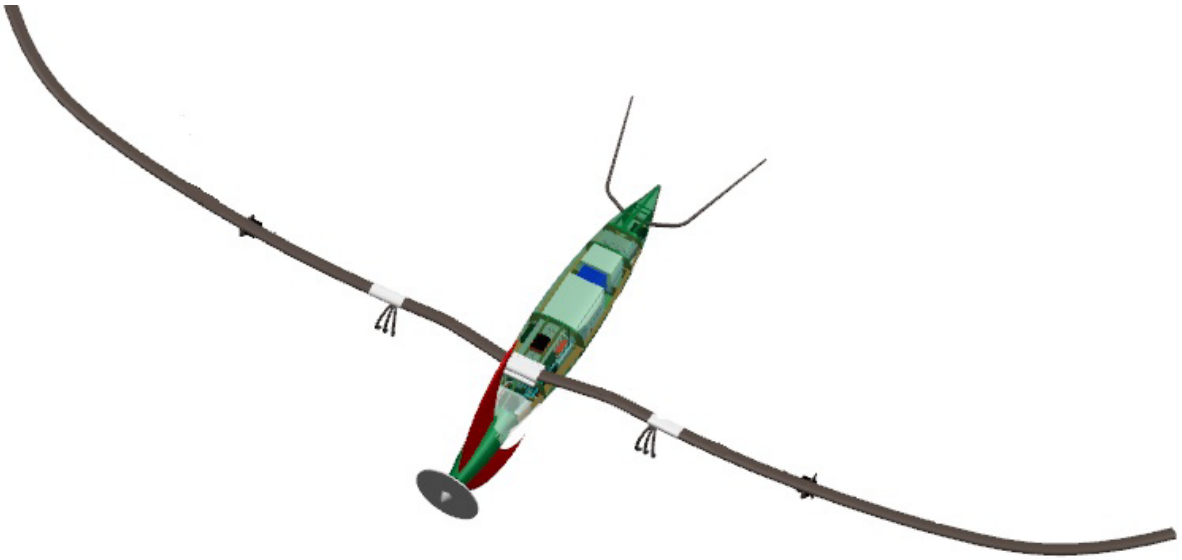

Fig. 26.1: The PtesLOsaur

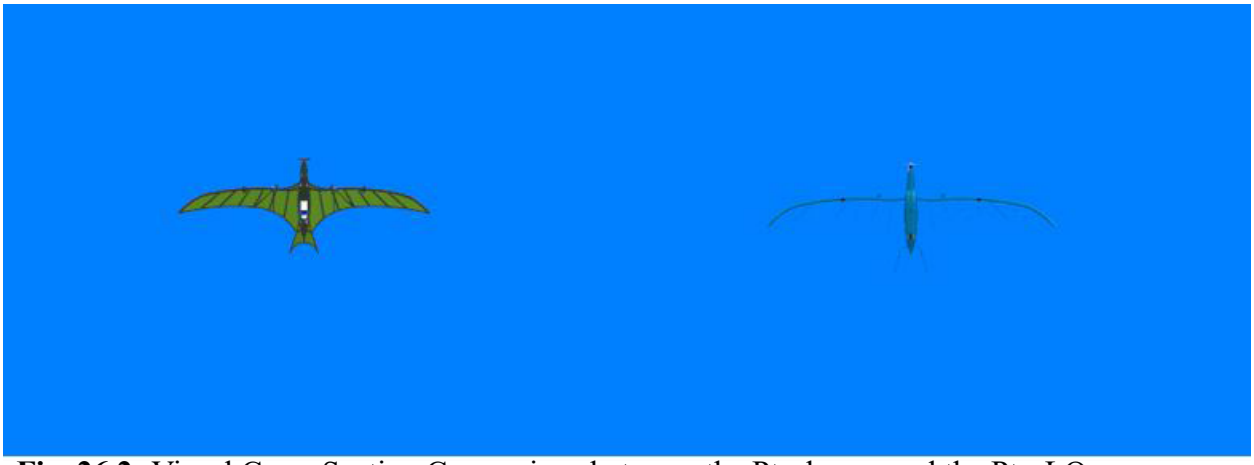

Fig. 26.2: Visual Cross Section Comparison between the Pteslasaur and the PtesLOsaur

26.1. Updated 3-View and Variant Models Summary and Recommendations

Summary

The major findings in this chapter are:

• The PtesLOsaur is a low observable design for public acceptance;

Recommendations

The author recommends that:

• Research additional low observable technology to further reduce the visual cross section and cost;

27. ADVANCED TECHNOLOGIES

27.1. LOW OBSERVABLE (LO) TECHNOLOGY

Between the weapon threats and privacy invasion, it is easy to find news articles where people are complaining about UAVs. Regardless of the design, this is a concern that should be considered in UAV design. Where traditional UAVs are foam or wooden-rib designs that are very hard to hide due to the structure materials, the Pteslasaur' s membrane wing is a perfect platform for LO technology. Rubber materials are commonly made into transparent or translucent colors, and the flexible ribs can be made from polycarbonate which is clear.

To take this one step further, there are now flexible display screens that could be wrapped around the bottom half of the fuselage and on the crest. Paired with a small camera on the top of the aircraft, the display screen can match the color and light emission of the sky above it. For display quality, an object can be hidden to the background from an observer only 2 meters away (~6.5 feet) using a 289 pixel per centimeter display, or 730 pixels per inch (ppi) display (Ref. 49). The only limitation to a hidden fuselage, is the power requirement would add small batteries spread around the aircraft fuselage or replace the LiDAR with one large battery.

27.2. ADVANCED ELECTRONICS

There is extra space on the wing fins where the aileron servos are located. Small cameras, like the hidden house security cameras, are added to the fins. This would provide two camera locations for stereoscopic vision. This would allow a pilot to have a 3-D video image for depth perception, opposed to a 2-D image that a single camera would provide. The stereoscopic vision would provide the pilot with a better view of the capture net during the recovery process.

27.3. ADVANCED TECHNOLOGIES SUMMARY AND RECOMMENDATIONS

Summary

The major findings in this chapter are:

- Using clear material for the wings, and active camouflage system on the fuselage makes a LO design;
- Cameras are added to the fins for stereoscopic vision

Recommendations

The author recommends that:

- Develop a low-power active camouflage for the fuselage;
- Have gyro-mounted cameras on the fins to create a less-shaky video image

28. RISK MITIGATION

The purpose of this section is to identify the risks associated with the design. Know the severity of the risks, there are steps that can be taken to mitigate the risks to achieve the entry into service date of 2020.

28.1. UNSTABLE YAW CONTROL

This design has a unique feature of a forward placed vertical tail. This design makes the Pteslasaur unstable in weathercock stability. This does create an increased risk of the pilot losing control of the aircraft with a $50k LiDAR inside. But this isn't the first time that an aircraft has flown with an unstable control. To ensure safety in the design, a few methods must be considered. During the control of an unstable mode, one consideration would be to make sure the time to double amplitude is sufficient for the pilot to identify the divergence and bring the aircraft back to a controlled flight. For this purpose, the servos selected for the crest were the fastest acting servos that could be found. While this increases the cost, it can help the pilot regain control over an aircraft. A slow articulating servo would not be able to move the control surface fast enough to counteract the aerodynamic forces when the UAV enters the unstable divergence from the flight path. It is otherwise recommended to have an autopilot control the aircraft where there a controller can be developed to correct for the instability.

28.2. WING MEMBRANE

Membrane wings have been used on micro-UAVs several times but they haven't been used on larger scale aircraft. To ensure the wing will perform as expected, it will require time for testing to understand the performance. This will require testing on different material types to figure out which one has the strength to keep its shape for flight but also have enough flexibility to morph to the airflow. The membrane shape is rather simple, so cutting material for testing can be done quickly. This will provide the opportunity for rapid testing of multiple designs and compare performance. With the rapid testing available, there should be time to select a reliable wing material in time for the entry into service date.

29. MANUFACTURING PLAN

The purpose of this section is to provide an insight into the manufacturing plan for the aircraft. The components of the aircraft will be determined along with the material and required quantities for the bill of materials (BOM).

Since the aircraft is small, it can be done in a single room with access to an oven for the composite curing. Being owned by a large company will simplify material acquisition and start-up funding, but the processes are small enough for small company ownership. Figure 28.1 shows the major components of the aircraft, and the materials required for production. Payload items are purchased so they are excluded from the figure.

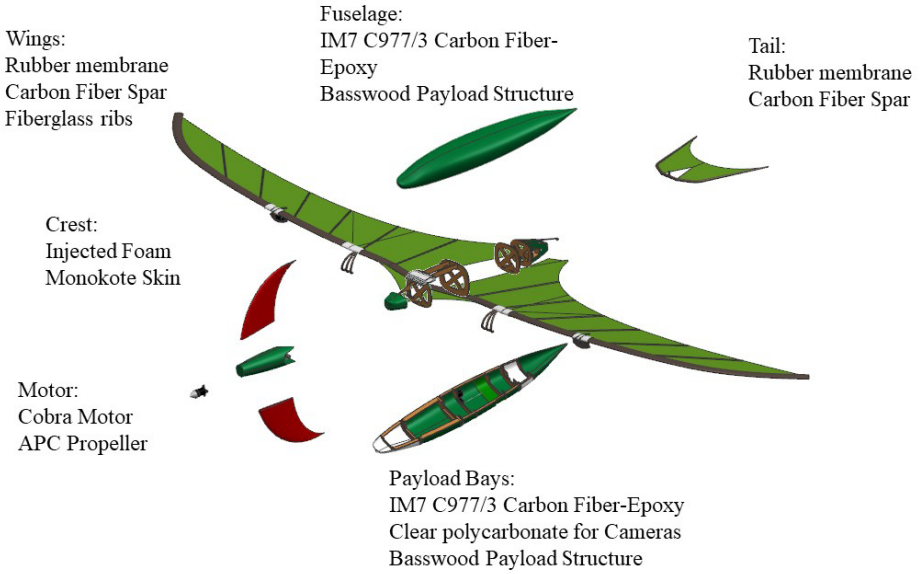

Fig. 29.1: Major Structural Components and Materials

The BOM shows all of the components that are required to produce this aircraft. This will provide the management office with a way to ensure they have a sufficient amount of materials to continue production and keep track of materials used. Table 28.1 (click to enlarge, click again to minimize) shows the full BOM. This includes the material, potential suppliers, type of process required to build as well as the full CG analysis used for Chapter 23.

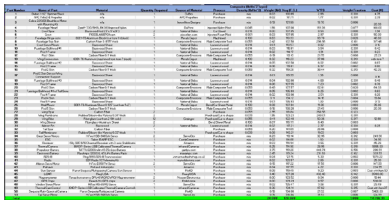

Table 29.1: Bill Of Materials

Due to the complex curvature of the fuselage, the composite layups will be done over a

male tool. A female tool will have challenges of not folding too much material into the tight curves at the front and back of the fuselage. While the skin on the removable payload pods could also be done in a female tool, the males tools will be used for simplicity. Having a single process helps insure quality of a part since it is easier to perfect one method opposed to constantly having two methods to consider.

The other consideration for composite structure is the work environment for the trimming processes. Trimming produces a lot of dust particles that are terrible for employee health and safety. The dust particles would also affect the bonding process used to build and attach the wood structure to the composite skins. For these two reasons, a partition wall will be used as the trimming room. Inside the trimming will always be done using high power vacuum tables and air powered tools with vacuum hoses attached. The two vacuums will increase production costs due to the power, but the focus is to protect the employees by reducing the amount of dust that stays floating in the air. Workers will also be required to have safety goggles to protect the eyes and a breathing mask to prevent inhaling the dust.

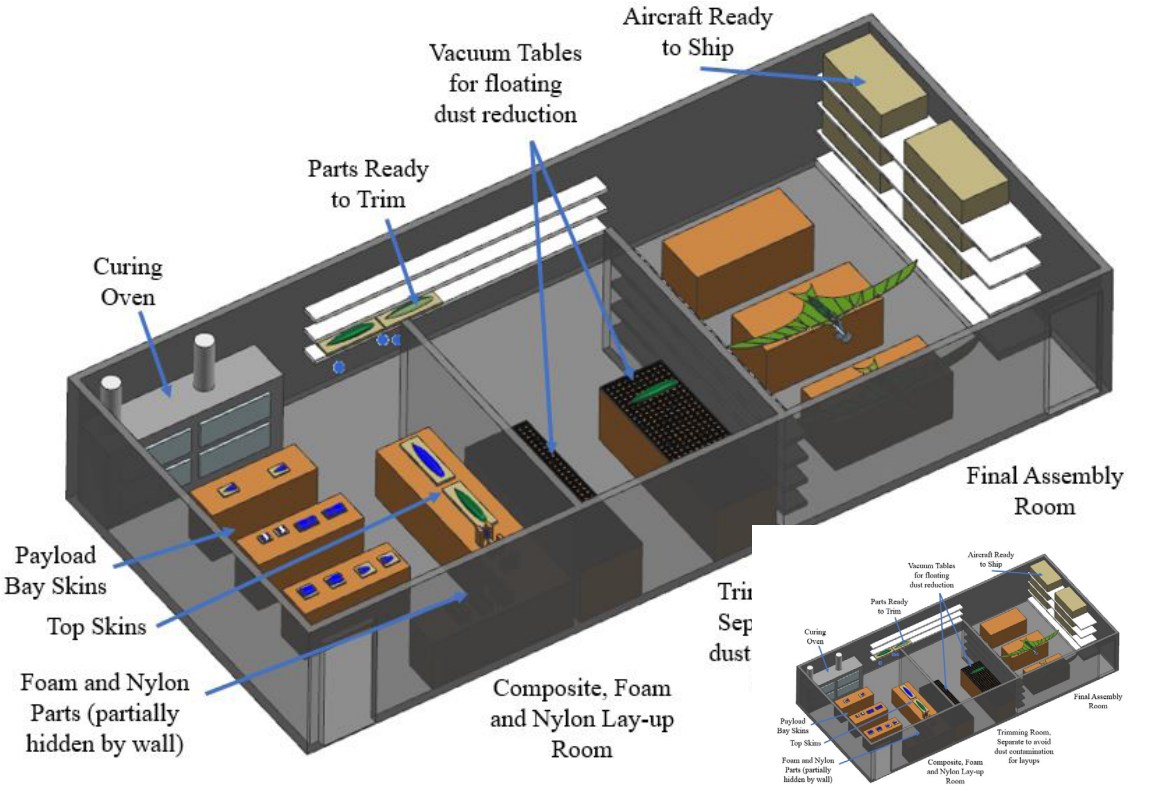

Fig. 29.2: Manufacturing Floor Plan

30. SPECIFICATION COMPLIANCE

The RFP has a set of required and tradable design options. Table 29.1 shows the RFP requirements alongside the Pteslasaur capabilities, this will show whether or not this design satisfies the proposal.

Table 30.1: Specification Compliance Checklist

Specification Requirements/ Aircraft Characteristics	Aircraft Performance	Objective Met	Chapter #
Operate from a Ford F-150	Operates from a Ford F-150	Yes	1
Cover 100 miles of powerlines per day	Covers 100 miles in 2 flights, total of 4.7 hours	Yes	5
Complies with Part 107 requirements	Under 55 pounds and cruise velocity is under 87 knots	Yes	5,6
Survive Wind Conditions	Designed for high gust loading	Yes	15
Autonomous Flight/ GPS Autopilot	Uses a Pixhawk 4.1	Yes	20
Operate with the RIEGL miniVux-1UAV LiDAR	Has space and power required for the full flight	Yes	20
High Resolution Still Camera (T)	Built into the Multi-Spectral Camera	Yes	20
Infrared Fixed Camera	Uses the 8640P camera from Infrared Cameras	Yes	20
Resistance to Magnetic Fields	Redundant GPS and magnetometers to mitigate noise from the power line magnetic fields	Yes	20
Operate from a 500x10 foot clearing, surrounded by 50 foot tress	Uses a catapult and net for short take-off and landing	Yes	13
Launch within 15 minutes of arrival	Only required the wing poles to be set in place, and flight plan is prepareed	Yes	20
Safe for Operators	Launch and Recovery can be completed from inside the truck	Yes	-
Visually Appealing/ Public Acceptance	It's a Pterosaur, so the public acceptance depends on who is looking at it	Maybe	27

30.1. OBJECTIVE FUNCTION DETERMINATION AND ASSESSMENT

The other metric for the design analysis is improving the objective function score. The objective function for this design was decided upon in Chapter 3 and the Pteslasaur score before a cost analysis is as follows:

OF=0.15*Range(=2 if over 200 miles, =1 if over 100 miles, 0 otherwise)

+0.15*(1 if it meets the 500ft clearing, 0 otherwise)

+0.2*(1 if Meets Payload Requirements, 0 otherwise)

+0.1*(8 hours/actual flight time, 0 if over 10 hours)2

+0.1*($25K/(Fly Away Cost))

+0.05*(Visually Appealing/Public Acceptance)

+0.05*(Safe for Operators=1 yes, or 0)

+0.15*(Interference resistance, 1=yes, 0 otherwise)

+0.05*([1 for each: Thermal iamging, HD optical, Vegetation Health]/3)

OF(Ptelasuar) = 0.15*2

+ 0.15* 1

+ 0.2*1

+0.1*(8/4.7)2

+ 0.1*(no cost analysis)

+ 0.05*0.5 (questionable public acceptance)

+ 0.05*1

+0.15*1

+ 0.05*(1+1+1)/3

= 1.2+0.1*($25k/unit cost)

31. Marketing Plan and Aircraft Design Summary

The purpose of this section is to start the marketing plan for the aircraft and how this aircraft will stay competitive in the market. This section and report will conclude with the preliminary market brochure for the aircraft. The initial brochure should then be sent to a advertising and graphics specialist for further refinement.

The Pteslasaur is entering into a very competitive market where there are a lot of designs competing for market control. This design was made to stand out in a couple of ways. Current electric motor designs all have limited ranges that would not be able to complete the required mission, so the Pteslasaur should be able to claim the 100-mile range as its primary market. If the LiDAR, which neither company from Chapter 3 wanted, is replaced with another battery the Pteslasaur would be the first UAV to break the 200-mile mark using electric power. Gas engines would still compete on a range basis, but electric motors run quieter which will increase public acceptance.

Keeping an eye on public acceptance, this design allows for logical integration of low-observable materials. An LO design with an electric motor would really decrease the public disturbance that has been talked about several times in the news. If the kids latch onto the idea of a flying dinosaur, a scaled model could quickly be developed for an RC aircraft toy plane.

Outside of the powerline surveillance industry, the UAV is equipped with sensors that are commonly used in the agriculture industry. With the growing demand for increased food production, crop health is becoming more important to monitor. The LiDAR would be useless, but removing the LiDAR opens up a lot of space for an operator to add any sensors that they consider important or extend the range that the UAV can scan per flight.

REFERENCES

1. Anon., "Linear Infrastructure Inspection Request for Proposal 2018-2019". AIAA Foundation Undergraduate Individual Aircraft Design Competition, pp. [online RFP], 1-11, URL: http://www.aiaa.org/designcompetitions/ [8, September 2018].
2. Anon. "2018 Ford F-150 XLT". *MinnesotaCars, MinnesotaCars Web Site* Image [https://www.minnesotacars.com/detail/2018-ford-f150-xlt/555082806/] MinnesotaCars, Inwood, Iowa 51240
3. Roskam, Jan, *Airplane Design: Part I, Preliminary Sizing of Airplanes,* DARcorporation, Lawrence, KS, 2005.
4. Roskam, Jan, Airplane Design: *Part II*, *Preliminary Configuration Design and Integration of the Propulsion System*, DARcorporation, Lawrence, KS, 2005.
5. Roskam, Jan, A*irplane Design: Part III, Layout Design of Cockpit, Fuselage, Wing,and Empennage: Cutaways and Inboard Profiles, DARcorporation,* Lawrence, KS, 1989.
6. Roskam, Jan, *Airplane Design: Part IV, Layout of Landing Gear and Systems,* DARcorporation, Lawrence, KS, 2010.
7. Roskam, Jan, Airplane Design: Part V, *Component Weight Estimation,* DARcorporation, Lawrence, KS, 1999.
8. Roskam, Jan, *Airplane Design: Part VI, Preliminary Calculation of Aerodynamic Thrust and Power Characteristics,* DARcorporation, Lawrence, KS, 2008.
9. Roskam, Jan, *Airplane Design: Part VII, Determination of Stability, Control and Performance Characteristics: Far and Military Requirements,* DARcorporation, Lawrence, KS, 1991.
10. Roskam, Jan, *Airplane Design: Part VIII, Airplane Cost Estimation: Design Development, Manufacturing and Operating,* DARcorporation, Lawrence, KS, 1990.
11. Taylor, J.W.S., "Jane's Online," published by Jane's Incorporation, London, UK., 2018. https://www.janes.com/
12. Anon., "Penguin C UAS". UAV Factory, UAV Factory Web Site [http://www.uavfactory.com/product/74] Bend, Oregon 97703
13. Anon, "Servicios con UAV/RPA" *Soluciones Integrales GIS, SiGIS Web Site* [http://www.sigis.com.ve/index.php/servicios-uav] Miranda State, Venezuala 1060
14. Anon, "Meet Albatross" *Applied Aeronautics, Applied Aeronautics Web Site* [https://www.appliedaeronautics.com/albatross-uav/] Austin, TX 78701
15. Applied Aeronautics, "The Albatross UAV-Ready to Launch" *DIY Drones Blogs, DIY Drones Web Site* [https://diydrones.com/profiles/blogs/the-albatross-uav-ready-to-launch]
16. Anon, "UAS: RQ-20B Puma™AE" AeroVironment, AeroVironment Web Site [https://www.avinc.com/uas/view/puma] Monrovia, CA 91016
17. Anon, "Delair DT26x LiDAR" Delair Aerial Intelligence, Delair Web Site [https://delair.aero/professional-drones/delair-dt26x-lidar-drone/] Labege, France 31670
18. Anon. "Long distance record for FAI Class F8 model plane", Barnard Microsystems, Web Site [http://www.barnardmicrosystems.com/UAV/milestones/atlantic_crossing_2.html] London, United Kingdom
19. Coleman, B., Zalog, J., Johnson, R., Technical Discussion on the Design Vectors". White River Valley Electric Cooperative. 14 September, 2018
20. Handley, T. Technical Discussion on the Design Vectors" FlyGuys. 26 September 2018
21. Barrett, R., "Report Block 1 Lecture," University of Kansas, Lawrence, Kansas, August 2016.
22. Anon, "RIEGL miniVUX-1UAV" RIEGL USA, Web Site [http://products.rieglusa.com/item/all-categories-unmanned-scanners/minivux-1uav--airborne-laser-scanners/riegl-minivux-1uav] Orlando Florida 32819
23. Anon. "PING1090 ADS-B Transceiver" uAvioni, Web Site [https://uavionix.com/downloads/ping1090/docs/uAvionix-ping1090-ADS-B-Transceiver-Data-Sheet.pdf] Palo Alto, California 94306
24. PX4 Dev Team. "Pixhawk 4" Dronecode Web Site [https://docs.px4.io/en/flight_controller/pixhawk4.html] 03, September 2018
25. Anon. "Sequoia+: Designed for Agriculture" PIX4D [https://pix4d.com/product/sequoia/]
26. Anon. "8640 P-Series | USB Calibrated Thermal Camera with Temperature Measurement" Infrared Cameras [https://infraredcameras.com/thermal-infrared-products/8640-p-series/] 26, September 2018
27. Anon. "Sensor Control Module| Thermal Infrared UAV Remote Management System" Infrared Cameras [https://infraredcameras.com/thermal-infrared-products/sensor-control-module/]
28. Anon. "Digi-Key Electronics CAM-M8Q-0" Digi-Key Electronics [https://www.digikey.com/product-detail/en/u-blox-america-inc/CAM-M8Q-0/672-1013-2-ND/6150646]
29. Barrett, R., "Report Block 1 Lecture," University of Kansas, Lawrence, Kansas, August 2016.
30. Anon. "Drone Energy Sources-Pushing the Bouundaries of Electric Flight" DRONEII.com, Drone Industry Insights [https://www.droneii.com/drone-energy-sources] Hamburg, Germany
31. Anon "Electric Power Transmission Lines" Homeland Infrastructure Foundation-level Data, Web Site [https://hifld-geoplatform.opendata.arcgis.com/datasets/electric-power-transmission-lines]

32. Anon “6kJ Protable Pneumatic Catapult” UAV Factory, UAV Factory Web Site [http://www.uavfactory.com/product/21] Bend, Oregon 97703

33. Anon. “C-2213-26 Specifications” Cobra Web Site [http://www.cobrasystem.net/web/Model/?n_cobra_t_product_id=25]

34. Anon. “TATTU 22000mAh 4S 25C Lipo Battery” GetFPV Web Site [https://www.getfpv.com/tattu-22000mah-4s-25c-lipo-battery.html?utm_source=google&utm_medium=cpc&adpos=1o1&scid=scplp2253&sc_intid=2253&gclid=Cj0KCQjw6MHdBRCtARIsAEigMxGTGdlFlnJZf6sXlAEiQU-X6KSaCkd8rgcNghYofHvtxz2QRTVtSX0aAj39EALw_wcB]

35. Anon. “LiPo 12000XL 4S 14.8V Battery Pack” MaxAmps.com Web Site [https://www.maxamps.com/lipo-12000xl-4s-14-8v-battery-pack]

36. Anon, “Bat” Wikipedia Web Site [https://en.wikipedia.org/wiki/Bat]

37. Barrett, R. M. “Technical Discussion on the Importance of Membrane Wing Concavity” The University of Kansas Aerospace Engineering Department. 6:00pm, 29 September 2018

38. Hu, H., Tamai, M., and Murphy, J., “Flexible-Membrane Airfoils at Low Reynolds Numbers, Journal of Aircraft, Vol. 45, No. 5, Septermber-October 2008. pp. 1767-1778

39. “Smith, R., Shyy, W., “”Computation of aerodynamic coefficients for a flexible membrane airfoil in turbulent flow: A comparison with classical theory,”” Physics of Fluids, August 1996 “

40. Witton, M. “Episode 55: Pterosaurs” , Palaeocast | Palaeontology Podcast Web Site [http://www.palaeocast.com/episode-55-pterosaurs/]

41. Béguin, B., “Development and Analysis of an Elasto-flexible Morphing Wing”, Technical University of Munich., June 2014

42. Thomas, A. “Why do birds have tails? The tail as a drag reducing flap, and trim control” Journal of Theoretical Biology, March 1996.

43. Sachs, G., “Tail effects on yaw stability in birds.” Journal of Theoretical Biology 249, 464-472. July 2007.

44. Anon. “Ford F150 Pickup 3D Model”, 3D CAD BROWSER Web Site [https://www.3dcadbrowser.com/download.aspx?3dmodel=15572]

45. National Aeronautics and Space Administration, “Transportation and Handling Loads”, NASA Space Vehicle Design Criteria (Structures). September 1971.

46. Barrett, R. M. “Technical Discussion on Longitudinal Stability Requirements”, The University of Kansas Department of Aerospace Engineering,

47. Bleischwitz, R., de Kat, R., Ganapathisubrammani, B., “Aeromechanics of membrane and rigid wings in and out of ground-effect at moderate Reynolds Numbers” University of Southampton, February 2016.

48. Anon. “Aerosonde Small Unmanned Aircraft System (SUAS)” Textron Systems Web Site [https://www.textronsystems.com/what-we-do/unmanned-systems/aerosonde]

49. Bennett, C. “Pterosaur Flight: The Role of Actinofibrils in Wing Function”. Historical Biology Volume 14, pp 255-284. 2000

50. McKee, K., Tack, D., “Active Camouflage for Infantry Headwear Applications” Humansystems Incorporated on behalf of the Department of National Defense. Feb. 2007

51. Roskam, Jan. Airplane Flight Dynamics and Automatic Flight Controls: *Part I*. DARcorporation, Lawrence, KS, 2011